Fall 1995

Heavy-Ion Interaction Models for Radiation Transport

Rajendra R. Dubey
Old Dominion University

HEAVY-ION INTERACTION MODELS FOR RADIATION TRANSPORT

by

Rajendra R. Dubey

M. Sc. August 1986, University of Bombay
M. S. December 1991, Old Dominion University

A Dissertation submitted to the Faculty of
Old Dominion University in Partial Fulfillment of the
Requirements for the Degree of

DOCTOR OF PHILOSOPHY

PHYSICS

OLD DOMINION UNIVERSITY

October 1995

Approved by:

Dr. Govind S. Khandelwal (Director)

ABSTRACT

This dissertation is concerned with finding the values for the nuclear cross sections used in the Boltzmann equation for space radiation transport and dose estimates. An extraordinary number of cross sections are required because of the large number of ion types and their extensive energy range, The Lippmann-Schwinger equation is numerically solved in momentum space for a first order optical potential (free space case) and calculations are made for the total and absorption cross sections for **nucleus-nucleus** scattering. Absorption cross sections are also calculated using a medium modified first-order optical potential in the Lippmann-Schwinger equation and are compared with experimental values. Results are presented for the absorption cross sections for ^{4}He-Nucleus and ^{12}C-Nucleus scattering systems and are compared with experimental values below 100 A MeV. The use of the in-medium nucleon-nucleon cross sections is found to result in a significant reduction of the free space absorption cross sections, in agreement with experiment. We have also reformulated the Glauber model of **heavy-ion** fragmentation to treat the cluster abrasion of alpha particles from α-cluster nuclei such as ^{12}C, ^{16}O, ^{20}Ne, ^{24}Mg, ^{28}Si, ^{36}Ar, and ^{40}Ca. Comparison of the calculated values is made with recent experimental data and good agreement is found. The energy dependence and the target mass dependence of cluster knockout cross sections for the ^{16}O projectile are discussed. The inclusion of clusters knockouts is shown to significantly modify transport properties of space radiations.

DEDICATION

This dissertation is dedicated to my father, mother, and my wife for the unfailing love, support, and encouragement they have shown to me throughout my life and also to Pryanka, Prasant and Shailesh.

ACKNOWLEDGMENTS

This dissertation would not have been completed without the encouragement and support of many people including my professors, colleagues, and family friends. Professor Govind S. Khandelwal has served as a guru and father figure since my arrival at Old Dominion University. When I first arrived at ODU, Dr. Khandelwal welcomed me by providing both academic challenges and funding grants so that I was able to carry on my studies and grow as a physicist. In the beginning, Dr. Khandelwal involved me in his atomic physics projects, which gave me an exposure to computational physics. That introduction to computers became the foundation for my basic career path. When I got interested in Nuclear and Radiation Physics, Dr. Khandelwal created an opportunity to become involved in his on going scientific research at NASA Langley Research Center. In my mind Dr. Khandelwal epitomizes the ideal of a real guru, requiring me to perform at a distinguished scholar level while ensuring that I had the resources and opportunities to achieve my academic goals. Without the direction and strong encouragement of my adviser, Professor Khandelwal, this dissertation would not have been possible.

The guidance and research expertise of Dr. Francis A. Cucinotta, NASA Langley Research Center, has been critical to this dissertation. Dr. Cucinotta has been generous in his willingness to help me in applying theoretical concepts and postulates to seek solutions for problems of concern to the

scientific community. He has extended my erudition and proficiency in new directions. During the last four years I have worked under his supervision, I have come to admire and esteem his extensive knowledge and hard work in the nuclear and radiation fields. I would like to extend my deepest appreciation to Dr. Cucinotta for his patience and valuable support. I would like to extend my gratitude to Dr. John W. Wilson, a distinguished physicist at NASA Langley Research Center, for providing me with an opportunity to work under his leadership.

I would like to extend my sincere gratitude to my father Ramkripal Dubey for providing me motivation and financial support at ODU. I am deeply grateful to my mother Ramadhari Devi for her love and patience during my stay at ODU. I would like to express my sincere thanks to my uncle, Dr. Surendra N. Tiwari, for his guidance, support, and confidence through all these years. I want to express my appreciation to my wife Sudha for her devoted love and patience during this seven year trial. I would also like to thank my children Pryanka and Prasant, my brother Shailesh, and our special friend Ms. Ruth Purushotham for their encouragement and understanding.

I would like to express my sincere gratitude to the faculty members of the Department of Physics at ODU in particular Dr. Cox, Dr. Harries, Dr. Hoy, and Dr. Van Orden for their encouragement and support. I am especially grateful to Dr. Pritchard for his assistance in the preparation of this dissertation. Thanks are also due to Dr. K. M. Maung of Hampton University

for his helpful suggestions and dedicated efforts during the research. I would also like to thank the other members of the dissertation committee, Dr. Heinbockel, and Dr. Kernell for their helpful comments.

Last but not least I would like to extend my sincere thanks to my family friends in particular Dr. V. K. Lakdawala, Dr. S. C. Mehrotra, Dr. D. K. Pandey, and Dr. R. K. Tripathi for their support in this endeavor.

I would like to acknowledge the support of the NASA langley Research Center grant NCC1-42, which provided the funding for this project.

TABLE OF CONTENTS

TABLE OF CONTENTS, Continue

LIST OF TABLES

LIST OF FIGURES

LIST OF FIGURES, Continued

Chapter 1

Introduction

The study of radiation hazards to the crew of manned space flights beyond the Earth's magnetosphere has been of great interest for many researchers for the last four decades. There are three main sources of radiation hazards present in the atmosphere: trapped particle radiation (Van Allen Belts), solar particle events (SPE), and galactic cosmic rays (GCR). The trapped radiation consists mostly of electrons and protons trapped in closed orbits by the earth's magnetic field. The galactic radiation consists mostly of protons, with a small admixture of helium ions and an even smaller component of heavier ions. The solar particle radiation consists mostly of protons, with a small contribution from helium ions and heavier particles. The differences between the last two categories are mainly in the vastly different distributions of particle energies involved and in the sporadic nature of the solar disturbances producing the solar particles as compared with the more slowly varying nature of galactic particle intensities. The effects resulting from large radiation doses acquired in a short period are of major concerns in the study of SPE transport. SPE's are characterized by their intensity, duration, and spectra of energetic particles. The primary particles in SPE's are protons in an energy range of 10 A MeV (10 MeV / nucleon) to several hundred A MeV.

The high energy particles such as protons, deuteron, triton, alpha, and other heavier ions present beyond the Earth's magnetosphere are the main

constituents of the GCR. These particles deposit a large quantity of energy per unit distance traveled in tissue or shielding materials. Therefore, they are much more hazardous to body tissues than are the X-rays. Nuclear reactions modify the composition of the galactic cosmic rays (GCR) in free space and in absorbers such as space craft and tissue. Due to this, the internal radiation environment within the spacecraft may change. This alteration in the environment depends on the geometry, thickness, and the type of materials used in the spacecraft. A transport model should express the transmitted flux as a function of spatial location, kinetic energy, and the direction of particle motions. There are three major areas of concern in the study of the processes involved in the transport of these radiation fields through the space shielding materials. These are: the ionized energy loss through collisions with atomic electrons; the nuclear elastic and inelastic collisions; and the nuclear reactions, such as fragmentation. Since fragmentation may result in light ion production, which may alter the transmitted radiation field, it becomes the leading area of concern.

The propagation of radiation fields is described by Wilson et. al. [1] using the Boltzmann equation, which can be derived by considering mass and energy conservation. The solution of the Boltzmann equation gives the particle flux and energy everywhere within the boundary of the target medium. In the straight-ahead approximation, we neglect the changes in the particle directions after collisions, since the kinetic energy of the SPE or GCR particles is very

high. One therefore considers the one dimensional Boltzmann equation [1] given by,

$$[\frac{\partial}{\partial x}-\frac{\partial}{\partial E}S_i(E)+\sigma_i(E)]\ \phi_i(x,\ E) = \sum_j \int \sigma_{ij}(E,\ E')\ \phi_j(x,\ E')\ dE' \quad (1)$$

In equation (1), ϕ_i is the flux (number of particles crossing a unit area per unit time) of type i ions at position x and E is the energy. The quantity $\sigma_i(E)$ is the corresponding macroscopic nuclear absorption cross section (per unit length). Here the stopping power $S_i(E)$ is the change in energy per unit distance and $\sigma_{ij}(E, E')$ is the cross section (per unit length) for producing ion i from a collision by ion j. Equation (1) can be written as [2]:

$$\begin{aligned}[\frac{\partial}{\partial x}-\nu_i\frac{\partial}{\partial E}S(E)+\sigma_i(E)]\ \phi_i(x,\ E) \\ = \sum_j \int_0^\infty f_{ij}(E,\ E')\ \phi_j(x,\ E')\ dE'\end{aligned} \quad (2)$$

where ν_i denotes the range-scaling parameter and is equal to Z_i^2/A_i, Z is the charge and A is the mass number. The quantity f_{ij} is the differential energy cross section and it obeys the relation,

$$\int_0^\infty f_{ij}(E,\ E')\ dE = m_{ij}\ \sigma_{abs} \quad (3)$$

where m_{ij} is the multiplicity of producing ion i from a collision by ion j, and σ_{abs}

is the corresponding macroscopic absorption cross section.

The method of calculation used in determining the stopping power has been described in reference [1]. The dominant contribution in a shielding calculation is associated with energy loss through ionization [3] due to a collision between an incoming charged particle and an orbital electron of the shielding material. These interactions involve many small energy exchanges along the path. A great deal of research has been devoted to the study of stopping power [4-12]. Bethe [4] derived an expression for the stopping power using the Born approximation. A detailed derivation of the Bethe expression for stopping power was fully reviewed by Lamkin [10]. Lamkin [10] and Chun [12], in their Ph. D. dissertations at Old Dominion University have considered the transport of energetic nucleons through extended bulk matter. They have developed an analytical approach to the nucleon transport problem called BRYNTRN that helps for numerical implementation. The BRYNTRN (Baryon Transport) code [13-17] represents one of the products of a collaboration between the NASA Langley Center and the Radiation Physics Group at Old Dominion University during the past 25 years. the BRYNTRN code provides the transport methodology for the typical radiation case using a varying thickness of aluminum slab shielding followed by the tissue media.

It is essential that the concepts of radiation physics that refer to the properties of the radiation field be augmented by quantities that relate to the interaction between the radiation field and matter. Among these radiological

quantities perhaps the most fundamental and important are the absorbed dose (D) and the dose equivalent (H). The absorbed dose is the amount of energy imparted by ionizing particles per unit mass of the material at the place of interest. Its unit is the RAD (100 erg per gm). The dose equivalent is defined as the product of the absorbed dose D, and the quality factor (Q) of a given radiation. The unit of dose equivalent is called the REM. The quantity Q is a dimension-less quantity as determined by International Commission on Radiation Protection (ICRP-60) [18].

The absorbed dose D due to energy deposition at a given location x by all particles is calculated according to [1] as

$$D(x) = \sum_j \int_0^\infty S_j(E)\ \phi_j(x, E)\ dE \qquad (4)$$

where $\phi_j(x,E)$ is the flux calculated from equation (2), and the quantity $S_j(E)$ is the stopping power.

The value of the dose equivalent H is computed as [1]

$$H(x) = \sum_j \int_0^\infty Q_j(E)\ S_j(E)\ \phi_j(x, E)\ dE \qquad (5)$$

The values of the dose equivalent H are used to specify radiation exposer limits.

This thesis is concerned with finding the values for the nuclear cross

sections used in equation (2) and applying the results to the area of radiation protection. The nuclear cross sections and the differential energy cross sections used in equation (2) are the major areas of concern in this thesis. The nuclear cross sections are calculated under the **Eikonal model** [19, 20]. We have also calculated the nuclear cross sections by numerical solutions of the **Lippmann-Schwinger** equation (exact solutions) and have compared them with the Eikonal model cross sections [21, 22]. Thus, we provide a major improvement to the nuclear data base. The differential energy cross sections are calculated using the **abrasion-ablation** model [23].

In this thesis, we are going to focus on the importance of nuclear interactions of light and heavy ions with materials and the production of light ions from the heavier elements in the GCR and in the shielding materials. The need for a sound theoretical basis for high-energy elastic and inelastic scattering calculations is becoming very important in the analysis of high energy experimental data. It is therefore necessary to review the basic assumptions of multiple scattering theory and compare the results based on it with experimental data wherever possible. In the multiple scattering approach, information for the two-nucleon system is introduced via the t-matrix. In the past, many authors [24-27] have used the forward angle and on-shell assumptions to calculate the t-matrix. The on-shell approach follows from the neglect of nuclear binding in the Green's function (impulse approximation), and means that only the particular form of the nucleon-nucleon (NN) t-matrix

which arises from the conservation of energy and momentum, needs to be used in the many-body problem. The second important assumption is the use of only the first order term of the optical potential in elastic and inelastic scattering calculations. In the first order optical potential, excitation of the projectile or target in intermediate states is neglected in the elastic scattering. The higher order terms of the optical potential correspond to correlation effects such as Pauli blocking [28]. The main approach in the study of high-energy scattering is the use of a microscopic optical potential that involves the formulation of scattering processes through a study of the interaction of each nucleon of the projectile with each target nucleon. Since the microscopic approach is more fundamental, and more information can be obtained about the scattering process, it is **the microscopic approach that we will take in the study of heavy-ion collisions** in this thesis. In the construction of the optical potential for **heavy-ion** collisions, a variety of approximations are discussed in chapter 3.

It is the purpose of this thesis to address nucleus-nucleus collisions through the microscopic first order optical potential based on the multiple scattering theory developed by Kerman, McManus, and Thaler [29], from now on referred as KMT. The KMT multiple scattering theory for proton-nucleus scattering has been studied extensively in relation to the Watson multiple scattering theory [30] by several authors [31-34]. The Watson multiple scattering theory rearranges the Born series, using the two-body amplitude for scattering of a projectile by a target. In the KMT multiple scattering theory,

the target nucleons are considered to be in ground states, i.e. excitation of the target nucleons is neglected in describing the first order optical potential. The advantage of the KMT approach is that the many body interactions can be approximated by two-body interactions.

Calculations of the reaction and absorption cross sections for a heavy ion projectile were well developed by Wilson and Townsend [19, 20] using an Eikonal approximation and a first order optical model. They used multiple scattering theory for scattering of two composite nuclei (neglecting three body interactions) developed by Wilson [35, 36]. The Eikonal approximation is based on a forward scattering assumption, and on considerations of the strength of the potential [37]. A second order solution (i.e. using a second order optical potential) to the Eikonal coupled-channels (ECC) model was developed by Cucinotta, Khandelwal, Maung, Townsend, and Wilson [35-36, 38-39] and was found to give improved accuracy over the first order solutions in limited studies for several collision pairs and energies.

In recent years, the validity of various approximations used frequently in multiple scattering theory have been investigated and this is another point of focus in our study presented here. There has recently been a systematic study of the Eikonal approximation using the microscopic optical potential by Wilson, Townsend, Cucinotta, and Khandelwal [35-36, 38-39]. The attractiveness of this study lies in the use of the two-body scattering amplitude in the optical potential, which involves two-body NN (nucleon-nucleon)

parameters. To test the reliability of the Eikonal approximation, in this dissertation, we compare the Eikonal model calculations for heavy-ion scattering with the results obtained from exact numerical solutions of the Lippmann-Schwinger equation.

Another purpose of this thesis is to accurately predict α-knockouts in heavy-ion collisions at high energy [40]. Much of this progress has been based on scattering experiments in which a proton is incident on a target. Analysis of these experiments reveals information about nuclear structure and the momentum distribution of nucleons in the nucleus. The large multiplicity of secondary α-particle in reactions suggests that the alpha knockout cross sections will have a wide range of uses in nuclear astrophysics and space radiation protection studies.

In a nuclear fragmentation reaction, in an inclusive measurement where light-ions are detected, the fragment momentum distribution is expected to be of Gaussian shape at small angles. The peak occurs at a velocity near that of the projectile. The reaction is usually described in a particle-spectator model. The spectator is assumed not to have interacted with the target, while the projectile fragments called participants collide elastically or inelastically with the target. The application of the Glauber theory [41] to these types of reactions has been made with reasonable success. The accuracy of the Glauber model for studying these reactions should be strongly questioned, since the energy conservation is ignored in this model. We expect this to be a serious

problem, because for reactions with three or more particles in the final state, validity of a small angle approximation in the Glauber model is not clear. We will treat this problem in Chapter 5.

The remaining chapters of this work are divided as follows. In Chapter 2, we discuss the multiple-scattering formalism for nucleus-nucleus collisions and the Eikonal approximation used in this dissertation. Using the Glauber model approach as discussed by Cucinotta, the Eikonal coupled channel (ECC) model is described. In Chapter 3, a first order optical potential for heavy-ion collisions based on the KMT model for multiple scattering is derived. The medium-modification of the optical potential is considered. In Chapter 4, we discuss one of the techniques used in solving the Lippmann-Schwinger equation in momentum space. We have extended the technique for the complex potential. In Chapter 5, a two step, participant-spectator model (abrasion-ablation) for fragmentation of the projectile or target is developed in terms of the Glauber profile function. The clustering effects in the heavy-ion fragmentation at the abrasion stage are discussed. We have extended the Glauber formulation of nuclear abrasion by considering energy conservation to generate response functions for exciting discrete levels of the pre-fragment. Finally, in Chapter 6, results of our calculations and future considerations are discussed.

Chapter 2

Review of Multiple Scattering Theory and the Eikonal Approximation

2.1 Introduction

In this chapter we will review multiple scattering theory and the Eikonal approximation useful in the solution of the problems of this dissertation. Our starting point is the non-relativistic Hamiltonian. The separation of the Hamiltonian into relative and overall center of mass (CM) coordinates is made. Next, we will discuss the approximation methods which are widely used in scattering theory. Approximate treatments are obviously necessary in complicated physical situations where exact solutions are not available. It is convenient, however, to consider these approximations whenever possible in the simple case of potential scattering where their interpretation is simpler and their range of validity can be checked accurately. The Glauber model approach [41] and the Eikonal coupled channel (ECC) model [38] are discussed.

2.2 Kinematics

The Hamiltonian for a projectile nucleus of mass number A_P and a target nucleus of mass number A_T interacting through a two-body potential is:

$$H = H_P + H_T + V \qquad (6)$$

where the projectile and target Hamiltonians are given by

$$H_P = \sum_{i=1}^{A_P} T_i + \sum_{i<j}^{A_P} V_{ij}(\vec{r}_i - \vec{r}_j) \tag{7}$$

and

$$H_T = \sum_{\alpha=1}^{A_T} T_\alpha + \sum_{\alpha<\beta}^{A_T} V_{\alpha\beta}(\vec{r}_\alpha - \vec{r}_\beta) \tag{8}$$

respectively. Roman subscripts refer to the projectile and Greek subscripts to the target. The interaction potential is given by

$$V = \sum_{\alpha, j} V_{\alpha j}(\vec{r}_\alpha - \vec{r}_j) \tag{9}$$

where $V_{\alpha j}$ is the two-nucleon potential. The kinetic energy operator is written in terms of the constituent momenta for the target as

$$T_\alpha = \frac{p_\alpha^2}{2m} \tag{10}$$

where m is the mass of the nucleon and

$$\vec{p}_\alpha = -i\hbar\vec{\nabla}_{r_\alpha} \tag{11}$$

We will assume $\hbar = 1$.

The target center of mass (cm) coordinate is given by

$$\vec{R}_T = \sum_{\alpha} \vec{r}_{\alpha} \tag{12}$$

with the relative vectors defined as

$$\vec{x}_{\alpha} = \vec{R}_T - \vec{r}_{\alpha} \tag{13}$$

The target momentum is given by

$$\vec{P}_T = \sum_{\alpha} \vec{p}_{\alpha} \tag{14}$$

and the constituent momenta relative to the target center of mass are

$$\vec{k}_{\alpha} = \frac{1}{A_T}\vec{P}_T - \vec{p}_{\alpha} \tag{15}$$

Equations (11) to (15) can also be written for the projectile nucleus. The projectile and the target Hamiltonians are now written as

$$H_P = \frac{1}{2mA_P}P_P^2 + h_P \tag{16}$$

and

$$H_T = \frac{1}{2mA_T}P_T^2 + h_T \tag{17}$$

where the internal Hamiltonians, h_P and h_T, do not depend on P_P and P_T,

respectively, nor do they depend upon their canonical position variables. The overall center of mass position is

$$\vec{R}_{cm} = \frac{A_P\vec{R}_P + A_T\vec{R}_T}{A_P + A_T} \tag{18}$$

and the relative coordinate between the projectile and the target is given by (Figure 1)

$$\vec{r} = \vec{R}_P - \vec{R}_T \tag{19}$$

The overall center of mass momentum relative to the overall center of mass is

$$\vec{P} = \vec{P}_P + \vec{P}_T \tag{20}$$

and the projectile momentum relative to the overall center of mass is

$$\vec{k} = \vec{P}_P - \frac{A_P}{A_P+A_T}\vec{P} \tag{21}$$

The total Hamiltonian is now written as,

$$H = \frac{1}{2m(A_P+A_T)}P^2 + \frac{1}{2\mu_R}k^2 + h_P + h_T + V \tag{22}$$

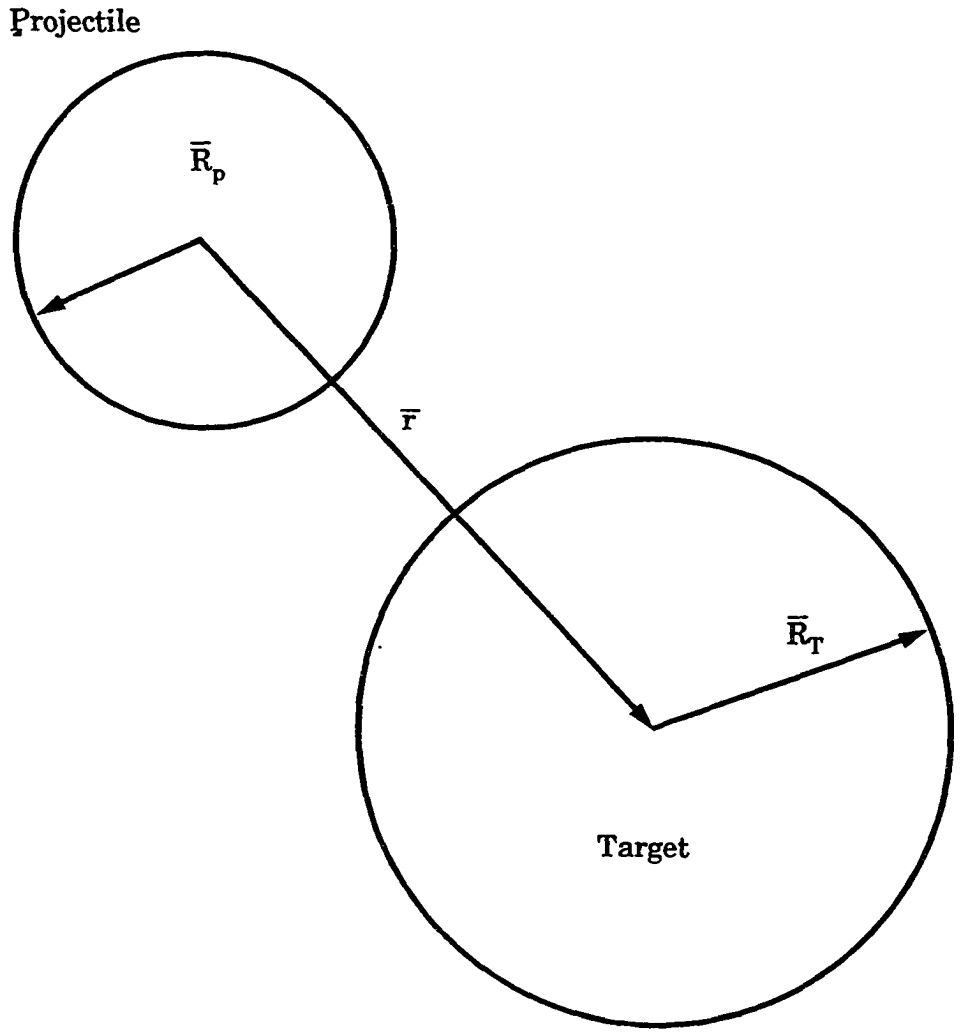

Figure 1. A schematic drawing of a nucleus-nucleus collision. A projectile with radius R_P strikes a target with radius R_T at the relative distance r.

with the reduced mass

$$\mu_R = \frac{m\, A_P A_T}{A_P + A_T} \tag{23}$$

and

$$V = \sum_{\alpha, j} V_{\alpha j}\, (\vec{x}_j - \vec{x}_\alpha + \vec{r}) \tag{24}$$

In equation (22), the over all center of mass energy is completely decoupled from the relative and internal energies as it appears only in the first term. The relative and internal energies are coupled through V. Denoting the complete set of projectile and target internal coordinates by ξ_P and ξ_T, respectively, the internal projectile and target wave functions $g_P(\xi_P)$ and $g_T(\xi_T)$ satisfy

$$h_P\, g_P(\xi_P) = \varepsilon_P\, g_P(\xi_P) \tag{25}$$

and

$$h_T\, g_T(\xi_T) = \varepsilon_T\, g_T(\xi_T) \tag{26}$$

We assume that these states are orthogonal and complete such that

$$\sum_n g(\xi)\, g^*(\xi') = \delta(\xi - \xi') \tag{27}$$

The relative motion eigenfunctions are given as continuum eigenstates by

$$\frac{1}{2\mu_R} k^2 \, \phi_{\vec{k}}(\vec{r}) = \varepsilon_k \, \phi_{\vec{k}}(\vec{r}) \tag{28}$$

with

$$\phi_{\vec{k}} = (2\pi)^{-3/2} \, e^{i\vec{k}.\vec{r}} \tag{29}$$

The corresponding closure relation is

$$\int \phi_{\vec{k}}(\vec{r}) \, \phi^*_{\vec{k}}(\vec{r}') \, dk = \delta(\vec{r}-\vec{r}') \tag{30}$$

Similarly, for the center of mass motion we have

$$\frac{1}{2m(A_P+A_T)} P^2 \, \phi_{cm}(\vec{R}_{cm}) = \epsilon_{cm} \, \phi_{cm}(\vec{R}_{cm}) \tag{31}$$

where

$$\phi_{cm} = (2\pi)^{-3/2} \, e^{i\vec{P}.\,\vec{R}_{cm}} \tag{32}$$

The interaction potential is assumed to be short-range. We assume that well-defined states of momenta are prepared in the entering state such that outside the interaction range these states are eigenstates of the free projectile target Hamiltonian given by

$$(H_P + H_T) \, \Phi = E \, \Phi \tag{33}$$

with

$$\Phi(\vec{r}, \vec{R}_{cm}, \xi_P, \xi_T) = \phi_k(\vec{r})\ \phi_{cm}(\vec{R}_{cm})\ g_P(\xi_P)\ g_T(\xi_T) \qquad (34)$$

and

$$E = \varepsilon_k + \varepsilon_{cm} + \varepsilon_P + \varepsilon_T \qquad (35)$$

Since the center of mass energy is decoupled, the quantity E - ε_{cm} will be conserved. The relative energy may change if the projectile or target eigenstates are altered in the collision.

2.3 Multiple Scattering Theory

In high-energy nucleus-nucleus scattering, many nucleons can interact mutually and the structure of multiple scattering is richer than nucleon-nucleus scattering. A simple picture of nucleus-nucleus scattering is to view the scattering in terms of each constituent of the projectile nucleus interacting with each constituent of the target nucleus. There may be other terms contributing to the scattering, such as a projectile constituent interacting consecutively with two different constituents of the target, i.e., double scattering. Similarly, there may be contributions to the scattering from interactions with other constituents of the target. The formalism describing this picture is called multiple scattering theory.

The nucleus-nucleus scattering processes are conveniently analyzed by

employing optical potential theory. Once the optical potential is determined, the original many-body scattering problem reduces to a two-body scattering problem. However, the price of reducing a many-body problem to a two-body situation is that the optical potential will be a complicated non-local, complex operator. Thus, for practical applications we shall require an approximation to determine the optical potential. An early exploitation of the optical model ideas in nuclear physics was made by Ostrofsky, Breit, and Johnson [42] in the study of alpha-decay of nuclei. Bethe [43] introduced the idea of an optical potential to describe low energy nuclear reactions within the compound nucleus model. The description of high energy nuclear collisions by means of the optical model formalism was initiated by Fernback, Serber, and Taylor [44] who first tried to describe elastic nucleon-nucleus scattering in terms of nucleon-nucleon collisions. They argued that, at high energies, a nuclear collision should proceed by way of collisions with individual target nucleons thus allowing the use of the known nucleon-nucleon cross sections. This multiple scattering analysis led to the conclusion that particles should move almost freely through nuclear matter at high energies. The fact that the optical potential is complex is worth noting. The imaginary part of the optical potential corresponds to absorption of the incident beam by target nuclei, and the real part of the optical potential corresponds to refraction of the beam without any disturbance to the target nuclei. Watson [30], and Kerman, McManus, and Thaler (KMT) [29] developed the formal theory of scattering of high energy nucleons by nuclei

in terms of the nucleon-nucleon scattering amplitude.

The full wave function satisfies

$$H\,\Psi = E\,\Psi \tag{36}$$

As we see from equation (6), equation (36) is an inhomogeneous equation. The solution of equation (36) can be written as a sum of the general solution of the homogeneous part and its particular solution. So, by making potential V = 0 we can make the projectile free and the resulting solution from the homogeneous equation will be given by equation (34).

Next, the particular solution of the inhomogeneous equation (36) can be written in terms of the Green's function G_0. The Green's function connects the incoming wave to the outgoing wave. The total solution of the inhomogeneous equation (36) can be written as

$$\Psi = \Phi + VG_0\Psi \tag{37}$$

where the Green's function G_0 is given by,

$$(E - H_P - H_T + i\eta)\,G_0 = 1 \tag{38}$$

The above equation (37) is known as the Lippmann-Schwinger equation. The first term (a plane wave) corresponds to zero potential, which implies no scattering. The second term describes the scattering of the projectile constituents by the target constituents. The transition operator T, which

transforms the plane wave into a scattered wave, is defined as

$$V|\Psi> = T|\Phi> \tag{39}$$

The reaction matrix R, which transforms the plane wave into a standing wave, is defined as

$$V|\Psi^S> = R|\Phi> \tag{40}$$

where Ψ^S denotes the standing wave. The relation between reaction matrix R and transition operator T is given by the Heitler integral equation [37]

$$R = T + i\pi T\,\delta(E - H_P - H_T)R \tag{41}$$

The transition probability for the system is given by the matrix element

$$T_{fi} = <\Phi|V|\Psi> \tag{42}$$

We can write the Lippmann-Schwinger equation for a transition operator as

$$T = V + VG_0T \tag{43}$$

The many-body Lippmann-Schwinger equation (43) for the nucleus-nucleus scattering can be written as

$$T = \sum_{\alpha, j} V_{\alpha j} + \sum_{\alpha, j} V_{\alpha j} G_0 T \tag{44}$$

From which we define

$$T_{\alpha j} = V_{\alpha j} + V_{\alpha j} G_0 T \tag{45}$$

Systematic iteration yields

$$T_{\alpha j} = V_{\alpha j} + V_{\alpha j} G_0 \sum_{\beta, j} V_{\beta j} + \ldots\ldots \tag{46}$$

The first term in the above equation (46) pertains to single scattering. The second term contains the multiple scattering terms. Separating the higher order terms, we can write

$$T_{\alpha j} = V_{\alpha j} + V_{\alpha j} G_0 V_{\alpha j} + \ldots. + V_{\alpha j} G_0 \sum_{\beta, j} V_{\beta j} \tag{47}$$

i.e.,

$$T_{\alpha j} = t_{\alpha j} + V_{\alpha j} G_0 \sum_{\beta, j} V_{\beta j} \tag{48}$$

where $t_{\alpha j}$ is defined as

$$t_{\alpha j} = V_{\alpha j} + V_{\alpha j} G_0 t_{\alpha j} \tag{49}$$

We see that $t_{\alpha j}$ describes the interaction between the projectile nucleon j and the target nucleon α. We see from equation (49) that if a projectile nucleon is scattered after one collision, it will miss all the other target nucleons. This approximation is called the single scattering approximation to the transition amplitude.

The KMT method of obtaining the optical potential is described in the next section. This method takes advantage of equation (49) to describe the optical potential in terms of the free nucleon-nucleon t-matrix $t^F_{\alpha j}$. The quantity $t^F_{\alpha j}$ has the following form:

$$t^F_{\alpha j} = V_{\alpha j} + V_{\alpha j}\, g_0\, t^F_{\alpha j} \tag{50}$$

where g_0 is the two-body Green's function

$$(E_{ON} - h + i\eta)\, g_0 = 1 \tag{51}$$

and h is the unperturbed hamiltonian (kinetic energy) of the nucleon-nucleon system. One can see from equation (49) that

$$V_{\alpha j} = \frac{t_{\alpha j}}{1 + G_0\, t_{\alpha j}} \tag{52}$$

From equations (50) and (52), we can derive the following relation between $t_{\alpha j}$ and $t^F_{\alpha j}$:

$$t_{\alpha j} = t^F_{\alpha j} + t^F_{\alpha j}\, (G_0 - g_0)\, t_{\alpha j} \tag{53}$$

We see that $t_{\alpha j}$ given by equation (49) does not have a two-body form since H_P and H_T are present in the propagator G_0. Thus, the motion of target and projectile nucleons is governed by their interactions with other projectile and target nucleons. Let us assume the energy of the projectile to be very large compared to h_P and h_T. Thus, in this approximation, we can replace the

operator $t_{\alpha j}$ by the free two-body transition amplitude $t^F_{\alpha j}$. This approximation is known as the impulse approximation. In the impulse approximation the target and projectile nucleons interact as if they were free particles. In this approximation we neglect the effect of the nuclear medium on the heavy-ion collision. The correlation effects come from the Pauli principle and the nuclear binding energy [28]. These corrections are important if the projectile energy is less then about 200 MeV. We will return to these effects in section 3.4 when we discuss the in-medium optical potential. Thus, from the above equation (53) we see that the impulse approximation is accurate if the difference between G_0 and g_0 is small. Thus, we can write $t_{\alpha j} \approx t^F_{\alpha j}$.

2.4 Eikonal Approximation

To describe the Eikonal approximation, it is useful to say a few words about the two other approximation methods that are widely used in applications to high energy problems. The first method we will mention is the Born series, which is simply the perturbative expansion of the scattering amplitude in powers of the scattering potential. That is, for a potential V(r) which is not too strong, the Lippmann-Schwinger equation may be solved by iteration, starting with a plane wave as the zero order approximation. The Born series for the wave function may then be substituted in the expression for scattering amplitude to obtain the Born series expression for the scattering amplitude. Very wide applications to scattering problems have been made of

the first term of the expansion. Its simplicity is often felt to compensate for all it may lack in accuracy. Unfortunately, the error retaining only the first term is substantial in nuclear collisions and it may be difficult to calculate the second and higher terms in the Born series. The rate at which the Born series converges depends on the strength of the potential V and the length of time the particle spends within the potential. Thus, for rapid convergence of the series the particle should spend less time within the interaction region. That is a weak potential or very high projectile energy is needed for rapid convergence. Unfortunately, these conditions are rarely fulfilled in nuclear collisions.

Another approximation, the W. K. B. method, corresponds to the classical limit of quantum mechanics. We assume the potential to be smooth enough that the distance over which it changes its value appreciably is large compared to the wave length (ka >>1 where k is wave number and a is the range of the potential). Now, if the kinetic energy of the particle is large enough, the scattering will be heavily concentrated at a small angle. This implies from the Heisenberg uncertainty principle that the scattering through a sufficiently small angle is never classical. We note that for classical scattering strong coupling is required. This is in contrast to the Born approximation, which requires the potential to be weak. Thus, the region of applicability of the W. K. B. method does not overlap with that of the Born approximation at all.

Semi-classical methods are useful approximation techniques when the variation of potential is not very large over a distance of the order of the de Broglie wavelength ($\lambda = h/p$) of the incident particle. This wave length is assumed to be small such that $ka >> 1$, where a is the range of the potential (short wave length condition). Furthermore, in contrast to the Born approximation, the strength V_0 of the scattering potential V does not have to be very weak if the inequality $E/V_0 >> 1$ is satisfied. These approximations embody what is known as the Eikonal approximation.

The Eikonal approximation [37] was originally introduced in quantum scattering theory by Moliere [45] and was considerably developed by Glauber [41] who proposed a many body generalization of the method. Let us consider high energy scattering (i.e., projectile scattered by a force center) such that $ka>>1$ and $\mid V_0 \mid /E<<1$, where V_0 is the strength of the potential. We start from the Lippmann-Schwinger equation

$$\Psi_{k_i}(\vec{r}) = \phi_{k_i}(\vec{r}) + \int G_0(\vec{r}, \vec{r}') \, u(\vec{r}') \, \Psi_{k_i}(\vec{r}') \, d\vec{r}' \qquad (54)$$

where u (r') is the reduced potential is defined as

$$u(\vec{r}') = \frac{2m \, v(\vec{r}')}{\hbar} \qquad (55)$$

the Green's function G_0 is given by the equation

$$G_0(\vec{r}, \vec{r}') = -(2\pi)^{3/2}\int \frac{e^{i\vec{k}.(\vec{r} - \vec{r}')}\, d\vec{k}'}{k'^2 - k_i^2 - i\eta} \tag{56}$$

and $\mathbf{k}_i$ is the incident wave vector.

We next write the wave function $\Psi_{ki}(\mathbf{r})$ as a product of a plane wave and another unknown function $\Phi(\mathbf{r})$

$$\Psi_{k_i}(\vec{r}) = (2\pi)^{-3/2} e^{i\vec{k}_i.\vec{r}}\ \Phi(\vec{r}) \tag{57}$$

The function $\Phi(\mathbf{r})$ used here is not to be confused with Φ used in equation (34). Substituting the above equation (57) into the Lippmann-Schwinger equation (54), we find that the function $\Phi(\mathbf{r})$ satisfies

$$\Phi(\vec{r}) = 1 - (2\pi)^{-3}\int d\vec{R} \int \frac{e^{i(\vec{k}' - \vec{k}_i).\vec{R}}\ u(\vec{r} - \vec{R})\ \Phi(\vec{r} - \vec{R})\ d\vec{k}'}{k'^2 - k_i^2 - i\eta} \tag{58}$$

where

$$\vec{R} = \vec{r} - \vec{r}' \tag{59}$$

The above equation (58) is still exact in the sense that no approximations are yet made. The momentum transfer is

$$\vec{q} = \vec{k}' - \vec{k}_i \tag{60}$$

and the wave vector $\mathbf{k}'$ defines the final wave vector after scattering has

taken place. If $\mathbf{k}'$ is close to the initial wave vector $\mathbf{k}_i$, $\mathbf{q}$ is a very small quantity. It would be convenient to apply the approximation which we have previously discussed. Basically, we will assume that $q/k_i << 1$. We choose the Z - axis in the direction of the incident wave vector $\mathbf{k}_i$. The integral over q_Z is done in the complex q_Z plane, where the integrand has a pole at $q_Z = i\eta$. For $Z > 0$ we choose the integration contour in the upper half plane and then apply Cauchy's theorem. In the lower half plane the integration value is zero since the value of the residue is zero. Thus, we can write equation (58) as

$$\Phi(x, y, z) = 1 - \frac{i}{2k_i}\int u(x, y, z-Z)\ \Phi(x, y, z-Z)\ dZ \qquad (61)$$

from which one obtains

$$\Phi(x, y, z) = e^{-\frac{i}{2k_i}\int_0^z u(x, y, z')\ dz'} \qquad (62)$$

One can see from equation (62) that $\Phi(x, y, z)$ is a negligibly varying function over distances of order $1/k_i$ because u/k_i^2 is very small. Using equation (62), we get from (57) the so called Eikonal wave function:

$$\Psi_E(x, y, z) = (2\pi)^{-3/2}\ e^{[i\vec{k}_i\cdot\vec{r} - \frac{i}{2k_i}\int_0^z u(x, y, z')\ dz']} \qquad (63)$$

We notice that only in the region where the potential is non zero does the modulating function $\Phi(\mathbf{r})$ modify the incident plane wave. Next, since the Eikonal wave function was obtained by performing the integration along the direction of incident wave vector i.e. Z-axis, we can say that the Eikonal method is used for small angle collisions. This makes sense because at high incident energy forward scattering dominates.

The scattering amplitude in the integral representation is

$$f = -\frac{(2\pi)^{2/3}}{4\pi}\int e^{-i\vec{k}_f \cdot \vec{r}'} u(\vec{r}')\ \psi_{k_i}(\vec{r}')\ d\vec{r}' \qquad (64)$$

Thus, we can write the Eikonal scattering amplitude from equations (63) and (64) as

$$f_E(\vec{q}) = -\frac{1}{4\pi}\int d\vec{r}\ e^{i\vec{q}.\vec{r}}\ u(\vec{r}) e^{-\frac{i}{2k_i}\int u(x, y, z')\, dz'} \qquad (65)$$

where $\mathbf{q}$ is the wave vector transfer. To evaluate the Eikonal scattering amplitude, we adopt a cylindrical coordinate system and decompose the $\mathbf{r}$ vector. A further small-angle approximation is now made by assuming the longitudinal momentum to be small such that

$$\vec{q}.\vec{r} = \vec{q}.\vec{b} + O(\theta^2) \qquad (66)$$

where $\mathbf{b}$ is the impact parameter and θ is the scattering angle. We can now

integrate (65) over z' yielding

$$f_E(\vec{q}) = \frac{k}{2\pi i}\int d^2\vec{b}\; e^{i\vec{q}.\vec{b}}\; (e^{i\chi(k_i,\,\vec{b})} - 1) \qquad (67)$$

where the Eikonal phase shift is defined by

$$\chi(k_i,\,\vec{b}) = -\frac{1}{2k_i}\int_{-\infty}^{\infty} u(\vec{b},\,z)\; dz \qquad (68)$$

Equation (67) gives the scattering amplitude for the system and is the main result of the Eikonal model. The scattering amplitude $f_E(q)$ is expressed in terms of an exponential function of phase shift. In deriving equation (67), we had assumed that the incident direction is along the Z-axis. We have also assumed for our convenience a cylindrical coordinate system. The scattering angle of the projectile is assumed to be small and incident energy $E>>V_0$ under the Eikonal approximation.

The generalization of the Eikonal approximation to a many body scattering problem is given by Glauber [46, 47] who applied it extensively to high-energy hadron-nucleus scattering. Wilson [35] has discussed the Eikonal approximation for a nucleus-nucleus optical model using a coupled channels formalism. In the Eikonal coupled channel (ECC) model [35, 38], the scattering amplitude is written in matrix form. The scattering amplitude matrix for all

possible projectile-target transitions is given by [35, 38]

$$\bar{f}(\vec{q}) = \frac{-ik}{2\pi}\hat{Z}\int e^{i\vec{q}.\vec{b}}\,[e^{i\bar{\chi}(\vec{b})} - \bar{1}]\,d^2b \qquad (69)$$

The matrix elements of χ are written as

$$<nm|\bar{\chi}(\vec{b})|n'm'> = \frac{1}{2\pi k_{NN}}\sum_{\alpha,j}\int d^2q\; e^{i\vec{q}.\vec{b}}\,F_{nn'}(-q)\,G_{mm'}(q)\,f_{NN}(q) \qquad (70)$$

where nm and n'm' are the initial and final states of the target and the projectile, F and G are the projectile and target form factors, f_{NN} is the two-body scattering amplitude, and k_{NN} is the relative momenta between the target and the projectile in the NN frame. The quantity k_{NN} is defined as

$$k_{NN} = \left[\frac{A_P + A_T}{A_P\,A_T}\right] k \qquad (71)$$

where k is given in equation (21).

A first order approximation to the elastic amplitude is obtained by neglecting all transitions between the ground and excited states. The χ is then diagonal and elastic scattering determined by [35, 38]

$$\chi(\vec{b}) = \frac{A_P A_T}{2\pi k_{NN}}\int d^2q\; e^{i\vec{q}.\vec{b}}\,F_P(-q)\,G_T(q)\,f_{NN}(q) \qquad (72)$$

where F_P and F_T are the projectile and target form factors respectively.

The Eikonal approximation satisfies the optical theorem in the high energy limit. The total cross section given by the optical theorem for the forward scattering amplitude is:

$$\sigma_{tot} = \frac{4\pi}{k} Im\ (f_E\ (\theta=0)\ ) \tag{73}$$

Let us consider a complex potential having azimuthal symmetry. Then, using equations (67) and (73) the total cross section can be written as

$$\sigma_{tot} = 4\pi \int_0^\infty b\ db\ [1-e^{(-Im\ \chi)}\ \cos(Re\ \chi)] \tag{74}$$

where Im and Re are imaginary and real quantities, respectively. The total elastic cross section can be found to be

$$\sigma_{tot}^{el} = 4\pi \int_0^\infty b\ db\ [1-e^{-Im(\chi)}\ \cos(Re(\chi))] - 2\pi \int_0^\infty b\ db\ [1-e^{-2Im(\chi)}] \tag{75}$$

The total absorption cross section is found by subtracting the total elastic scattering cross section equation (75) from equation (74) as

$$\sigma_{abs} = 2\pi \int_0^\infty b\, db\, [1 - e^{-2\, Im(\chi)}] \qquad (76)$$

We use equation (72) to calculate the quantity χ in the optical limit. The total and absorption cross sections under the Eikonal approximation can be calculated using equations (74) and (76).

Chapter 3

Generalized KMT Model and First Order Optical Potential for Multiple Scattering

3.1 Introduction

Heavy-ion elastic and inelastic scattering calculations represent an important subject in cosmic ray studies. In the optical potential approach, the many-body problem for scattering of a projectile by a target can be reduced to a two-body problem through an effective interaction potential called the optical potential. Therefore, the main task of microscopic calculations is to describe the two-body nucleon interactions in terms of the fundamental information about the two nucleon system. As discussed previously, in the multiple scattering approach, the two-body interaction is introduced via the t-matrix which is the solution to the problem of scattering of two nucleons. The optical potential is a complex potential in which the imaginary part describes the absorption in nuclear reactions. The systematic study of the first order optical potential has been done by several authors [31-34, 48-52]. The purpose of this chapter is to develop a first order optical potential for heavy-ion collisions based on multiple scattering theory.

The optical potential is a useful theoretical tool in the analysis of heavy-ion collisions. Usually for a nucleus, it is parameterized by a complex Woods-Saxon or harmonic oscillator potential. The elastic scattering is often found to

be fairly insensitive to the detailed interior shape. The theoretical derivation of the optical potential for a nucleon-nucleus system has been attempted in several ways by various authors [31-34, 48-52]. The simplest way may be the double folding model, where the effective nucleon-nucleon (NN) interactions are folded over the density distributions of projectile and target [31-34]. In order to reproduce the energy dependence of the optical potential, however, the strength of the effective interaction has to be renormalized. This suggests that for a many-body problem the Pauli principle has to be considered [53-56]. In the case of nucleon-nucleus scattering, modification of the effective interaction by the presence of the nuclear medium has been taken into account explicitly by solving the Bethe-Goldstone equation in nuclear matter, by several authors [57-59]. Many-body effects may be expected to be even more important in heavy-ion collisions. We will also treat the medium modified optical potential in this chapter. For high energy collisions, anti-symmeterization between projectile and target constituents is neglected.

3.2 First order Optical Potential

To define the optical potential, the projection operator technique of Feshbach [60] may be used. The projection operators P and Q project on and off channels of interest. To define our optical potential for heavy-ion collision, we first define a projection operator P_{0P} for the projectile, which projects on the projectile ground state and P_{0T} for the target which projects on the target

ground states. Let Q_{0P} be a projection operator, which projects onto the complimentary space of the projectile excited states. Let Q_{0T} be a projection operator, which projects onto the complementary space of the target excited states. Thus, we can write

$$P_{0P} + Q_{0P} = 1 \tag{77}$$

and

$$P_{0T} + Q_{0T} = 1 \tag{78}$$

Let ϕ_{0P} and ϕ_{0T} be the projectile and target ground state wave functions. For elastic scattering, both the initial and final states for target and projectile are ground states. Thus, we can write

$$\langle\psi|T|\Phi\rangle = \langle\psi|P_{0P}P_{0T}\ T\ P_{0P}P_{0T}|\Phi\rangle \tag{79}$$

Now we can express G_0 using equations (77) and (78) as

$$G_0 = (P_{0P}\ P_{0T} + Q_{0P}\ Q_{0T} + P_{0P}\ Q_{0T} + Q_{0P}\ P_{0T})\ G_0 \tag{80}$$

Using the above result we can write equation (43) as

$$T = V + V\ (P_{0P}P_{0T}+Q_{0P}Q_{0T}+P_{0P}Q_{0T}+P_{0T}Q_{0P})\ G_0\ T \tag{81}$$

which can be rewritten as

$$(1-V\,(Q_{0P}Q_{0T}+P_{0P}Q_{0T}+Q_{0P}P_{0T})\,G_0)\;T = V + VP_{0P}P_{0T}G_0T \quad (82)$$

or

$$T = U + U\,P_{0P}\,P_{0T}\,G_0T \quad (83)$$

We have used the fact that P_{0P} and P_{0T} commute with G_0 and we have defined the optical potential operator U as

$$U = (1 - V\,(Q_{0P}\,Q_{0T}+P_{0P}Q_{0T}+Q_{0P}P_{0T})\,G_0)^{-1}V \quad (84)$$

To get the microscopic content of the optical potential, we rearrange equation (84), and get

$$U = V + V\,G_0\,(Q_{0P}\,Q_{0T} + P_{0P}\,Q_{0T} + Q_{0P}P_{0T})\,U \quad (85)$$

where the presence of Q_{0P} and Q_{0T} in the above equation (85) indicates the excitation (of the projectile or target or of both) in the reaction processes describing U. We can write U as $\Sigma\, U_{\alpha j}$ and rewrite equation (85) as

$$U_{\alpha j} = V_{\alpha j} + V_{\alpha j}G_0\,(Q_{0P}Q_{0T}+P_{0P}Q_{0T}+Q_{0P}P_{0T})\sum_{\beta,\,j} U_{\beta j} \quad (86)$$

Following Watson [30], we define an operator $\tau_{\alpha j}$ as

$$\tau_{\alpha j} = V_{\alpha j} + V_{\alpha j} G_0 (Q_{0P} Q_{0T} + P_{0P} Q_{0T} + Q_{0P} P_{0T}) \tau_{\alpha j} \qquad (87)$$

and write equation (86) as

$$U_{\alpha j} = \tau_{\alpha j} + \tau_{\alpha j} G_0 \, (Q_{0P} Q_{0T} + P_{0P} Q_{0T} + Q_{0P} P_{0T}) \sum_{\beta \neq \alpha, j} U_{\beta j} \qquad (88)$$

Thus, we can obtain the Watson multiple scattering series for the optical potential as

$$U = \sum_{\alpha, j} \tau_{\alpha j} + \sum_{\beta \neq \alpha, j} \tau_{\beta j} G_0 \, (Q_{0P} Q_{0T} + P_{0P} Q_{0T} + Q_{0P} P_{0T}) \, \tau_{\beta j} + .. \qquad (89)$$

In the first order approximation to the optical potential, we take the first term of equation (89). Using equations (49) and (87), the relation between $t_{\alpha j}$ and $\tau_{\alpha j}$ can be written as

$$\tau_{\alpha j} = t_{\alpha j} - t_{\alpha j} G_0 P_{0P} P_{0T} \tau_{\alpha j} \qquad (90)$$

We will also employ the anti-symmetry in the target and projectile, so we can write

$$\langle \phi_{0P} \phi_{0T} | \sum_{\alpha, j} \tau_{\alpha j} | \phi_{0P} \phi_{0T} \rangle = \langle \phi_{0P} \phi_{0T} | A_P A_T \tau | \phi_{op} \phi_{0T} \rangle \qquad (91)$$

Thus, we get the transition amplitude due to first order optical potential as

$$T = A_P A_T \tau (1 + P_{0P} P_{0T} G_0 T) \tag{92}$$

Substituting τ in terms of t we get

$$T = A_P A_T t \ (1 - P_{0P} P_{0T} G_0 \tau) \ (1 + P_{0P} P_{0T} G_0 T) \tag{93}$$

or

$$T = A_P A_T t + (A_P A_T - 1) \ t P_{0P} P_{0T} G_0 T \tag{94}$$

We can write equation (94) as

$$T' = U' + U' P_{0P} P_{0T} G_0 T' \tag{95}$$

where

$$T' = \frac{A_P A_T - 1}{A_P A_T} \ T \tag{96}$$

and

$$U' = (A_P A_T - 1) \ t \tag{97}$$

where

$$t = \sum_{\alpha, j} t_{\alpha j} \tag{98}$$

Equation (97) is the result for the first order optical potential for nucleus-nucleus scattering. Equation (97) is known as the scaled optical potential. In deriving the above relation, we took the approach of KMT. The advantage of the KMT approach is that the many-body operator T is approximated by the two-body transition amplitude t. On the other hand, the Watson multiple scattering quantity τ given in equation (87) has terms Q_{0P} and Q_{0T}, which allow only intermediate states in which the target and projectile nucleons are excited. Thus, in nuclear matter one requires the intermediate momenta of the target and the projectile to be greater than the fermi momentum. This raises the difficulty of handling the anti-symmetry.

3.3 Model Calculation for the First Order Optical Potential

In the first-order optical model in the impulse approximation, the optical potential is the matrix element of the free two-body amplitude over target and projectile ground states. Thus

$$\langle f|U|i\rangle = \frac{A_P A_T - 1}{A_P A_T} \langle O_P O_T | \sum_{\alpha, j} t_{\alpha j} | O_P O_T \rangle \tag{99}$$

At this point, we digress to discuss $t_{\alpha j}$ and recall that the optical potential has a spin dependence that arises from the spin dependence of the t - matrix. From symmetry principles, one can write the non-relativistic t-matrix for nucleon-nucleon scattering in terms of Pauli spin operators as [61]

$$t = A + C(\vec{\sigma}_1+\vec{\sigma}_2).\vec{n} + M\vec{\sigma}_1.\vec{m}\vec{\sigma}_2.\vec{m} + G\vec{\sigma}_1.\vec{n}\vec{\sigma}_2.\vec{n} + H\vec{\sigma}_1.\vec{l}\vec{\sigma}_2.\vec{l} + D(\vec{\sigma}_1.\vec{m}\vec{\sigma}_2.\vec{l} + \vec{\sigma}_1.\vec{l}\vec{\sigma}_2.\vec{m}) \quad (100)$$

where σ is the Pauli spin operator and **l**, **m**, and **n** define a right-hand coordinate system. The quantities A, M, G, H, and D are functions of q and beam energy.

If we consider only spin zero nuclei, and the spin projection of the target and projectile nucleus is integrated out, the terms of t that are linear in the projectile and target nucleon spin vanish. Thus, only the first term A is left in equation (100). Therefore, we write

$$A(q) = \frac{-\hbar^2}{(2\pi)^2\mu} f_{NN}(q) \quad (101)$$

We fold the optical potential [31-34] over initial and final states and write it in terms of target and projectile form factors. Thus, we get the optical potential

in equation (99) for spin-zero spin-zero, nucleus-nucleus scattering as

$$\langle f|U|i\rangle = \frac{A_P A_T - 1}{A_P A_T}\int d\vec{q}\; e^{i\vec{q}.\vec{r}}\; A(q)\; F_P(q)\; G_T(q) \qquad (102)$$

where F_P is the projectile form factor and G_T is the target form factor. The two-body scattering amplitude in equation (101) is parameterized as

$$f_{NN}(q) = \frac{\sigma(\alpha + i)}{4\pi}\; k_{NN}\; e^{\frac{-Bq^2}{2}} \qquad (103)$$

where σ is the nucleon-nucleon total cross section, α the ratio of the real part to the imaginary part of the forward two-body amplitude and B the slope parameter. The quantity k_{NN} is the relative momentum between particles α and j in the NN frame. The values of σ, α and B are taken as iso-spin averaged values:

$$\sigma = \frac{Z_P Z_T + N_P N_T}{A_P\, A_T}\; \sigma_{pp} + \frac{Z_P N_P + Z_P N_T}{A_P\, A_T}\; \sigma_{np} \qquad (104)$$

$$B = \frac{Z_P Z_T + N_P N_T}{A_P\, A_T}\; B_{pp} + \frac{Z_P N_P + Z_P N_T}{A_P\, A_T}\; B_{np} \qquad (105)$$

and

$$\alpha = \frac{(Z_P + Z_T)\sigma_{pp}\ \alpha_{pp} + (N_P + N_T)\sigma_{np}\ \alpha_{np}}{(A_P + A_T)\ (\sigma_{pp} + \sigma_{np})} \qquad (106)$$

where np indicates the neutron-proton and pp indicates the proton-proton quantities. There are substantial differences between pp and np total cross sections. This implies that one should carefully distinguish between pp and np scattering when applying NN cross sections in heavy-ion collisions. The one body form factor is written in terms of the charge form factor $F_{ch}(q)$ as

$$F(q) = \frac{F_{CH}(q)}{F_p(q)} \qquad (107)$$

where $F_p(q)$ is the proton form factor. For light nuclei ($A < 16$), we used the harmonic well distribution

$$F_{CH} = (1 - sq^2)\ e^{-aq^2} \qquad (108)$$

where values of the parameters s and a are given in reference [20]. For medium and heavy mass nuclei ($A \geq 17$) where the Woods-Saxon density is

appropriate, we have from reference [62]:

$$\rho_{CH}(r) = \frac{\rho_0}{1 - e^{(\frac{r - R}{c})}} \tag{109}$$

where ρ_0 is the normalization constant. The Fourier transform of equation (109) gives the charge form factor as

$$F_{CH}(q) = \frac{4\pi}{q} \rho_0 \phi(q) \tag{110}$$

where

$$\phi(q) = \pi R c \left[\frac{-\cos(Rq)}{\sinh(\pi cq)} + \frac{\pi c}{R} \frac{\sin(Rq) \coth(\pi cq)}{\sinh(\pi cq)} - \frac{2C}{\pi R} \sum_{m=1}^{\infty} (-1)^m \frac{mCq\, e^{-(\frac{mR}{c})}}{[(Cq)^2 + m^2]^2} \right] \tag{111}$$

The series in equation (111) converges rapidly, and the first three or four terms are accurate for most applications. Values for the parameters c and R are taken from reference [20].

We use equation (107) to calculate the projectile and target form factors. The two-body scattering amplitude is calculated from equation (103). Once we know the two-body scattering amplitude and form factors, the desired optical potential is calculated using equation (102).

3.4 Medium-Modified Optical Potential

For many years various authors have studied the microscopic optical potential for the nucleon-nucleus scattering system [31-34]. There are several correlation effects to be taken into account for the medium modified optical potential [28]. It is well known that in-medium nucleon-nucleon (NN) scattering differs from bare NN (i.e. when the effect of the nuclear medium is neglected) scattering at intermediate energies. This is mainly due to correlation effects such as Pauli blocking of the intermediate and final states and nuclear binding effects [53-56]. In conjunction with the nucleus-nucleus collision, Faessler and co-workers have studied in-medium NN scattering based on a non-relativistic Brueckner calculation and the Reid soft-core potential. The bare NN cross sections and the in-medium NN cross-sections have been calculated using relativistic [63-68], as well as non-relativistic [69] Brueckner theory. Recently Li and Machleidt [70, 71] have obtained the in-medium elastic NN cross sections using a microscopic nuclear matter model in an energy range from 50 to 300 A MeV. They found that the in-medium NN scattering angular distributions are very different from those of free space (i.e. the bare NN cross sections). This suggests that the in-medium NN scattering cross section must be used in the optical model nucleus-nucleus scattering for energy below 300 A MeV.

Our aim in this thesis is to calculate the total cross sections for the nucleus-nucleus collisions in which the NN cross sections are important inputs.

The aim of the present section is to assess the manifestation of many-body effects in the total cross section calculations for heavy-ion collisions. As discussed above, there are several ways of introducing the in-medium effects in the case of heavy-ion collisions. We adopt a simple method where, to calculate the medium modified two-body scattering amplitude, we make use of the medium modified energy dependent two-body NN cross sections given in reference [70, 71]. The medium modified two-body scattering amplitude is used as an input for the optical potential. We use the resulting optical potential to solve the Lippmann-Schwinger equation in momentum space. We will investigate the effects that the use of the in-medium NN cross sections will have on the absorption cross sections in the energy range of 18-83 A MeV in a later chapter.

Several authors have calculated the medium modified optical potential [53-56]. Usually, one introduces the Pauli blocked final momentum $k > K_F$ (Fermi momentum) in the two-body Green's function g_0. This method requires a lot of computational time and many partial waves in the case of heavy-ion collisions. Therefore, in our calculations, we introduced a simple method in which we incorporated the in-medium NN cross sections given in reference [70, 71] in the two-body scattering amplitude.

3.5 Model Calculations for Medium Modified Optical Potential

From equation (103) we see that in the calculation of the medium modified optical potential, the effect of the quantity α on the reaction cross sections is small, since the major contribution comes from the imaginary part of the optical potential. We also note that in the Eikonal approximation, the reaction cross sections are independent of the parameter α (in equation 103). The slope parameter B (in equation 103) has been calculated by taking into account the medium effects for low energies (<200 MeV/nucleon), where the interaction is nearly isotropic [70]. Our analysis shows that the values of B do not significantly differ from the free space values (values based on the first order optical potential). As a test, using these two sets of values did not have an appreciable effect in the calculations performed as part of this thesis. Since reference [70] does not have values of B for the energies of our interest, we have used free space values for these energies.

As discussed earlier Li and Machleidt [70, 71] have derived the in-medium elastic NN cross sections using a microscopic nuclear matter model in the energy range from 50 to 300 MeV/nucleon. They found that there is strong density dependence in the in-medium cross sections. With increase of density, the cross sections decrease. This indicates that proper treatment of the density dependence of the in-medium NN cross sections is important. They also found that the in-medium total NN cross sections and the in-medium np-scattering angular distribution are very different from those of free space. This suggests

that in-medium NN scattering cross sections must be used in the microscopic calculations. The two-body, medium-modified, energy-dependent, proton-proton and proton-neutron total cross sections given by Li and Machleidt [70, 71] can be written as

$$\sigma_{pp}(E, \rho) = [23.5 + 0.00256(18.2 - E^{0.5})^{4.0}] * [\frac{1.0 + 0.1667\ e^{1.05\rho^3}}{1.0 + 9.704\ \rho^{1.2}}] \quad (112)$$

$$\sigma_{np}(E, \rho) = [31.5 + 0.092\ abs(20.2 - E^{0.53})^{2.9}] * [\frac{1.0 + 0.0034\ E^{1.51}\ \rho^2}{1.0 + 21.55\ \rho^{1.34}}] \quad (113)$$

where E is the beam energy in MeV / nucleon and ρ is the matter density in fm^{-3}. To accommodate the density dependence of equations (112) and (113) in the optical potential, one has to consider the density dependence of both the projectile and target in the folding of the NN scattering amplitude with the projectile and target densities (102). This requires excessive computational time and will be treated in future calculations. Here, we use the value of the saturation density of normal nuclear matter which from Reference [70] is 0.18 fm^{-3}. We have used this value for the quantity ρ_0 in the calculation of matter density. We will use the in-medium quantities σ_{pp} and σ_{np} of equations (112) and (113) in our calculations.

Chapter 4

Momentum Space Method and Nucleon-Nucleon Scattering

4.1 Introduction

There are several techniques for solving the Lippmann-Schwinger equation. In this part of our work, we are going to describe one of the techniques to solve the Lippmann-Schwinger equation in momentum space. In doing the calculations in co-ordinate space, the numerical solution of the Lippmann-Schwinger equation becomes complicated. The second point to note is that, in momentum space, we can do the relativistic calculations just by changing the Green's function. However, it is difficult to obtain an optical potential for solving the Lippmann-Schwinger equation [68]. In the non-relativistic case, the Lippmann-Schwinger equation can easily be solved in momentum space [27]. Hence, we take the momentum space calculation approach. The following approach was used by several authors [72, 73] for a real potential. We have extended it for the case of a complex potential. The basic equations are more or less the same as in the case of a real potential. However, modifications were made to incorporate the complex nature of the potential.

4.2 Nucleon-Nucleon Scattering

The Lippmann-Schwinger equation for the free two body transition

operator t (t -matrix) in operator form is given by equation (50) and can be rewritten as

$$t = U + U\, g_0 t \tag{114}$$

where U is the two-body interaction potential defined by equation (97) and g_0 is the free two body propagator defined by

$$(E - h + i\eta)\, g_0 = 1 \tag{115}$$

where h is the unperturbed Hamiltonian (kinetic energy) of the nucleon-nucleon system. We want to work in the center of mass (CM) momentum space. If $\mathbf{k}_1$ and $\mathbf{k}_2$ are the wave vectors of the two nucleons in the lab system, we define the relative wave vector $\mathbf{k}$ as

$$\vec{k} = \frac{\vec{k}_1 - \vec{k}_2}{2} \tag{116}$$

and the relative energy E_k as

$$E_k = \frac{\hbar^2 k^2}{2\mu} \tag{117}$$

where

$$\mu = \frac{m_1 m_2}{m_1 + m_2} \tag{118}$$

is the reduced mass. If we now take the on-shell matrix element of t in

equation (114) we get

$$\langle \vec{k}' | t | \vec{k} \rangle = \langle \vec{k}' | U | \vec{k} \rangle + \int \frac{\langle \vec{k}' | U | \vec{k}'' \rangle \langle \vec{k}'' | t | \vec{k} \rangle \, d\vec{k}''}{E_k - E_k'' + i\eta} \quad (119)$$

where we have taken **k** as the on-shell wave vector. Next, we define the R-matrix which satisfies

$$\langle \vec{k}' | R | \vec{k} \rangle = \langle \vec{k}' | U | \vec{k} \rangle + P \int \frac{\langle \vec{k}' | U | \vec{k}'' \rangle \langle \vec{k}'' | R | \vec{k} \rangle \, d\vec{k}''}{E_k - E_k''} \quad (120)$$

where P denotes the principle value of the integral. The R- matrix is related to the t-matrix by the Heitler equation (41). Next we do the partial wave decomposition of equation (120) and write the above equation as

$$R_l(k', k) = U_l(k', k) + \frac{2\mu}{\hbar^2} \int_0^\infty \frac{U_l(k', k'') \, R_l(k'', k) \, k''^2 dk''}{k^2 - k''^2} \quad (121)$$

where we have used the following expression for the partial wave decomposition

$$\langle \vec{k}' | R | \vec{k} \rangle = \sum_l \frac{(2l+1)}{4\pi} R_l(k', k) \, P_l(k', k) \quad (122)$$

and the P_l are the Legendre polynomials.

The on-shell t_l is related to the on-shell R_l via the Heitler equation by

$$t_l = \frac{R_l(k, k)}{1 + \frac{i\pi\mu}{\hbar^2} k R_l(k, k)} \tag{123}$$

The scattering amplitude for nucleus-nucleus scattering is related to the T-matrix through

$$f(q) = -(2\pi)^2 \frac{E_P E_T}{E_P + E_T} T(q) \tag{124}$$

where E_P and E_T are the projectile and target total energies. We can calculate T(q) from

$$T(q) = \sum_{l=0}^{\infty} \frac{(2l + 1)}{4\pi} t_l P_l(\cos\theta) \tag{125}$$

Thus, once t_l is found from equation (123) (by matrix inversion as described below), the scattering amplitude can be obtained by using equations (124) and (125). The expression for the scattering amplitude given by equation (124) requires an infinite number of partial waves for the t-matrix as seen from equation (125). However, in practice, it is usually necessary to truncate the sum to a finite number of partial waves. The result obtained is very reasonable for low energies. It is well known that, for higher partial waves and for higher energies, the Born approximation becomes accurate when $T(q) \approx U(q)$. We will

utilize this fact to our advantage in order to estimate the contribution of higher partial waves. First, we rewrite equation (125) as

$$T(q) = \sum_{l=0}^{l_{max}} \frac{2l+1}{4\pi} t_l P_l(\cos\theta) + \sum_{l_{max}+1}^{\infty} \frac{2l+1}{4\pi} t_l P_l(\cos\theta) \quad (126)$$

where $l_{max} + 1$ is the partial wave beyond which the Born approximation is valid. This can be easily done by comparing the quantity U_l and the calculated t_l for each partial wave while solving equation (123). From the Born approximation for the second term of equation (126) we obtain

$$\begin{aligned} T(q) = &\sum_{l=0}^{l_{max}} \frac{2l+}{4\pi} t_l P_l(\cos\theta) + \sum_{l_{max}+1}^{\infty} \frac{2l+1}{4\pi} U_l P_l(\cos\theta) \\ &+ \sum_{l=}^{l_{max}} \frac{2l+1}{4\pi} U_l P_l(\cos\theta) - \sum_{l=0}^{l_{max}} \frac{2l+1}{4\pi} U_l P_l(\cos\theta) \end{aligned} \quad (127)$$

where we have added and subtracted a term. Now, the second and the third terms can combine to give us the three dimensional U(q) since it is a sum of all partial waves for U. Therefore, we finally get

$$T(q) = \sum_{l=0}^{l_{max}} \frac{2l+1}{4\pi} t_l P_l(\cos\theta) - \sum_{l=0}^{l_{max}} \frac{2l+1}{4\pi} U_l P_l(\cos\theta) + U(q) \quad (128)$$

Equation (128) is the final result which tells us that in order to obtain the contributions from higher partial waves, we have to calculate t_l only up to a certain l_{max} at which the Born approximation is valid. The quantity T(q) is then obtained by summing t_l from l values varying from 0 to l_{max}. The quantity U(q) given by equation (102) is to be added. In the end, the second term in equation (128) has to be subtracted to avoid the double counting.

The phase shift δ_l is introduced through

$$t_l = -\frac{\hbar^2}{\pi\mu}\frac{e^{2i\delta_l} - 1}{2ik} \tag{129}$$

The total elastic cross section and the absorption cross section can be calculated from

$$\sigma_{el} = \frac{\pi}{k^2}\sum_{l=0}^{\infty}(2l + 1)\left|\eta_l\, e^{2iRe(\delta_l)} - 1\right|^2 \tag{130}$$

where

$$\eta_l = e^{(-2Im\delta_l)} \tag{131}$$

and

$$\sigma_{abs} = \frac{\pi}{k^2}\sum_{l=0}^{\infty}(2l + 1)\,(1 - \eta_l^2) \tag{132}$$

The total cross section is given as

$$\sigma_{tot} = \frac{2\pi}{k^2} \sum_{l=0}^{\infty} (2l + 1) \, [1 - \eta_l \cos(2Re(\delta_l))] \qquad (133)$$

In order to obtain the cross sections given in equations (130), (132), and (133) one must calculate δ_l from equation (129). The quantity t_l should be calculated from equation (123), once one knows the values of R_l. In the next section we describe the method used to calculate the quantity R_l.

4.3 Technique for Momentum Space Calculation

In this section, we describe the technique used in the calculation of the t matrix in momentum space. We decompose the integral equation (121) into two parts in such a way that the first part will have the pole at the mid point between the limits. Thus,

$$\int_0^{\infty} \frac{U_l(k', k'')R_l(k'', k) \, k''^2 dk''}{k^2 - k''^2} = \int_0^{2k} \frac{U_l(k', k'')R_l(k'', k) \, k''^2 dk''}{k^2 - k''^2} + \int_{2k}^{\infty} \frac{U_l(k', k'') \, R_l(k'', k) \, k''^2 \, dk''}{k^2 - k''^2} \qquad (134)$$

Note that the second integral in the above equation (134) does not have a pole. Since the pole is now at the mid point between the limits, we can use

the even number point Gaussian quadrature rule [74]. The Gaussian quadrature rule is

$$\int_{-1}^{+1} f(x)\, dx = \sum_{i=1}^{N} f(x_i)\, w_i \qquad (135)$$

where x_i and w_i are standard Gaussian points and weights. Therefore, we need to transform the limits of integration of (134) from -1 to +1. For the first integral with limits from 0 to 2k, we use the transformation

$$S = mx + c$$

$$S = 0 \; ; \; x = -1 \qquad 0 = -m + c \qquad (136)$$

$$S = 2k \; ; \; x = +1 \qquad 2k = m + c$$

Thus, c = k and m = k, and dS = mdx = dS = kdx. Therefore,

$$\int_{0}^{2k} f(S)\, dS = \sum_{i=1}^{N} f(S(x_i))\, k\, w_i \qquad (137)$$

Now, if we define a new weight w'_i by

$$w_i' = k\, w_i \qquad (138)$$

then equation (137) becomes

$$\int_0^{2k} f(S)\, dS = \sum_{i=1}^{N} f(S(x_i))\, w_i' \tag{139}$$

For the second integral in equation (134), with limits from 2k to ∞, we choose the transformation

$$S = d + b \tan\left(\frac{\pi}{4}(x + 1)\right) \tag{140}$$

so that when S = 2k and x = -1 one gets 2k = d. When S = ∞ and x = +1, we choose b = 2k. Actually the choice of b = 2k is arbitrary. From equation (140) we get

$$dS = b \sec^2\left(\frac{\pi}{4}(x + 1)\right) \frac{\pi}{4}\, dx \tag{141}$$

therefore

$$\int_{2k}^{\infty} f(S)\, dS = \sum_{j=1}^{M} f(S(x_j))\, b \sec^2\left(\frac{\pi}{4}(x_j+1)\right)\frac{\pi}{4}\, w_j = \sum_{j=1}^{M} f(S(x_j))\, w_j' \tag{142}$$

where w'_j is the modified weight and is defined as

$$w_j' = 2k \sec^2\left(\frac{\pi}{4}(x_j + 1)\right) \frac{\pi}{4}\, w_j \tag{143}$$

Now, the integral equation for the second term in (134) can be written as a single sum

$$\int_0^\infty f(S)\, dS = \sum_{n=1}^{N+M} f(S(x_n))\, w_n' \qquad (144)$$

Here, for the case n ≤ N, the quantities $S(x_n)$ and W_n are to be calculated from equations (136) and (138). For the case n ≥ N+1, they have to be calculated from (140) and (143). Let us define in equation (134)

$$Z_l(k', k'') = \frac{2\mu}{\hbar^2} \frac{U_l(k', k'')\, k''^2}{k^2 - k''^2} \qquad (145)$$

Then equation (134) becomes

$$R_l(k', k) = U_l(k', k) + \int_0^\infty Z_l(k', k'')\, R_l(k'', k)\, dk'' \qquad (146)$$

Now, if we write the integral in (146) as a sum according to equation (144) it becomes

$$R_l(S_i, S_{on}) = U_l(S_i, S_{on}) + \sum_{n=1}^{N+M} Z_l(S_i, S_n)\, R_l(S_n, S_{on})\, w_n' \qquad (147)$$

where the indices i and n run as i, n = 1, 2, 3, -, -, N, N+1, -, -, (M+N). Here, R_l and U_l are one dimensional column matrices with (M+N) components and

$Z_l(S_i, S_n)$ is a (N+M) X (N+M) square matrix. Since we are interested in the on-shell value of R_l i.e. $R_l(S_{on}, S_{on})$, we increase the dimension of R_l and U_l by one component. Then the (N1 = M+N+1)th component represents the on-shell value. That is, i and n run as i, n = 1, 2, 3, -, -, -, (M+N+1), where S_{N+M+1} represents the on-shell grid point.

Now, we have to increase the square matrix $Z_l(S_i, S_n)$ by one row and one column. When n = N1, it will blow up. In order to avoid the singularity, we simply put $Z_l(S_i, S_{N1}) = 0$. Thus, we can write equation (147) as

$$R_l(S_i) = U_l(S_i) + \sum_{n=1}^{N1} Z_l(S_i, S_n)\, R_l(S_n)\, w_n' \qquad (148)$$

or

$$R_l(S_i) - \sum_{n=1}^{N1} Z_l(S_i, S_n)\, R_l(S_n)\, w_n' = U_l(S_i) \qquad (149)$$

i.e.,

$$\sum_{n=1}^{N1} [\, \delta_{in} - Z_l(S_i, S_n)\, w_n' \,]\, R_l(S_n) = U_l(S_i) \qquad (150)$$

where we left the second index S_{on} for R_l and U_l. Now, we define

$$\Lambda_l(S_i, S_n) = \delta_{in} - Z_l(S_i, S_n)\, w_n' \qquad (151)$$

and rewrite equation (150) as

$$\sum_{n=1}^{N1} \Lambda_l(S_i, S_n)\, R_l(S_n) = U_l(S_i) \qquad (152)$$

or

$$R_l = \Lambda_l^{-1}\, U_l \qquad (153)$$

Therefore, our task is to form a column matrix $U_l(S_i)$ and the N1 X N1 square matrix $\Lambda_l(S_i, S_n)$ and solve the matrix equation (153) using a matrix inversion technique. Once the column solution $R_l(S_i)$ is obtained, the last component $R_l(S_{N1})$ is our desired on-shell R_l value.

Chapter 5

Alpha-Cluster Model

5.1 Introduction

If we consider the effect of high energy nuclei on a physical system a large nuclear cross section data base is required as an input. An accurate data base is essential in order to assess the effects of space radiations. The accuracy and importance of such a data base for radiation transport calculations has been discussed by Wilson, Townsend, and Cucinotta in their several papers [35-36, 38-39]. The high energy optical potential described in previous chapters, has been applied in the Eikonal approximation giving reliable prediction for both the total and absorption cross sections. The resulting model is closely related to the Glauber approximation for heavy-ion collisions [35, 38]. The Glauber model has been used by several authors in the study of inclusive heavy-ion inelastic scattering [75-80]. We will use the Glauber model for heavy-ions of interest to us in this chapter.

In the last four decades, the production of heavy-ion fragments has been studied by several authors [75-80]. During these years, a wealth of data has been accumulated about the production of heavy fragments especially from nucleon-nucleus collisions. The introduction of heavier projectiles introduces an important experimental advantage: one can study the heavy-ion fragments which are produced by the break-ups of the projectile or of the target nucleus.

The heavier fragments from a target nucleus have low velocities, while the projectile fragments are produced near the beam velocities. A reach variety of phenomenon occur in heavy-ion collisions including the production of many fragments with masses smaller than the colliding nuclei. At large energies the target and projectile can decompose into their constituents. This leads to final states with many particles.

High energy fragmentation reactions proceed in two steps. In the first abrasion stage of the reaction, the projectile and target constituents (participant) interact, forming a fireball (overlap region) and two relatively cold spectator pieces called the pre-fragments. The nucleons which take part in interactions in the overlap of the participating nuclei are called the participants. The nucleons that are outside the overlap zone are called spectators (Figure 2). In the overlap zone, part of the beam energy is converted into heat. In the process called abrasion, most participant nucleons have left and the nuclei remain with odd shapes. The target and projectile spectator pieces, called pre-fragments are left in excited states. In the second stage, the pre-fragments left over after abrasion, decay into stable fragment nuclei by particle emission as well as gamma rays. This two-step model was first proposed by Serber [75] and was called 'cascade-evaporation' model. Later, the name 'abrasion-ablation' model has come into use with Bowman, Swiatecki, and Tsang [76].

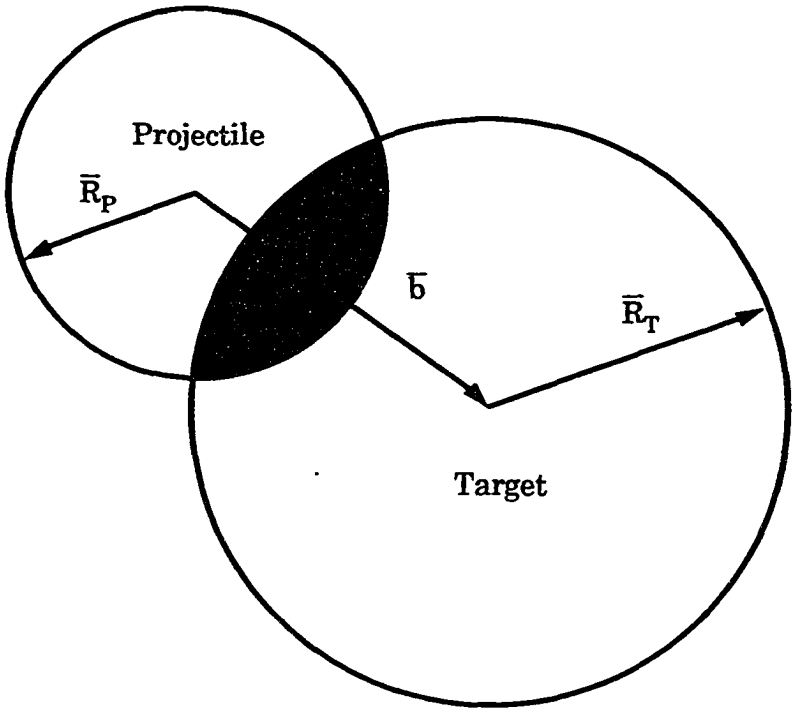

Figure 2. A systematic drawing of the abrasion-ablation model. A systematic drawing of a nucleus-nucleus collision. A projectile with radius R_P strikes a target with radius R_T at impact parameter b. The nucleons in the overlap (shaded) area are called participants. The remaining portion of the target and projectile represents the spectator.

There are several phenomena of nuclear behavior that suggest the clustering of nucleons into groups within a nucleus. The earliest and perhaps simplest nuclear model to consider such characteristics is the alpha-particle model. Heavy nuclei that spontaneously decay by alpha-particle emission have decay rates suggesting at least a tendency for preformation of alpha-particle clusters in nuclear matter. In the simplified theory of nuclear matter, the fact that four nucleons in their ground states could strongly interact played an important role in accounting for the binding energy of nuclei. The nuclei with N = Z and the so called alpha-particle like nuclei, have large binding energies. This suggests viewing such nuclei as consisting of alpha-particle clusters with weak inter-cluster bond energy. The presence of well known clustering effects may manifest themselves in the abrasion step of heavy-ion fragment which we shall investigate herein.

The projectile energies higher than about 500 A MeV fall in the relativistic energy region. These energies are large compared to nucleon separation energy or fermi energy. Nuclear clustering has been ignored in the description of relativistic heavy-ion collision where the abrasion-ablation models [77-80] are typically used for peripheral reactions. For 4n nuclei such as ^{12}C and ^{16}O, we should expect a significant contribution from direct alpha knockout in the production of fragments in the abrasion stage. Early work in the study of clustering effects in nuclear fragmentation included the use of the Glauber model for evaluating the knockout cross section [81], the diffractive

excitation model [82], and inclusion of cluster effects in the internuclear cascade model [83]. The alpha cluster model is a convenient method for representing deformed ground states and rotational bands in the 4n nuclei [84, 85]. We should expect the pre-fragment levels formed after the abrasion of alpha particles to be selective of rotational bands and somewhat distinct from the levels occurring after nucleon abrasion. In this chapter, we will consider the energy transfer spectrum of the projectile fragments for 4n nuclei using the Glauber model.

The excitation energy transferred to the projectile nucleus in the collisional overlap with the target has often been treated in an ad hoc manner in the abrasion-ablation model, using an average excitation energy which is introduced through assumptions largely independent of the collisional dynamics. In the work of Bowman, Swiatecki, and Tsang [76], the excitation energy is determined by the excess surface energy after abrasion in a liquid drop model. The first paper on the Glauber formulation of abrasion by Hufner, Schafer, and Schurmann [77] used a Thomas-Reiche-Khun sum rule with center of mass corrections to estimate an average pre-fragment excitation energy. The frictional spectator interaction which accounts for final state interactions of the abraded projectile nucleons with the pre-fragments was introduced by Oliveira, Donangelo, and Rasmussen [79] using some simplified assumptions on the average energy deposited and trajectories of the out going particles. More recently, Gaimard and Schmidt [80] introduced a diabetic

model which relates the excitation energy to the vacancies created in the single-particle levels in the nucleus from abrasion. The large number of methods for estimating excitation energies in the abrasion-ablation models lead us to identify an explicit calculation of the energy transfer spectrum as an important step in the understanding of these models.

In this chapter, we extend the Glauber formulation of nuclear abrasion in two ways. First, we introduce abrasion response functions which are analogous to the response functions used to describe the quasielastic peak in electron or proton scattering, however generalized to collision dynamics of heavy-ion fragmentation. In this way, we are able to reformulate the abrasion cross section as a differential spectrum in the energy transfer to the projectile nucleus averaged over the energy of the abraded particles. Our second extension of the abrasion model is to consider the abrasion of the nuclear clusters which we specialize to the example of alpha cluster knockout, including the multiple-alpha knockout process. The rigid alpha-particle expansion of the Glauber scattering series [86] is used in our calculations. The cluster abrasion model is developed for the general case of an arbitrary number of cluster knockouts using a factorized form for the alpha-cluster wave-function of the projectile nucleus.

5.2 Glauber Model for α Clusters

In the Glauber model, the scattering operator for a nucleus-nucleus collision is written as

$$f(\vec{q}) = \frac{ik}{2\pi}\int d^2b\ e^{i\vec{q}.\vec{b}}\ \Gamma(\vec{b}) \qquad (154)$$

where k is the projectile-target relative wave number, **b** is the impact parameter, and **q** is the momentum transfer. The interaction of the projectile nucleon with the target nucleon is represented by the profile function

$$\Gamma(\vec{b}) = 1 - \prod_{\beta,\, j}[1 - \Gamma_{\beta j}(\vec{b} - \vec{s}_\beta - \vec{s}_j)] \qquad (155)$$

where β and j label the target and projectile constituents, respectively. In equation (155), $\mathbf{s}_j$ is the projection of the projectile nucleon on the plane perpendicular to the impact parameter **b**, and $\mathbf{s}_\beta$ is the projection of the target nucleon on the plane perpendicular to the impact parameter **b**. The quantity $\Gamma_{\beta,\,j}$ is the two-body profile function with the internal nuclear coordinates having components r = (s, z). The geometry is shown in Figure 3.

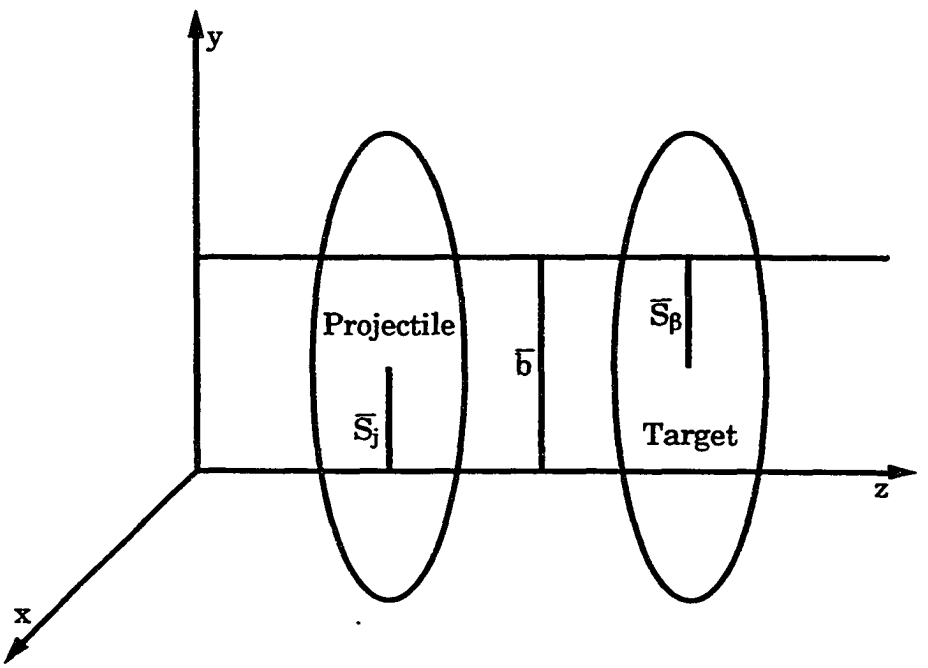

Figure 3. The geometry of $\Gamma_{\beta j}$, the two-body profile function with internal nuclear coordinates having component $r = (s, z)$. The subscripts j and β label the projectile and target constituents.

For a projectile nucleus with a number N_c of α clusters we introduce

$$Q_{j_c\beta} = \prod_{j=1}^{4}[1 - \Gamma_{j\beta}(\vec{b} - \vec{s}_j - \vec{s}_\beta)] \tag{156}$$

such that the profile function becomes

$$\Gamma(\vec{b}) = 1 - \prod_{j_c=1}^{N_c}\prod_{\beta=1}^{A_T} Q_{j_c\beta} \tag{157}$$

The cluster model wave function is an anti-symmetrized product of the intrinsic wave functions of a core nucleus (for ^{16}O core is ^{12}C) and an alpha particle and their wave function $\phi(\mathbf{r})$ of the relative motion such that

$$\Psi_{A_P} = A[\Phi_c(\vec{r}_c)\ \Phi_\alpha(\vec{r}_\alpha)\ \phi(\vec{r})] \tag{158}$$

Similarly, the core wave function ϕ_c ($\mathbf{r}_c$) (for ^{12}C core is ^{8}B) can be written as

$$\Phi_c = A[\chi_{C'}(\vec{r}_{c'})\ \Phi_\alpha(\vec{r}_\alpha)\ \psi(\vec{r})] \tag{159}$$

where $\psi(\mathbf{r})$ is the wave function of relative motion between two alpha particles for the core. The quantity $\chi_{C'}$ is the wave function for the ^{8}B core. The Glauber model is formulated within a frozen nucleus approximation. This means that the relative motion wave functions $\phi(\mathbf{r})$ and $\psi(\mathbf{r})$ should be taken to be the same in the calculations. However, they will be treated as distinct herein. In order to consider the coupling to the excited states of the core nucleus in the fragmentation, specific internal states of relative motion must be included.

In describing the fragmentation of the target into α-clusters, we will neglect multi-step contributions where alpha particles are dissolved and reformed in intermediate states. The profile function is then averaged over the intrinsic alpha-particle wave function in equation (157) in a rigid alpha-particle model by defining

$$Q_{\alpha N}(\vec{b}-\vec{s}_j-\vec{s}_\beta) = \langle\Phi_\alpha|\prod_{j=1}^{4}[1-\Gamma_{\beta j}(\vec{b}-\vec{S}_{j_c}-\vec{s}_j'-\vec{s}_\beta)]|\Phi_\alpha\rangle \quad (160)$$

where we have introduced projectile coordinates $\mathbf{r}'_j$ relative to the nuclear coordinates $\mathbf{R}_{jc}$ with $\mathbf{S}_{jc}$ the transverse component of $\mathbf{R}_{jc}$. Only the relative part of the projectile wave function is then employed in the remainder of this chapter.

5.3 Cluster Abrasion Response Function

We now consider the evaluation of the energy transfer spectra of the projectile fragments from the knockout of α particles. We can write

$$\langle O_P O_T|f(\vec{q})|XF^*\rangle = \frac{ik}{2\pi}\int d^2b\ \langle O_P O_T|\Gamma(\vec{b})|XF^*\rangle\ e^{i\vec{q}.\vec{b}} \quad (161)$$

where O_P and O_T are the projectile and target initial states respectively, and we have denoted target final states by $|X>$. The quantity F^* refers to projectile fragment states (relative motion part only).

If we sum over all final states of the target, we can write

$$\frac{d\sigma}{dE_{F^*}} = \sum_X \frac{1}{(2\pi)^2}\int d^2q\ d^2b\ d^2b'\ e^{i\vec{q}.(\vec{b}-\vec{b}')}\ \delta(E_i-E_f) \tag{162}$$

$$\int \prod_{j_c=1}^{n_c} [\frac{d\vec{k}_{j_c}}{(2\pi)^3}] <O_P O_T|\Gamma^+(\vec{b}')|XF^*\vec{k}_{j_c}><\vec{k}_{j_c}F^*X|\Gamma(\vec{b})|O_P O_T>$$

where $\mathbf{k}_{jc}$ are the wave vectors of the abraded clusters and n_c is the number of abraded α clusters. We have introduced the delta function to ensure energy conservation.

The closure relation for the target final states can be written as

$$\sum |X><X| = 1 \tag{163}$$

In the energy conservation term, which is included in equation (162), the change in energy of the target can be written as

$$E_T - E_X = E_T - \sqrt{(P_T - q)^2 + M_X^2} \tag{164}$$

We see from equations (163) and (164), that the state dependence of the target final state energy prevents the use of closure on the target states in equation (162). However, when energy conservation is not considered closure can be made in equation (162) [78].

If we consider

$$E_T - E_X = E_T - \sqrt{(P_T - q)^2 + M_X^2}$$
$$= E_T \left[1 - \sqrt{1 + \frac{q^2 + M_X^2 - M_T^2}{E_T^2}}\right] \quad (165)$$

we expect that performing the closure on $|X>$ will be valid for a sufficiently large E_T. Proceeding with closure on the final target states, we write

$$\frac{d\sigma}{dE_{F^*}} = \frac{1}{(2\pi)^2}\int d^2q\ d^2b\ d^2b'\ e^{i\vec{q}\cdot(\vec{b}-\vec{b}')}\ \sigma_{n_c}(\vec{b},\ \vec{b}',\ \vec{q},\ E_{F^*}) \quad (166)$$

where we have defined

$$\sigma_{n_c}(\vec{b},\ \vec{b}',\ \vec{q},\ E_{F^*}) = \langle O_T|\{\int \prod_{j_c=1}^{n} \left[\frac{d\vec{k}_{j_c}}{(2\pi)^3}\right] \delta(E_i - E_f)$$
$$\langle O_P|\Gamma^+(\vec{b}')|F^*\vec{k}_{j_c}\rangle\langle\vec{k}_{j_c}F^*|\Gamma(\vec{b})|O_P\rangle\}|O_T\rangle \quad (167)$$

In order to consider the energy conserving delta function in equation (167), we introduce the Fourier transform pair

$$\sigma_{n_c}(t) = \int dE\ e^{-iEt}\ \sigma_{n_c}(E) \quad (168)$$

and

$$\sigma_{n_c}(E) = \int \frac{dt}{2\pi} e^{iEt} \sigma_{n_c}(t) \tag{169}$$

In the projectile rest frame, we have

$$E_i - E_f = S_n + (E_T - E_X) - T_{F^*} - \epsilon_{F^*} - \sum_{j_c} \frac{k_{j_c}^2}{2\mu} \tag{170}$$

where S_n is the separation energy, T_{F^*} is the recoil energy of the prefragments, and ε_{F^*} is the excitation energy of the prefragments. Fourier transforming into temporal space with respect to the energy $E = T_{F^*} + \varepsilon_{F^*} - S_n - (E_T - E_X)$, we find

$$\sigma_{n_c}(t) = \langle O_T | \{ \prod_{j_c=1}^{n_c} [\frac{d\vec{k}_{j_c}}{(2\pi)^3}] \, e^{-i\sum_{j_c} (\frac{k_{j_c}^2 t}{2\mu})} \tag{171}$$

$$\langle O_P | \Gamma^*(\vec{b}') | F^* \vec{k}_{j_c} \rangle \langle F^* \vec{k}_{j_c} | \Gamma(\vec{b}) | O_P \rangle \} | O_T \rangle$$

We consider an alpha cluster participant-spectator factorization of profile functions as

$$\Gamma(b) = 1 - \prod_{l_c=n_c+1}^{N_c} Q_{l_c} \prod_{j_c=1}^{n_c} Q_{j_c} \tag{172}$$

where

$$Q_{j_c} = \prod_{\beta=1}^{A_T} Q_{\alpha N} \tag{173}$$

If we neglect the anti-symmetrization between the alpha knockouts and the core (prefragments), we can approximate the projectile wave function of equation (158) by

$$|O_P> = |F> \prod_{j_c=1}^{n_c} \phi(\vec{R}_{j_c}) \tag{174}$$

Using equations (173) and (174) in equation (171), we find

$$\sigma_{n_c}(t) = <O_T|\{ \binom{N_c}{n_c} <F| \prod_{l_c} Q_{l_c}^{+}(\vec{b} - \vec{S}_{l_c}) |F^*>$$

$$<F^*| \prod_{l_c=n_c+1}^{N_c} Q_{l_c}(\vec{b} - \vec{S}_{l_c}) |F> \prod_{j_c=1}^{n_c} [\int \frac{d\vec{k}_{j_c}}{(2\pi)^3} d\vec{R}_{j_c} d\vec{R}'_{j_c} e^{i\vec{k}_{j_c}\vec{x}_{j_c}} \tag{175}$$

$$e^{-i\frac{\vec{k}_{j_c}^2 t}{2\mu}} Q_{j_c}^{+}(\vec{b}' - \vec{S}'_{j_c}) Q_{j_c}(\vec{b} - \vec{S}_{j_c}) \phi^{+}(\vec{R}'_{j_c}) \phi(\vec{R}_{j_c})]\} |O_T>$$

where $\mathbf{x}_{jc} = \mathbf{R}_{jc} - \mathbf{R}'_{jc}$.

Using the coherent approximation for the target wave function leads to

$$\sigma_{n_c}(t) = \binom{N_c}{n_c} P^{N_c-n_c}(\vec{b}, \vec{b}') \Lambda_{n_c}(\vec{b}, \vec{b}', t) \tag{176}$$

where

$$P^{N_c-n_c}(\vec{b}, \vec{b}') = \langle O_T F | \prod_{l_c} Q_{l_c}^{+}(\vec{b}' - \vec{S}_{l_c}') | F^* \rangle$$
$$* \langle F^* | \prod_{l_c} Q_{l_c}(\vec{b} - \vec{S}_{l_c}) | F O_T \rangle \tag{177}$$

describes the projectile prefragments (spectators). The response function

$$\Lambda_{n_c}(t) = \langle O_T | \int \prod_{j_c=1}^{n_c} [d\vec{R}_{j_c} d\vec{R}_{j_c}' \frac{d\vec{k}_{j_c}}{(2\pi)^3} e^{i\vec{k}_{j_c}\vec{x}_{j_c}} e^{-i\frac{k_{j_c}^2 t}{2\mu}}$$
$$\phi_{n_c}^{+}(\vec{R}_{j_c}') \phi_{n_c}(\vec{R}_{j_c}) Q_{j_c}^{+}(\vec{b}' - \vec{s}_{j_c}') Q_{j_c}(\vec{b} - \vec{s}_{j_c})] | O_T \rangle \tag{178}$$

describes the abrasion dynamics. Evaluating the integrals over $\mathbf{k}_{j_c}$ in equation (178) leads to

$$\Lambda_{n_c}(t) = \langle O_T | \int \prod_{j_c=1}^{n_c} [d\vec{R}_{j_c} d\vec{R}_{j_c}' (\frac{\mu}{2\pi i t})^{\frac{3}{2}} e^{-\frac{\mu x_{j_c}^2}{2it}}$$
$$\phi_{n_c}^{+}(\vec{R}_{j_c}') \phi_{n_c}(\vec{R}_{j_c})] Q_{j_c}^{+}(\vec{b}' - \vec{S}_{j_c}') Q_{j_c}(\vec{b} - \vec{S}_{j_c}) | O_T \rangle \tag{179}$$

and in energy space the result is

$$\Lambda_{n_c}(\vec{b},\ \vec{b}',\ E_F^*) = \langle O_T | \int \prod_{j_c=1}^{n_c} [\ d\vec{R}'_{j_c}\ d\vec{R}_{j_c}\ \rho(\vec{R}_{j_c},\ \vec{R}'_{j_c})$$

$$Q^+_{j_c}(\vec{b}' - \vec{S}'_{j_c})\ Q_{j_c}(\vec{b} - \vec{S}_{j_c})\ ] \tag{180}$$

$$* \frac{\mu}{2}\left(\frac{1}{2\pi}\right)^{\frac{3n_c}{2}} \frac{\xi_{n_c}^{\frac{3n_c}{2}-1}}{\bar{x}_{n_c}^{\frac{3n_c}{2}-1}} J^{(1)}_{\frac{3n_c}{2}-1}(\xi_{n_c}\ \bar{x}_{n_c}) | O_T \rangle$$

where $\rho(r, r') = \phi(r)\ \phi^+(r')$ and J_m is the cylindrical Bessel function of the first kind of order m and we define

$$\xi_{n_c} = \sqrt{2\mu[T_{F^*} + \epsilon_{F^*} - S_{n_c} - (E_T - E_X)]} \tag{181}$$

and

$$\bar{x}_{n_c} = \sqrt{\sum_{j_c=1}^{n_c} x_{j_c}^2} \tag{182}$$

The Bessel functions appearing in equation (180) provide a distribution in T_{F^*} resulting from the production spectra of abraded clusters. If we assume forward peak density matrices, a small argument expansion of the Bessel

functions can be developed [87, 88] resulting in

$$\Lambda_{n_c}(\vec{b}, \vec{b}', E_{F*}) \propto C_{n_c}[T_{F*} + \epsilon_{F*} - S_{n_c} - (E_T - E_X)]^{n_c-1} \Lambda_1^{n_c}(\vec{b}, \vec{b}', \frac{\xi_{n_c}}{\sqrt{n_c}}) + O(\xi_{n_c}^4 \vec{x}_{n_c}^4) \tag{183}$$

where Λ_1 is found after evaluating the profile functions in the optical limit

$$\Lambda_1(\vec{b}, \vec{b}', E_{F*}) = \frac{\mu\xi_1}{(2\pi)^2}\int d\vec{R}\, d\vec{R}'\, \rho(\vec{R}, \vec{R}')\, j_0(\xi_1 x) * (e^{\Omega_{\alpha T}(\vec{b}-\vec{s}, \vec{b}'-\vec{s}')}-1) \tag{184}$$

with

$$\Omega_{\alpha T} = \frac{A_T}{(2\pi k_{\alpha N})^2}\int d^2q\, d^2q'\, e^{i\vec{q}.(\vec{b}-\vec{s})}\, e^{-i\vec{q}.(\vec{b}'-\vec{s}')} * F_T(\vec{q}-\vec{q}')\, f_{\alpha N}(\vec{q})\, f_{\alpha N}^{+}(\vec{q}') \tag{185}$$

where F_T is the form factor of the target nucleon and $f_{\alpha N}$ is the alpha nucleon elastic scattering amplitude. The iteration of the $\Omega_{\alpha T}$ function in equation (184) represents the multiple scattering of the abraded α-particle with the target.

The coefficients C_{nc} in equation (183) are found in reference [88] where $C_1 = 1$, $C_2 = \pi/4$, $C_3 = \pi/105$, $C_4 = \pi^2/240$. Let us assume in equation (157) that

$$q^2 + M_T^2 - M_X^2 \ll E_T^2 \tag{186}$$

It then follows that

$$\frac{d\sigma}{dE_{F*}} = \binom{N_c}{n_c} \int d^2b \; C_{n_c} (T_{F*} + \epsilon_{F*} - S_{n_c})^{(n_c-1)} \\ * \; P^{N_c - n_c}(\vec{b}) \; \Lambda_1^{n_c}(\vec{b}, \frac{\xi_{n_c}}{\sqrt{n_c}}) \tag{187}$$

The formalism we have described can be used to consider the abrasion of several alpha clusters in heavy-ion reactions.

5.4 Wave Functions in the α- Cluster Model

The formalism for the abrasion of α clusters described above can be generalized for the projectile or the target. We use the model of Coelho [89] which considers virtual states of relative motion of an α particle with a core in the projectile or target ground state. For the case of ^{12}C, the ground state wave function can be written using Jacobi coordinates as [89]

$$\Psi(\vec{u}, \vec{v}) = \sum_{L, M} C_L \; \phi_{L, M}(\vec{u}) \; \psi_{L, -M}(\vec{v}) \langle 00 | L, L, M, -M \rangle \tag{188}$$

where

$$\vec{u} = \vec{R}_3 - \frac{1}{2}(\vec{R}_1 + \vec{R}_2)$$
$$\vec{v} = \vec{R}_1 - \vec{R}_2 \qquad (189)$$

Only L = 0, 2, 4 virtual states are allowed if the dissociation of α particles in intermediate states is neglected. The allowed angular momentum values correspond to the ^{8}Be ground state (L = 0), first excited state at 2.9 MeV (L = 2), and second excited state at 11.4 MeV (L = 4). Coelho finds [89], using a harmonic oscillator basis, that the spectroscopic constants obey the relation

$$\sum_{L = 0, 2, 4} |C_L|^2 = 1 \qquad (190)$$

For $\phi_{L, M}$ we use an Eckart wave function which has the correct long range behavior [89-91]

$$\phi_{L, M}(\vec{U}) = N(1-e^{-\frac{u}{R}})^n \frac{e^{-\alpha_L U}}{u} Y_{L, M}(\hat{U}) \qquad (191)$$

with n = 4. The value of R (2.6 fm) is found by fitting to the ^{12}C ground state form factor by the method described by Noble [91], and the quantity α_L is defined as

$$\alpha_L = \sqrt{-2\ \mu_R\ \epsilon_L} \qquad (192)$$

For the ^{8}Be core we use [90]

$$\psi_{0,0}(\vec{v}) = N\left[1 - \frac{4}{3}\left(\frac{v}{a}\right)^2 + \frac{4}{15}\left(\frac{v}{a}\right)^4\right] e^{-\frac{v^2}{2a^2}} Y_{0,0}(\hat{v}) \quad (193)$$

and

$$\psi_{2,-M}(\vec{v}) = N\left(\frac{v^2}{a^2} - \frac{2}{3}\frac{v^4}{a^4}\right) e^{-\frac{v^2}{2a^2}} Y_{2,-M}(\hat{v}) \quad (194)$$

where N represents a normalization constant and from reference [87] we use a = 1.03 fm. Using the model wave function (equations 188-191), the excitation cross section for the abrasion of a single α cluster becomes (considering the ground state wave function for the core)

$$\frac{d\sigma}{dE_{F*}}\Big)_{Inel} = \frac{\mu\xi_{L'}}{(2\pi)^2}\int d^2b \sum_{L,M}\sum_{L',M'} C_L\, C^{+}_{L'} \quad (195)$$

$$\langle 00|L, L, M, -M\rangle\langle 00|L', L', M', -M'\rangle^{+}\, \Lambda_{LM,L'M'}(\vec{b})$$

where

$$\Lambda_{LM,L'M'}(\vec{b}) = \int d\vec{u}\, d\vec{u}'\, j_0\left(\xi'_L \frac{(n_c-1)}{n_c}|\vec{u} - \vec{u}'|\right) \quad (196)$$

$$\phi_{LM}(\vec{u})\, \phi^{+}_{L'M'}(\vec{u}')\, \left(e^{\Omega_{\alpha,T}\left(\vec{b} - \frac{2}{3\vec{u}}, \vec{b} - \frac{2}{3\vec{u}'}\right)} - 1\right) P_{LM,L'M'}(\vec{b}, \vec{u}, \vec{u}')$$

and

$$P_{LM,\,L'M'}(\vec{b},\,\vec{u},\,\vec{u}') = \int d\vec{v}\; d\vec{v}'\; \rho_{LM}(\vec{v})\; \rho_{L'M'}(\vec{v}')$$

$$e^{i[\,\chi_{aN}(\vec{b} - \frac{\vec{v}}{2} - \frac{\vec{u}}{3}) - \chi^{*}_{aN}(\vec{b} + \frac{\vec{v}}{2} + \frac{\vec{u}}{3})\,]} \qquad (197)$$

$$e^{i[\,\chi_{an}(\vec{b} + \frac{\vec{v}'}{2} + \frac{\vec{u}'}{3}) - \chi^{*}_{an}(\vec{b} - \frac{\vec{v}'}{2} + \frac{\vec{u}'}{3})\,]}$$

where ρ_{lM} is the transition density of the core. The total knockout cross sections can be written as

$$\sigma = \int d^2b \sum_{L,\,M} \sum_{L',\,M'} C_L\, C^{*}_{L'} \langle 00|L,\,L,\,M,\,-M\rangle \qquad (198)$$

$$\langle 00|L',\,L',\,M',\,-M'\rangle\; \Delta_{LM,\,L'M'}(\vec{b})$$

where

$$\Delta_{LM,\,L'M'}(\vec{b}) = \int d\vec{u}\; d\vec{u}'\; \phi_{LM}(\vec{u})\; \phi^{*}_{L'M'}(\vec{u}') \qquad (199)$$

$$(e^{\Omega_{aT}(\vec{b} - \frac{2}{3\vec{u}},\, \vec{b} - \frac{2}{3\vec{u}'})} - 1)\; P_{LM,\,L'M'}(\vec{b},\,\vec{u},\,\vec{u}')$$

where $P_{L,M,\,L',M'}$ is given by equation (197). We have used the optical limit for

the profile function with

$$\chi_{\alpha N}(\vec{b}) = \frac{A_T}{2\pi k_{\alpha N}} \int d^2q \; e^{i\vec{q}.\vec{b}} \; F_T(\vec{q}) \; f_{\alpha N}(\vec{q}) \qquad (200)$$

and we use the two-body scattering amplitude

$$f(q) = \frac{\sigma(\alpha + i)}{4\pi} \; k_{NN} \; e^{-\frac{Bq^2}{2}} \qquad (201)$$

Equation (195) is simplified through introduction of the vectors

$$\vec{g} = \vec{u} - \vec{u}' \qquad \vec{h} = \frac{1}{2} (\vec{u} + \vec{u}') \qquad (202)$$

which allows for factorization of many of the integrals in equation (195) which are evaluated numerically. For the evaluation of the double alpha abrasion contribution we consider only the ^{8}Be ground state in our calculations. The alpha-particle form factor is assumed as Gaussian with a radius parameter of 1.33 fm. The elastic alpha-nucleon scattering amplitude is evaluated in the Glauber model as described in Reference [86].

Chapter 6

Results and Discussion

6.1 Calculations Using the Lippmann-Schwinger Equation

Many authors have solved the Lippman-Schwinger equation for a real potential in momentum space. We have numerically solved the Lippman-Schwinger equation for the optical potential in momentum space (see chapter 4). Using the technique described in previous chapters, the total and absorption cross sections are calculated using equations (132) and (133). The proton-nucleus, alpha-nucleus, and carbon-nucleus total and absorption cross sections are calculated. The total and absorption cross sections under the Eikonal model are calculated using equations (74) and (76). By comparing the results based on exact solutions of the Lippmann-Schwinger equation and Eikonal model solutions, we provide an important validation of data bases used in cosmic-ray studies. The absorption cross sections are calculated by using the medium modified optical potential in the Lippmann-Schwinger equation. The Eikonal model is unable to account for nuclear medium corrections, although such studies may be done in the future using momentum space methods. The inclusion of medium corrections provides improvements in nuclear data bases.

The total and absorption cross sections for nucleon, ^{4}He, and ^{12}C projectiles colliding with different target nuclei have been calculated in an energy range from 25 A to 1000 A MeV. By using the Lippmann-Schwinger

calculation and the Eikonal model, theoretical predictions for total and absorption cross sections are compared in Figures 4 through 9 with representative experimental data [92-96]. All physical inputs (form factors and two-body amplitudes) are kept identical in the Lippmann-Schwinger and in the Eikonal model calculations. The agreement is excellent between the Lippmann-Schwinger calculation, the Eikonal model, and the experimental data at higher energy for total and absorption cross sections.

Results of calculations of the total cross sections for the nucleon-nucleus, ^{4}He-nucleus, and ^{12}C- nucleus systems are shown in Figure 4, 5, and 6 respectively. We observe from our calculations that, at a lower energy the percentage differences between the Eikonal model values and the exact (Lippmann-Schwinger) values are higher when compared with those at a higher energy. This is an indication that the Eikonal model prediction for scattering cross sections is fairly accurate at higher energies. The Eikonal model results are consistently lower than the exact results because of the forward scattering assumption of the Eikonal approximation. Although the scattering is dominated by forward angles at high energies, some contribution from large-angle scattering is always present and is not included in the Eikonal model. We also observe that both the Eikonal model and the exact results are well within the range of experimental data. At low energies, an improvement in the calculations will most likely be obtained by considering the corrections to the impulse approximation; correlation effects [53-56, 97-98], or

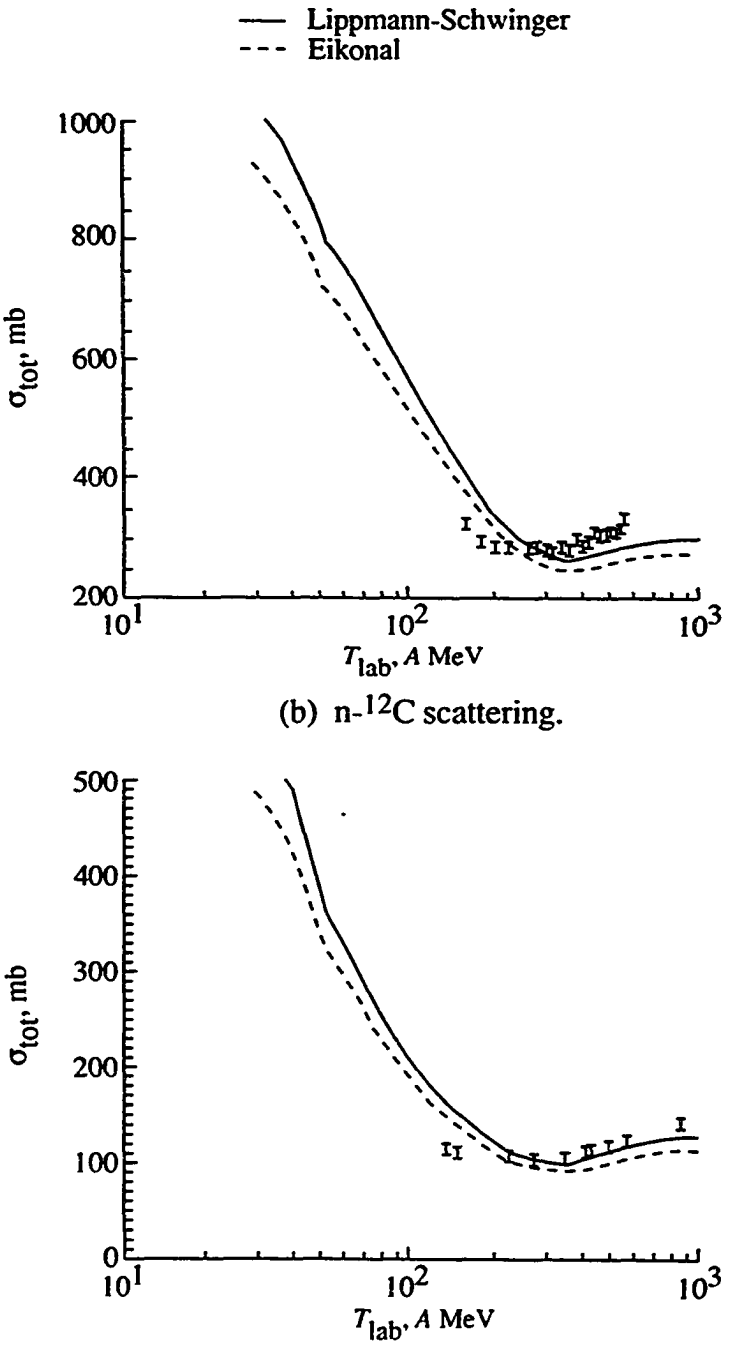

Figure 4. Comparison of the total cross section calculation using the Eikonal approximation with the exact solution for a nucleon-nucleus system in the energy range from 25 A to 1000 A MeV. Available experimental data are shown by error bars.

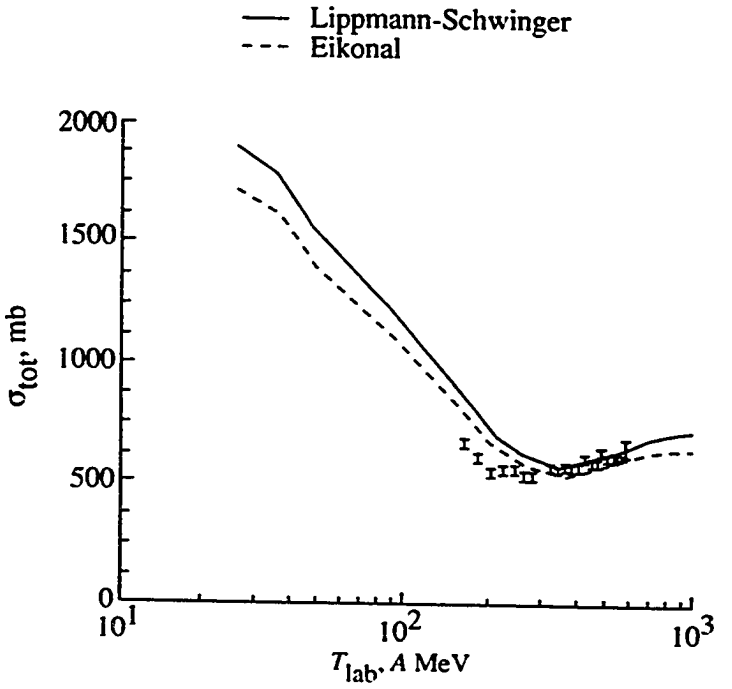

(d) n-^{27}Al scattering.

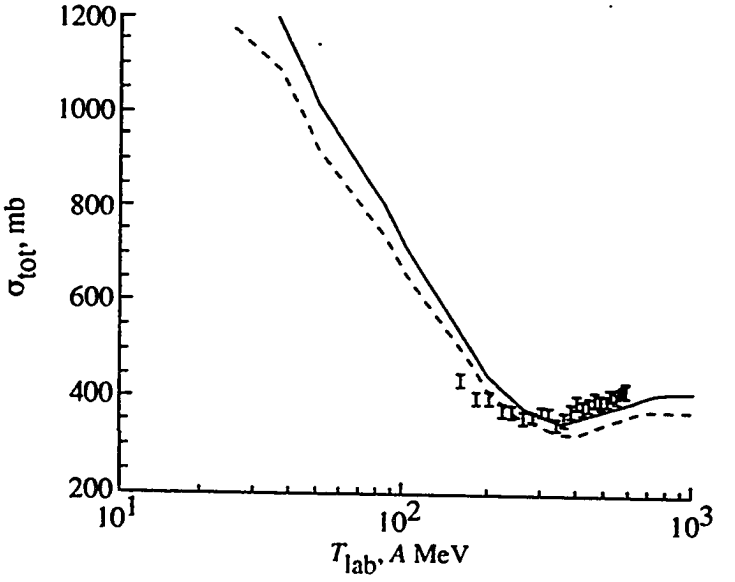

(c) n-^{16}O scattering.

Figure 4, continued

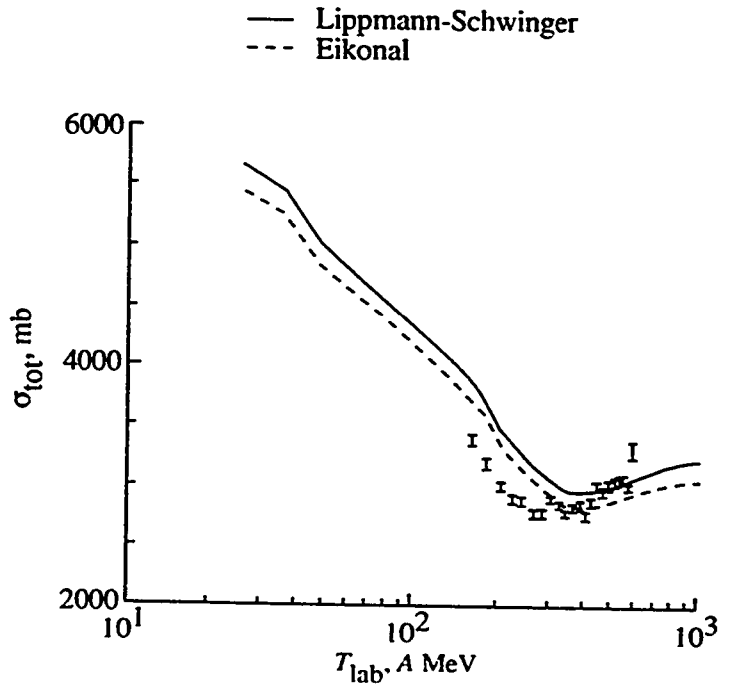

(f) n-^{208}Pb scattering.

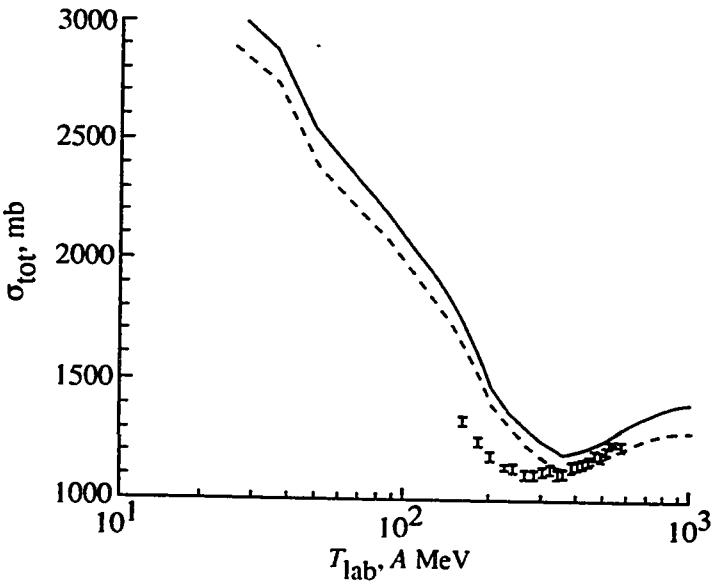

(e) n-^{64}Cu scattering.

Figure 4, continued

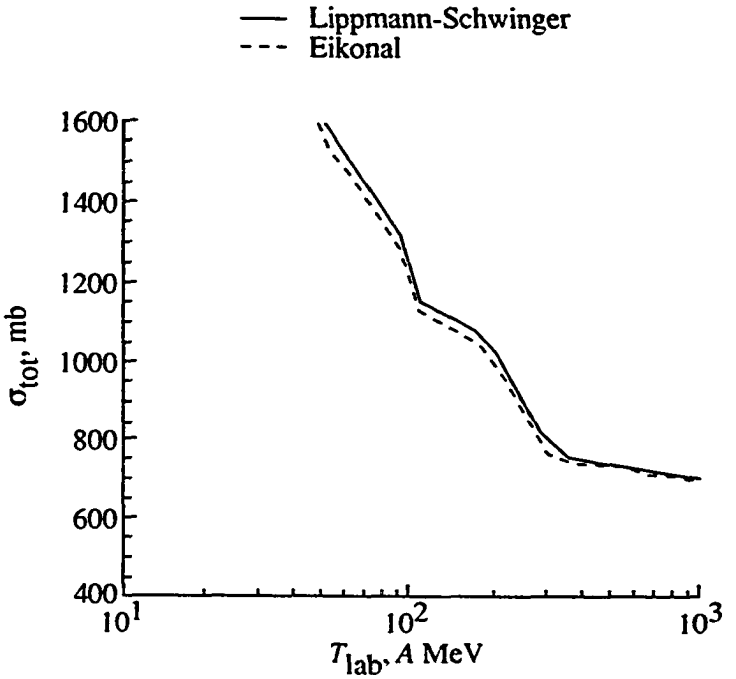

(b) ^{4}He-^{16}O scattering.

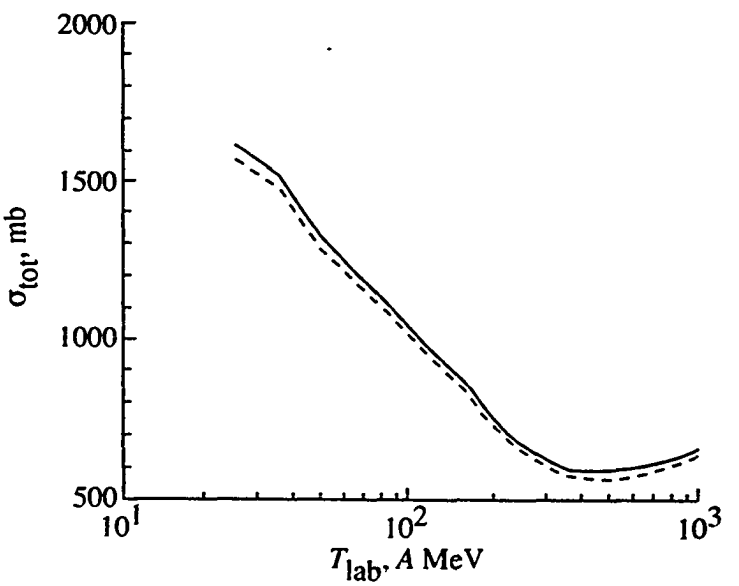

(a) ^{4}He-^{12}C scattering.

Figure 5. Comparison of the total cross section calculation using the Eikonal approximation with the exact solution for a helium-nucleus system in the energy range 25 A to 1000 A MeV.

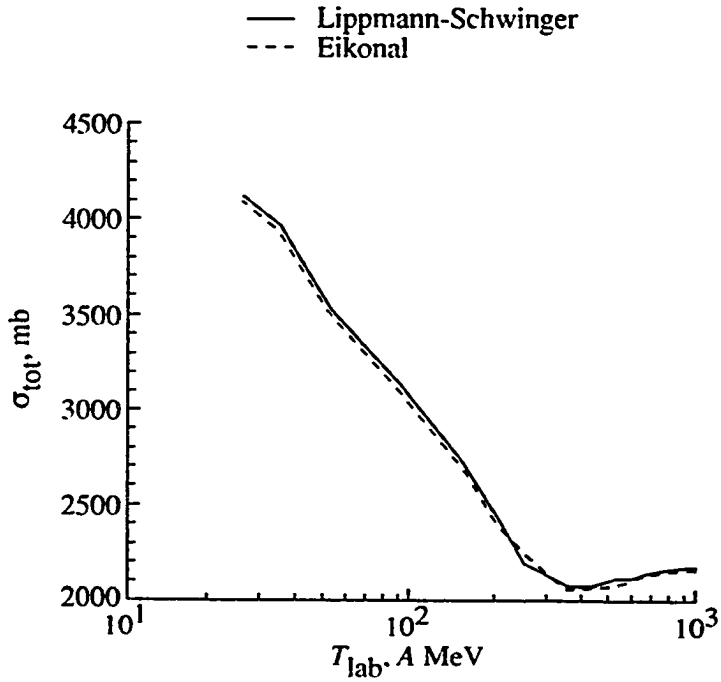

(d) ^{4}He-^{64}Cu scattering.

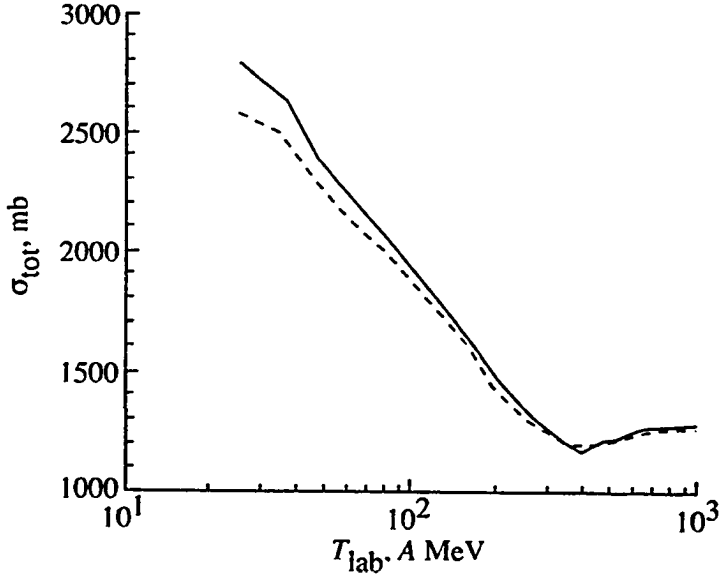

(c) ^{4}He-^{27}Al scattering.

Figure 5, continued

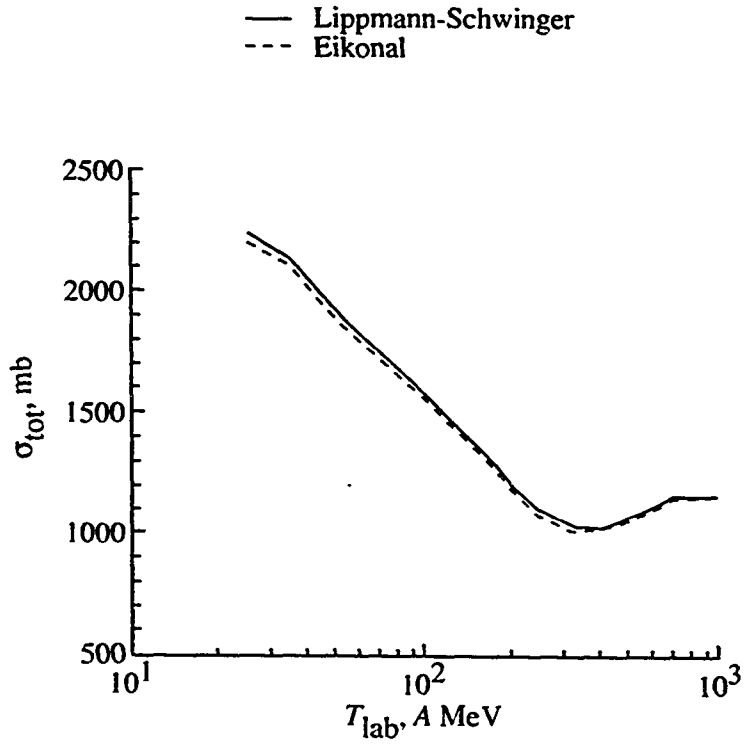

Figure 6. Comparison of the total cross section calculation using the Eikonal approximation with the exact solution for the ^{12}C-^{12}C system in the energy range 25 A to 1000 A MeV.

perhaps relativistic effects [63-68].

In Figures 7, 8, and 9 we present comparisons of the exact calculation of the absorption cross section to the Eikonal model solution for the nucleon-nucleus, ^{4}He-nucleus, and ^{12}C-nucleus systems, respectively. Experimental data are shown in these comparisons if available. The Eikonal model is seen to represent the exact solution quite well for projectile energies greater than 200 A MeV, but below 200 A MeV, the differences are large. In some cases, the Eikonal model represents the experimental data better than does the exact solution. This is a definite indication that the first order optical potential is not completely adequate. Table 1 presents a comparison of the experimental data from Reference [94] with the results of Eikonal and Lippmann-Schwinger calculations for ^{12}C-nucleus absorption cross sections at an energy of 83 A MeV. Although the calculated values agree satisfactorily with the experimental values, further investigations of optical potential theory, including nuclear medium effects, will be required for the theoretical evaluation of absorption cross sections with high precision at lower energies.

Figure 10 shows the number of partial waves required to calculate the total, absorption, and elastic cross sections at energies of 100 A and 1000 A MeV for the nucleon-^{12}C and ^{12}C-^{12}C systems. We observe that if we increase the energy of the projectile, we will need more partial waves for cross section calculations. Figure 11 shows the total and absorption cross sections as functions of the slope parameter at energies of 100 A and 1000 A MeV for the

Table 1. Absorption cross sections for ^{12}C-nucleus systems.

E_{lab} = 83 A MeV

System	σ_r (mb) (experimental)	σ_r (mb) (Lippmann)	σ_r (mb) (Eikonal)
$^{12}C + ^{12}C$	960 ± 30	874	849
$^{12}C + ^{27}Al$	1400 ± 40	1419	1477
$^{12}C + ^{40}Ca$	1550 ± 60	1737	1750
$^{12}C + ^{56}Fe$	1810 ± 100	1997	2123

*For ^{12}C-nucleus, the experimental data is from S. Kox et al. [94].

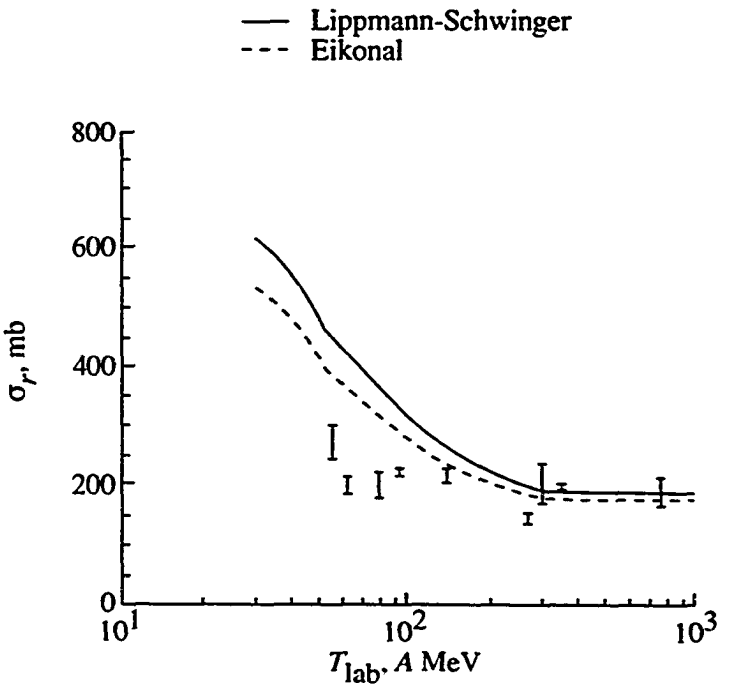

(b) n-^{12}C scattering.

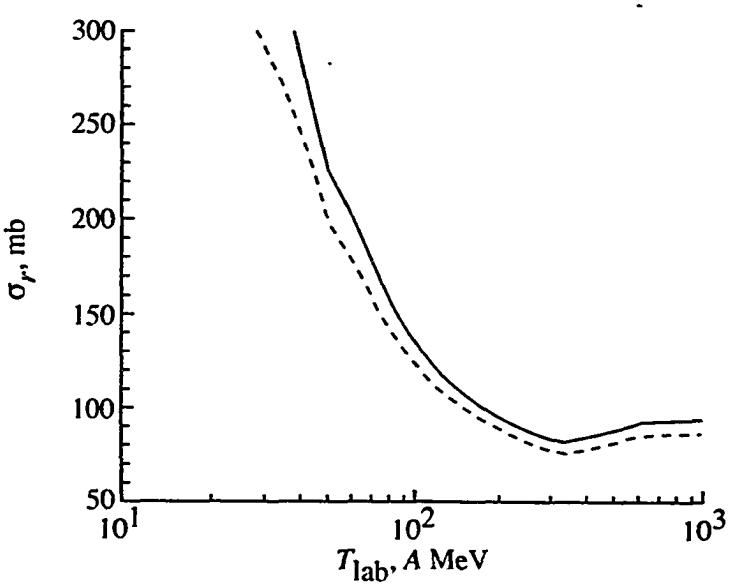

(a) n-^{4}He scattering.

Figure 7. Comparison of the absorption cross section calculation using the Eikonal approximation with the exact solution for a nucleon-nucleus system in the energy range 25 A to 1000 A MeV. Available experimental data are shown by error bars.

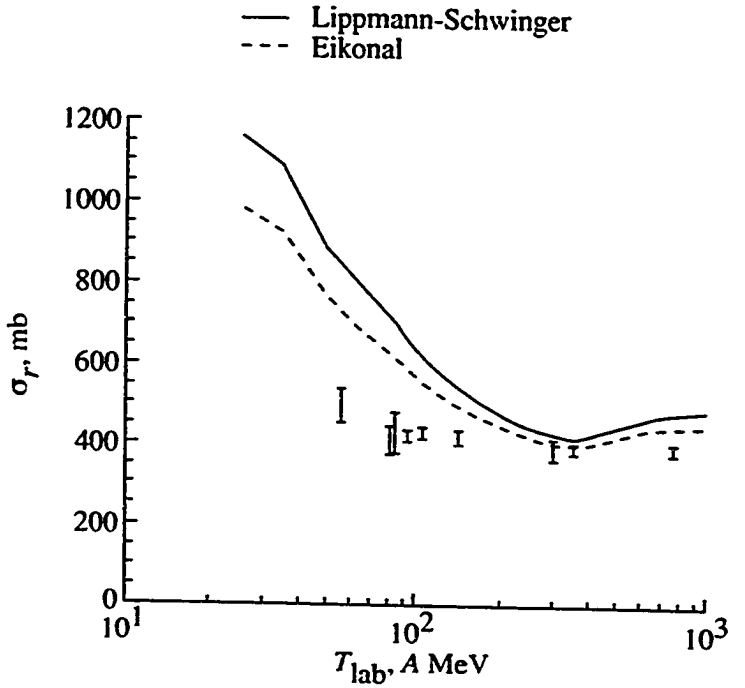

(d) n-^{27}Al scattering

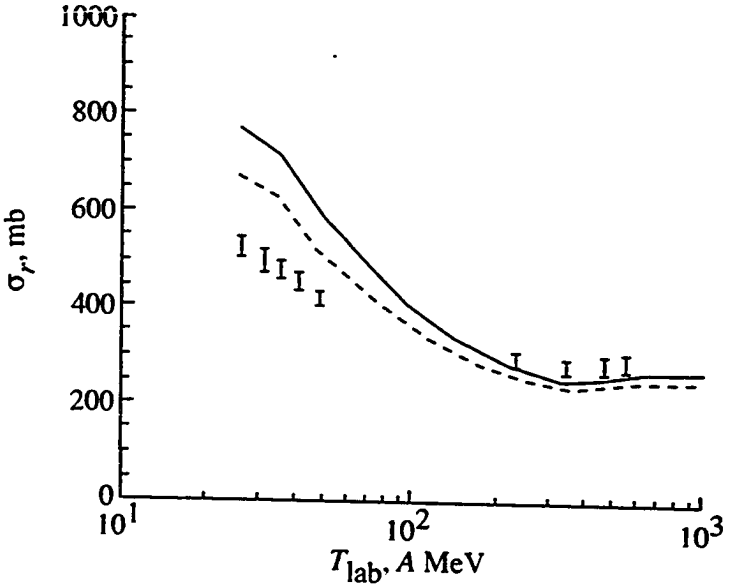

(c) n-^{16}O scattering.

Figure 7, continued

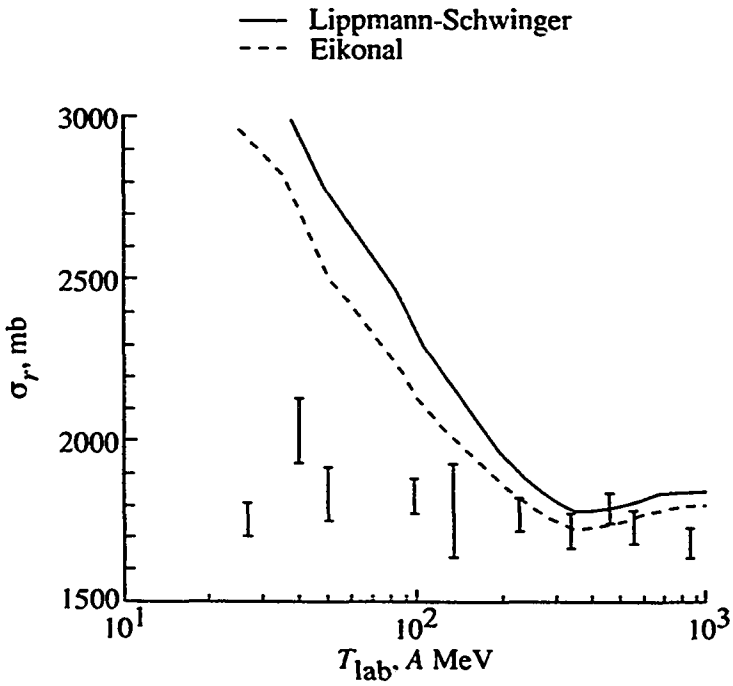

(f) n-^{208}Pb scattering

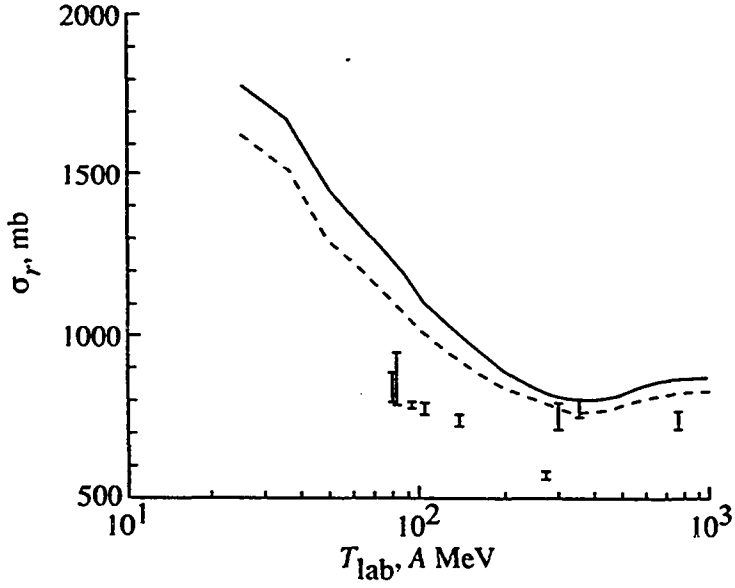

(e) n-^{64}Cu scattering

Figure 7, continued

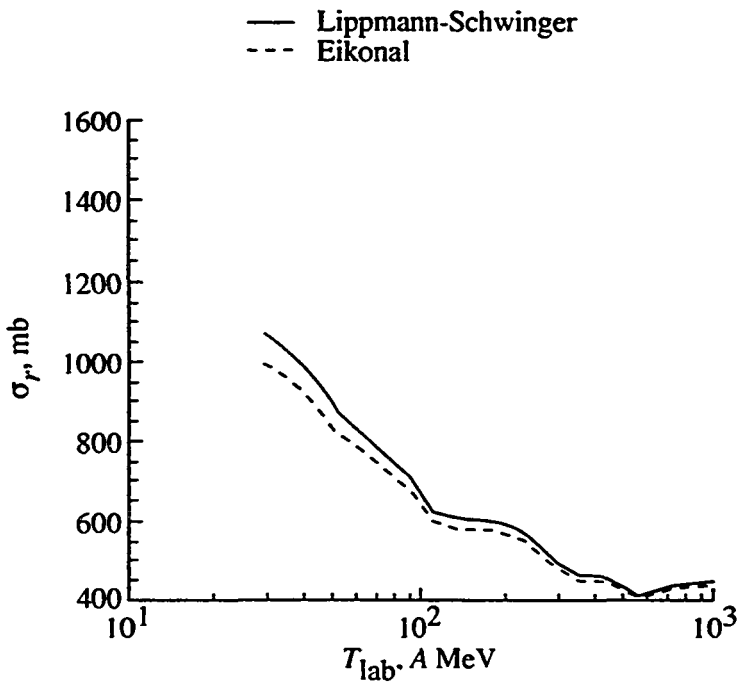

(b) ^{4}He-^{16}O scattering.

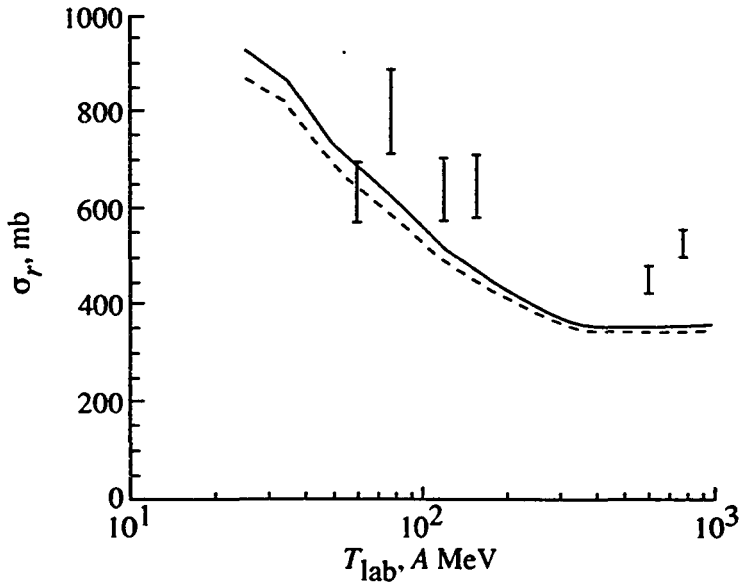

(a) ^{4}He-^{12}C scattering.

Figure 8. Comparison of the absorption cross section calculation using the Eikonal approximation with the exact solution for a helium-nucleus system in the energy range 25 A to 1000 A MeV. Available experimental data are shown by error bars.

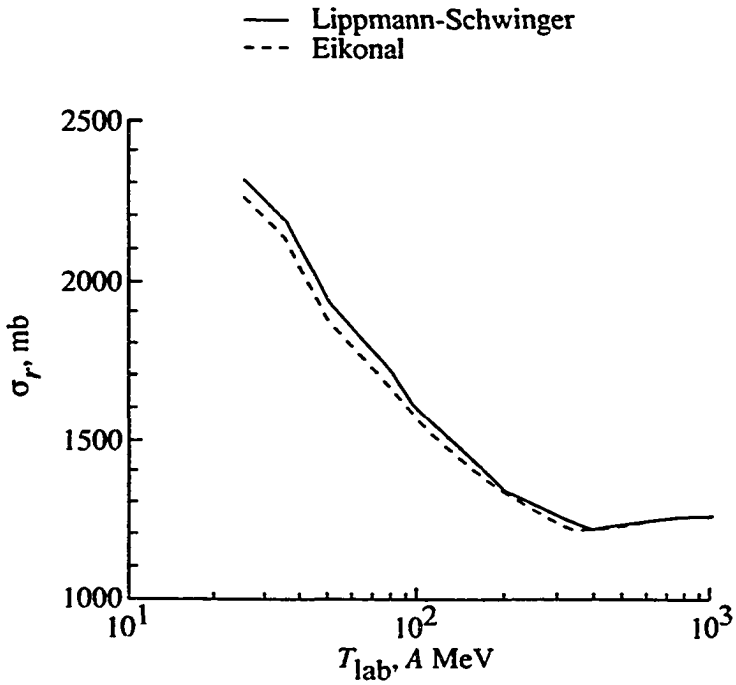

(d) ^{4}He-^{64}Cu scattering.

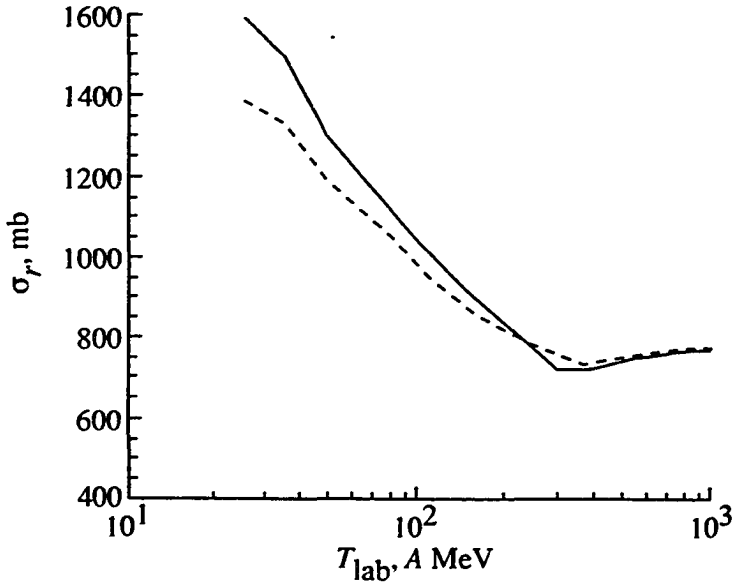

(c) ^{4}He-^{27}Al scattering.

Figure 8, continued

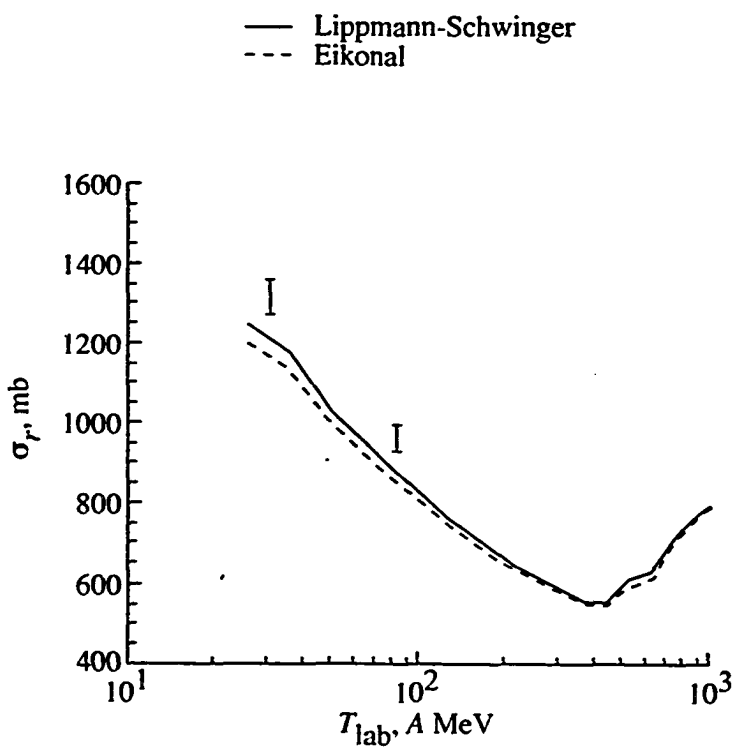

Figure 9. Comparison of the absorption cross section calculation using the Eikonal approximation with the exact solution for the ^{12}C-^{12}C system in the energy range 25 A to 1000 A MeV. Available experimental data are shown by error bars.

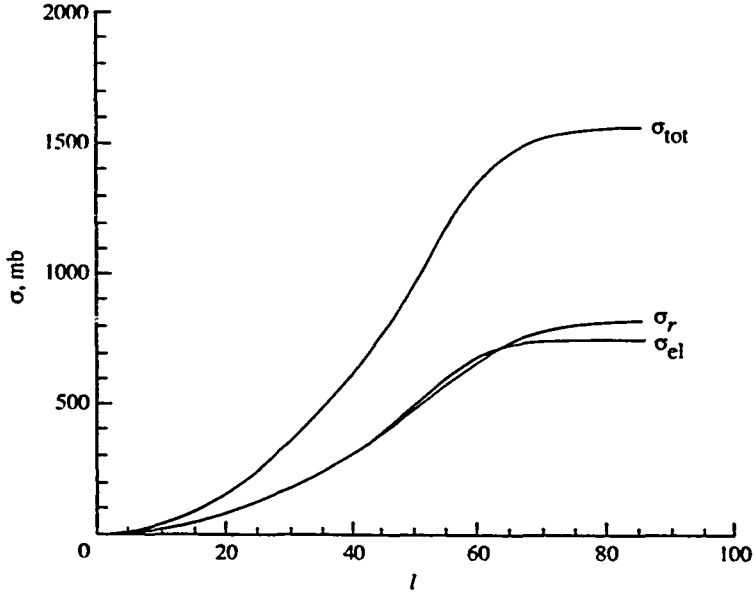

(b) 100 A MeV for ^{12}C - ^{12}C system.

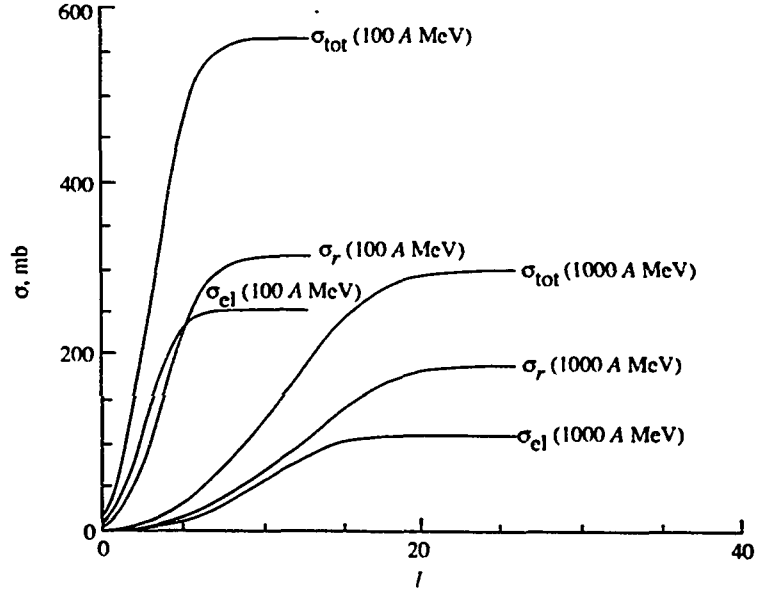

(a) 100 A and 1000 A MeV for n - ^{12}C system.

Figure 10. The total, absorption, and elastic cross sections as a function of number of partial waves.

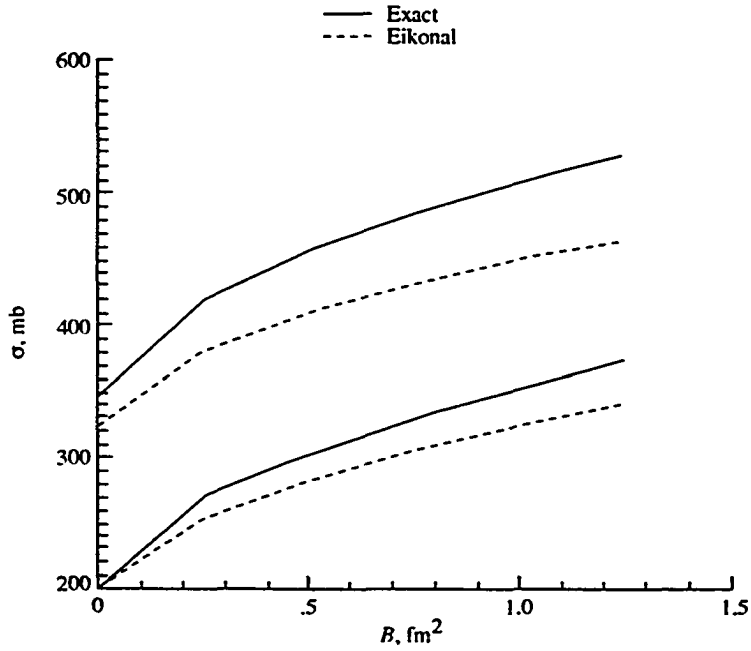

(b) 1000 A MeV for n - ^{16}O system.

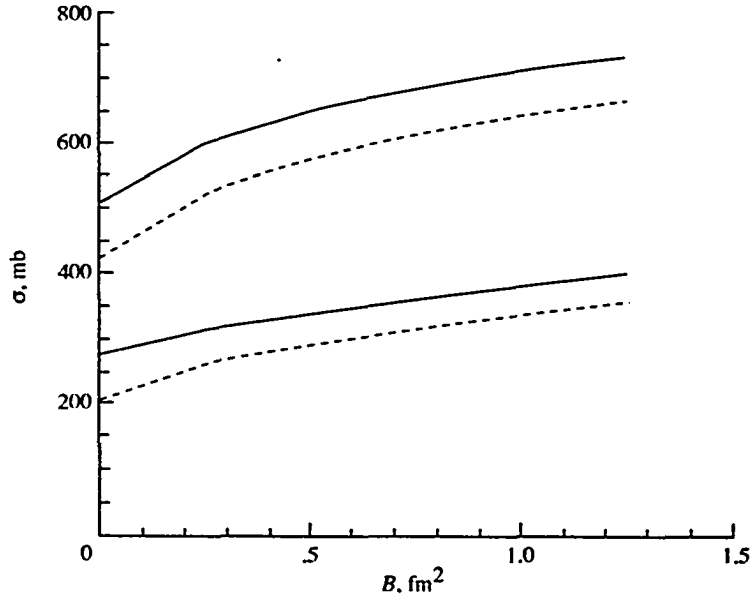

(a) 100 A MeV for n - ^{16}O system.

Figure 11. The total and absorption cross sections for the exact and the Eikonal calculations as a function of slope parameter.

nucleon-^{16}O system. We observe from our calculations that because the total and absorption cross sections saturate at large values of the slope parameter, limiting values of the cross sections are reached.

We next use the medium modified optical potential for theoretical predictions of the absorption cross section and the results are compared with the representative experimental data [99] in Figure 12 for alpha-nucleus collisions. Using the formalism described in previous chapters, absorption cross sections for the projectiles ^{4}He and ^{12}C colliding with different target nuclei have been calculated in an energy range of 18-83 A MeV. The agreement between calculated values of absorption cross sections using the medium modified optical potential and experimental data is excellent. We see in Figure 12 that, at lower energies the absorption cross sections using the medium modified optical potential are much different from the values obtained using the free space optical potential. This suggests that correlation effects such as Pauli blocking are dominant at lower energies. The experimental and the theoretical absorption cross sections using the medium modified optical potential are in good agreement. We also see that the medium modified calculation reduces the values about 15% at all energies in the alpha-nucleus collision.

The ^{12}C- nucleus data for absorption cross sections for 83 MeV per nucleon are shown in Table 2. Experimental data are taken from reference [94]. We observe from Table 2 that, as the mass of the target increases, the use

Table 2. Absorption cross sections (medium modified) for ^{12}C-nucleus systems. E_{lab} = 83 A Mev

System	σ_r (mb) (Experimental)	σ_r (mb) (in-medium)	σ_r (mb) (free space)
$^{12}C + ^{12}C$	960 ± 30	816	874
$^{12}C + ^{27}Al$	1400 ± 40	1369	1419
$^{12}C + ^{40}Ca$	1550 ± 60	1580	1737
$^{12}C + ^{56}Fe$	1810 ± 100	1970	1997

*For ^{12}C-nucleus, the experimental data is from S. Kox et al. [94].

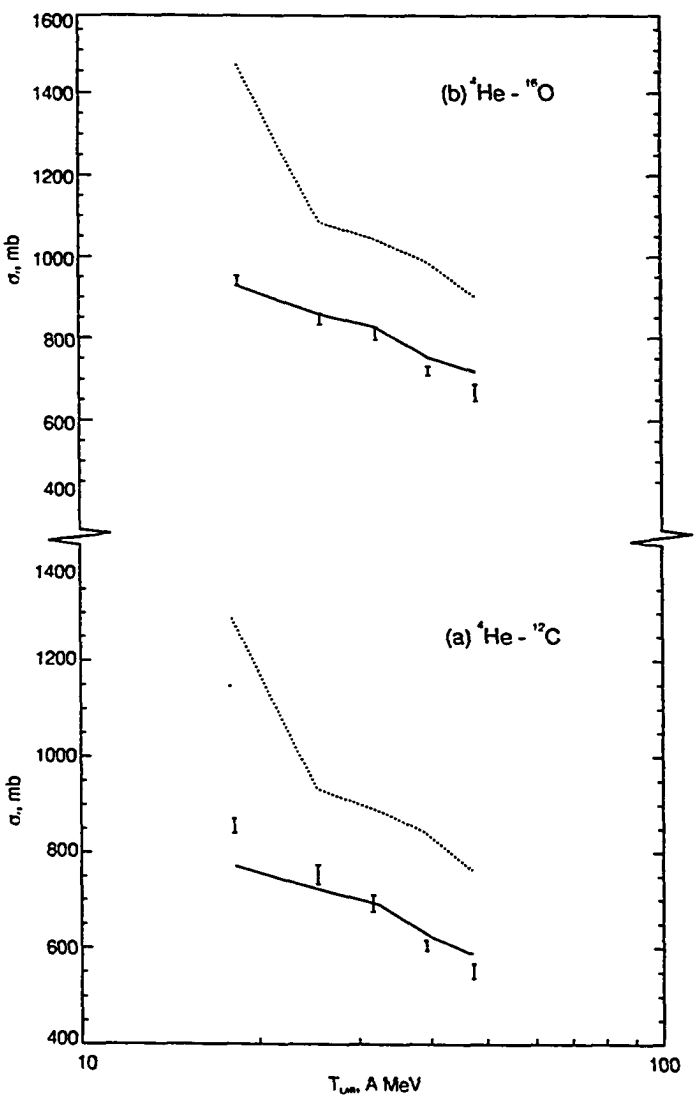

Figure 12. Comparison of theoretical absorption cross sections calculations using the Lippmann-Schwinger equation to the experimental data. The dash line using the free space and the solid line the in-medium nucleon-nucleon total cross sections.

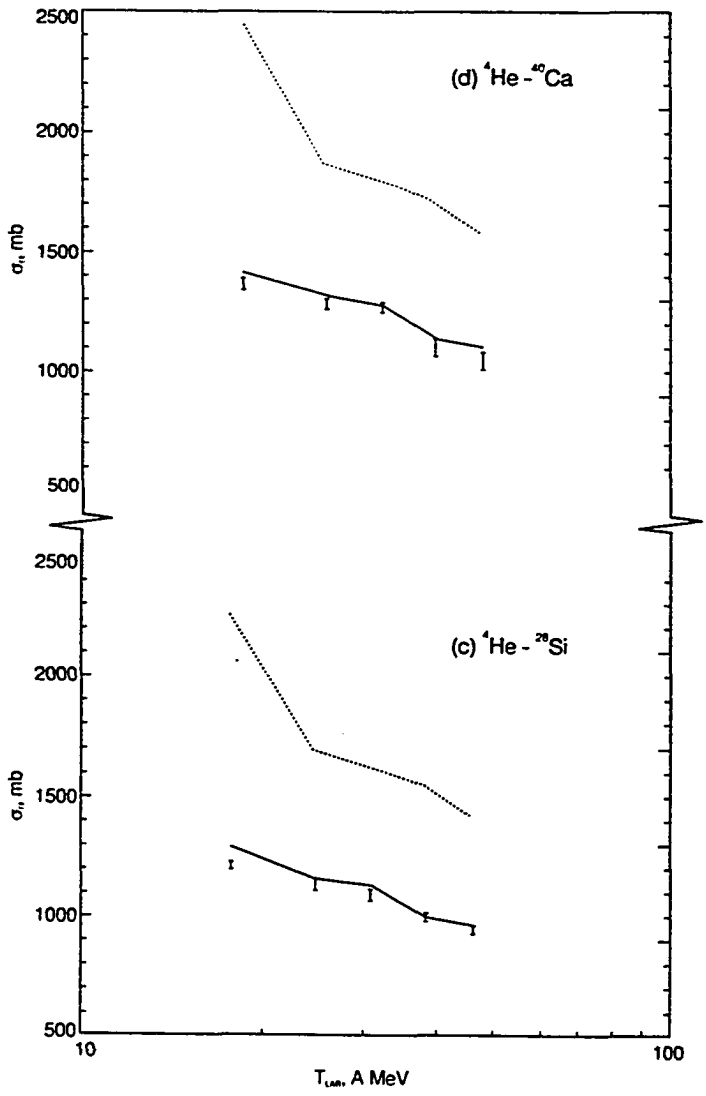

Figure 12, continued

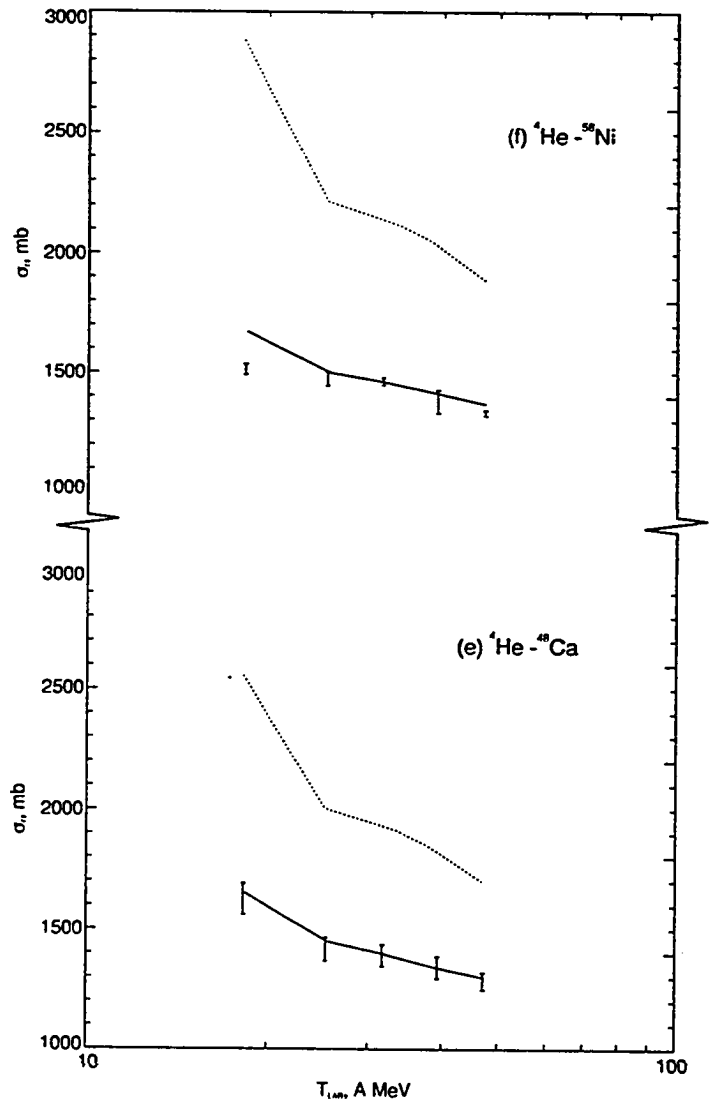

Figure 12, continued

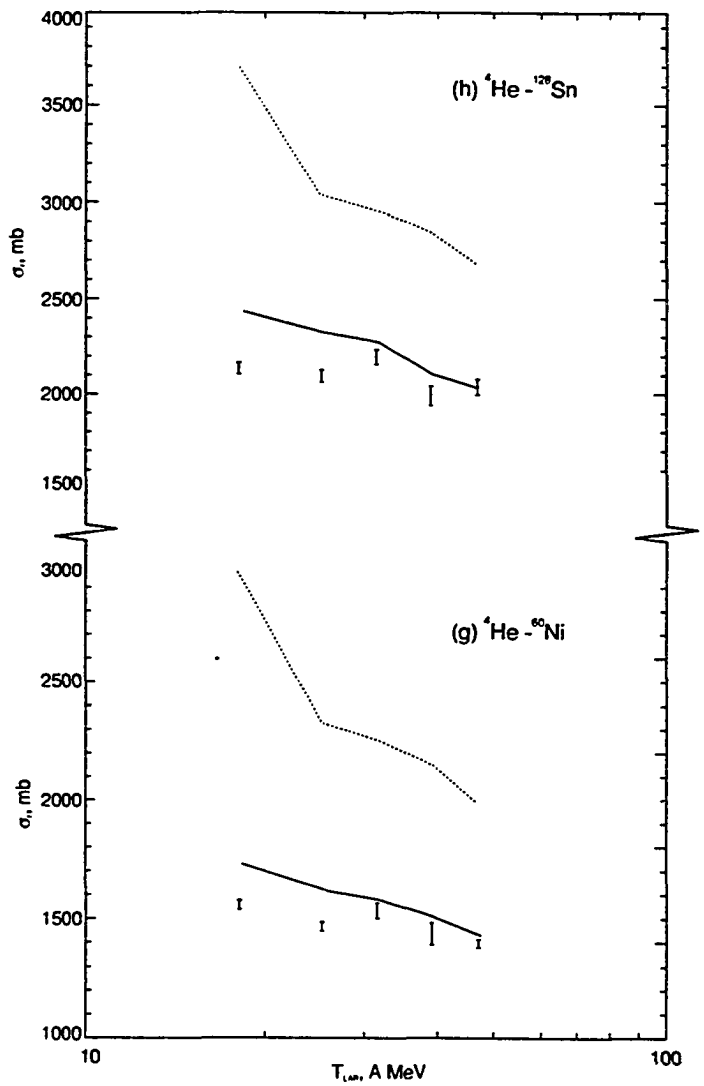

Figure 12, continued

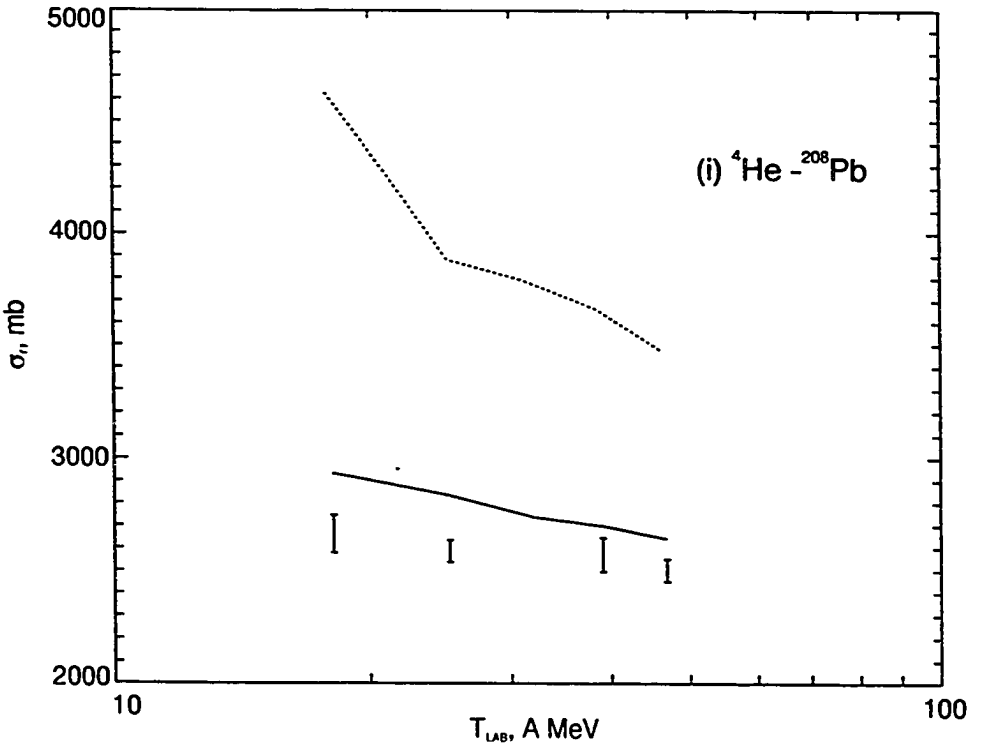

Figure 12, continued

of in-medium NN cross sections gives improved agreement with the experimental data.

Experimental data showed that using in-medium NN cross sections rather than free space NN cross sections provides improved absorption cross sections values. We therefore conclude that in-medium total NN cross sections should be used in optical model calculations below 200 MeV/nucleon.

The Eikonal approximation is computationally efficient since it requires only a few numerical integrations. The exact solution using the Lippmann Schwinger equation requires many partial waves even for nucleon-nucleus scattering. Therefore, one prefers the Eikonal approximation for heavy-ion collisions.

6.2 Calculations Using the Abrasion-Ablation Model

Next, in this chapter we are going to discuss the results obtained from theoretical calculations of knockout spectra and we will compare them with the available experimental data. The knockout spectra and knockout cross sections are calculated from equations (195) and (198). The relation between wave functions and the spectroscopic factors is given by Coelho [89]. The ground state wave function is given by equation (193). For obtaining the transition densities, Woods-Saxon and harmonic oscillator potentials are used. The quantity χ is calculated under the optical limit from equations (200) and (201). The inclusion of knockout of alpha clusters gives good agreement between

theory and experiment.

In Figure 13, we show results for a single α-particle abrasion from a ^{12}C projectile interacting with a ^{12}C target at a projectile energy of 2.1 A GeV. Contributions to the energy transfer cross section from the transitions L = 0 and 2 to L' = 0 and 2 states in the case of a ^{8}Be core are shown. The $0 \rightarrow 0$ transition (ie., where ^{8}Be is a spectator), is seen to dominate with a broad distribution in energy transfers. The diagonal transition $2 \rightarrow 2$, also contributes. However, the off-diagonal transition ($0 \rightarrow 2$) of the core contributes very little indicating that ^{8}Be acts as a true spectator.

Engelage et. al. [100] have measured the excitation spectrum for $^{12}C \rightarrow 3\ \alpha$ using the Heavy-Ion Super-conducting Spectrometer (HISS) for a 2.1 A GeV beam. Excitation energy is the invariant mass of the projectile fragments minus the ^{12}C rest mass. In Figure 14, we compare the measurements with our calculated values for the energy transfer spectrum of the projectile spectators. The contributions from the abrasion of two α particles, where we have included only the L = 0 state of ^{8}Be in the initial and intermediate states, are allowed for the calculation. The HISS detector had insufficient granularity at low energy values due to poor resolution in resolving α pairs with relative momenta of less than 75 MeV/c [100]. Figure 14 shows their corrected and uncorrected data [100]. We find that the cluster abrasion model is in good agreement with the data that includes the granularity correction. Our calculations show that the peak in the energy distribution lies below that of

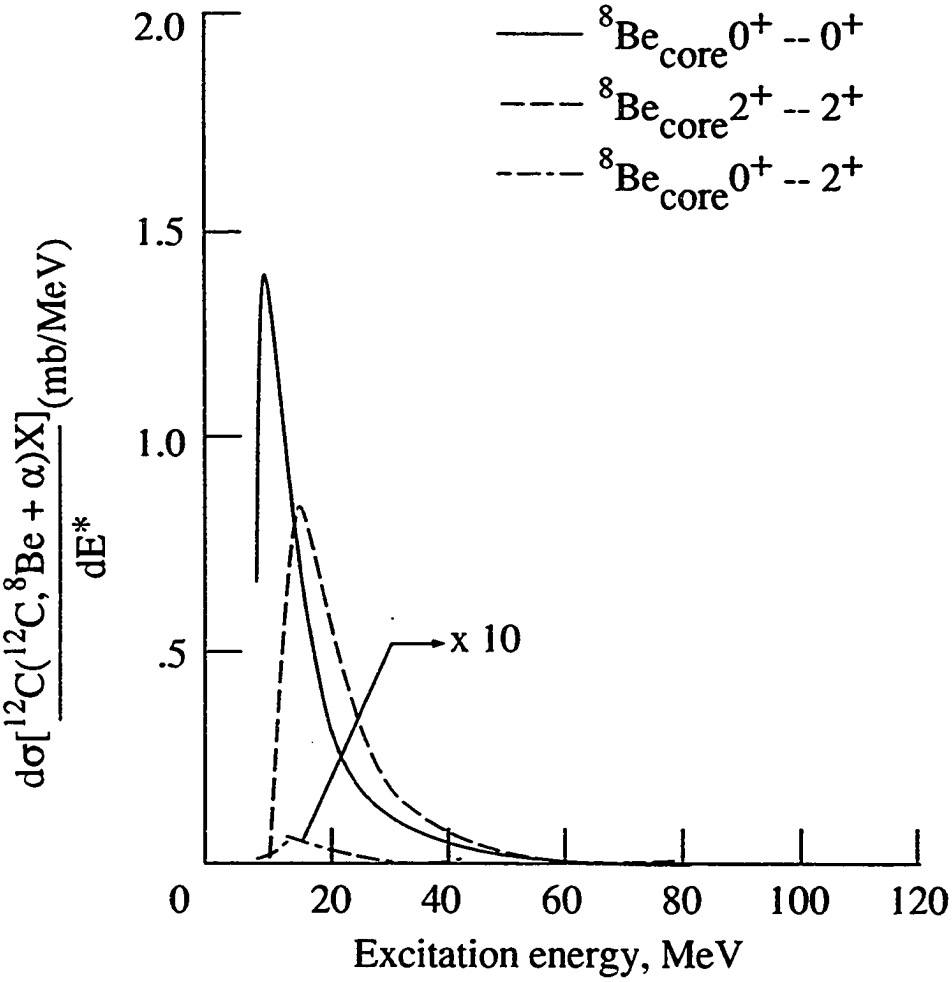

Figure 13. Theoretical excitation spectra for ^{12}C (^{12}C, $^{8}Be+\alpha$)X reactions at 2.1 A GeV. Shown are contributions of several $^{8}Be+\alpha$ states of relative motion in initial and final states.

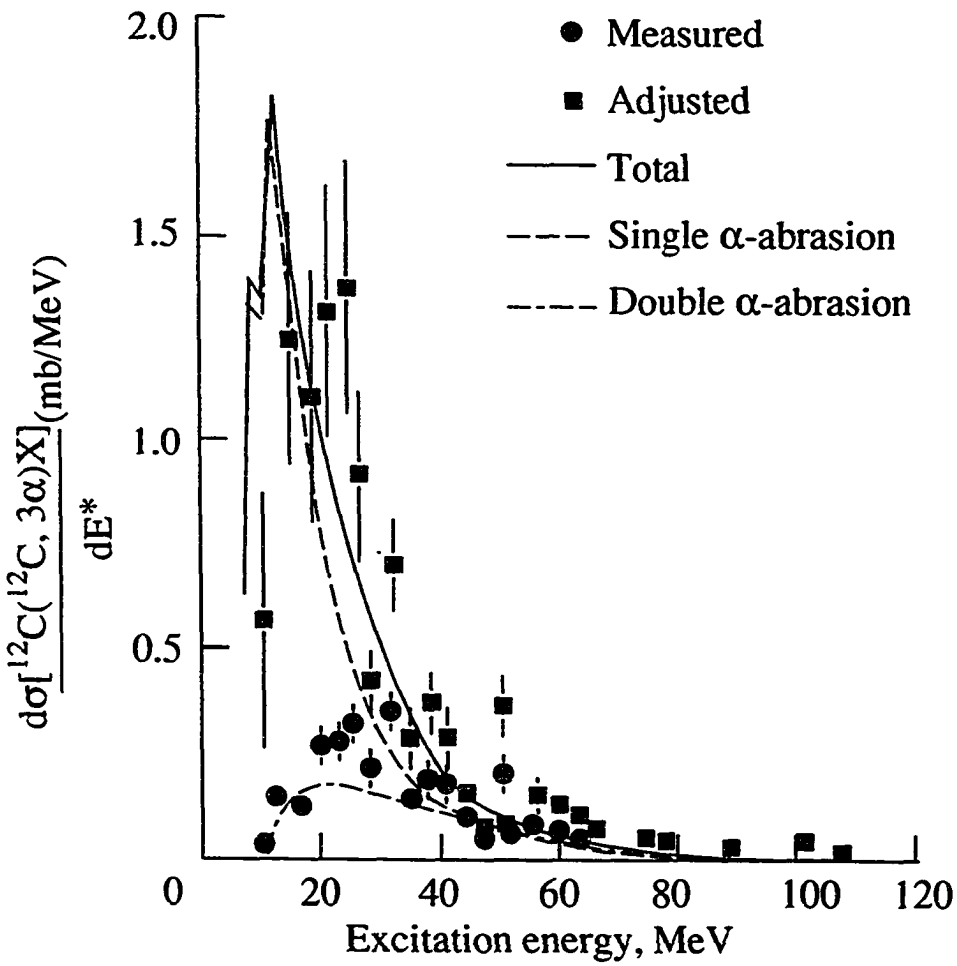

Figure 14. Comparson of theoretical and experimental excitation spectra for ^{12}C (^{12}C, 3α)X reactions at 2.1 A GeV. Calculations are for single and double alpha abrasion.

the experimental data. We have also done calculations with a wave function of the form $\phi_{L,M} = \sqrt{N}\, u^4 \exp(-u^2/2a^2)\, Y_{L,M}$. However, the results of this procedure greatly overestimated the experimental values above 50 MeV. Although we expect that improved agreement with experiment could be achieved by using cluster wave functions from a microscopic formulation, some effect from the use of a target closure approximation and final state interactions may modify our comparison.

The excitation of several low lying levels of ^{12}C may lead to 3 α final states [101]. Several of these states have been investigated previously at high energies using a proton [102] and α-particles [103] beams. The experiments of Blanpiad et. al. [102] resolved the excited states at 7.7, 9.6, 10.8, and 14.1 MeV using 800 MeV protons. The gross features of these measurements are adequately described in the distorted wave Born approximation (DWBA) or coupled-channel model [102, 104]. To estimate the contribution of these states to the experiment described above, we have used the DWBA with the closure approximation [105] for an unobserved ^{12}C target in an inclusive reaction. For the 0^+ state at 7.7 MeV, we find a narrow peak below 10 MeV in the excitation cross section and we expect similar peaks for the other low lying states. These states are not resolved by the HISS detector. The integrated cross section for these states has been estimated previously [104], and is found to give only a small contribution to the ^{12}C absorption cross section.

The model developed in Chapter 5 describes the excitation spectrum of

a projectile that fragments into α particles. This description is based on multiple quasielastic α-nucleon scattering with a broad distribution in energy transfers due to the kinetic energy distribution of the alpha particles or core intermediate states. The abrasion response functions will also describe the excitation spectrum following nucleon abrasion through multiple quasielastic nucleon-nucleon scattering. In the future, these response functions will be used [106] to describe the measurements of Webb et. al. [107] using the HISS detector for the excitation energy in the fragmentation channel.

The cluster effects, for ^{16}O projectiles of 2.1 A GeV energy bombarded on several targets are shown in Figure 15. The dashed line shows the nucleon knockout cross sections with ablation. We see that the calculations based on just the assumption of the nucleon knockouts can not give results to agree with the experiment. The thick dashed line represents the alpha knockout cross sections. The solid line shows the total (nucleon + alpha) knockout cross sections. The resultant database is an improvement over our initial assumption of only nucleon knockouts. Thus, we can say that the effect of alpha clustering is most apparent in α- ^{16}O collisions. The addition of the alpha knockout cross section (leaving ^{12}C in the ground state) to the non-elastic cross section (solid line) brings good agreement with the LBL oxygen beam data of Olson et. al. [108]. The inclusion of the alpha cluster effect is important in filling the gap between experiment and theory.

Figure 16 shows the results for several projectiles with 600 A MeV beam

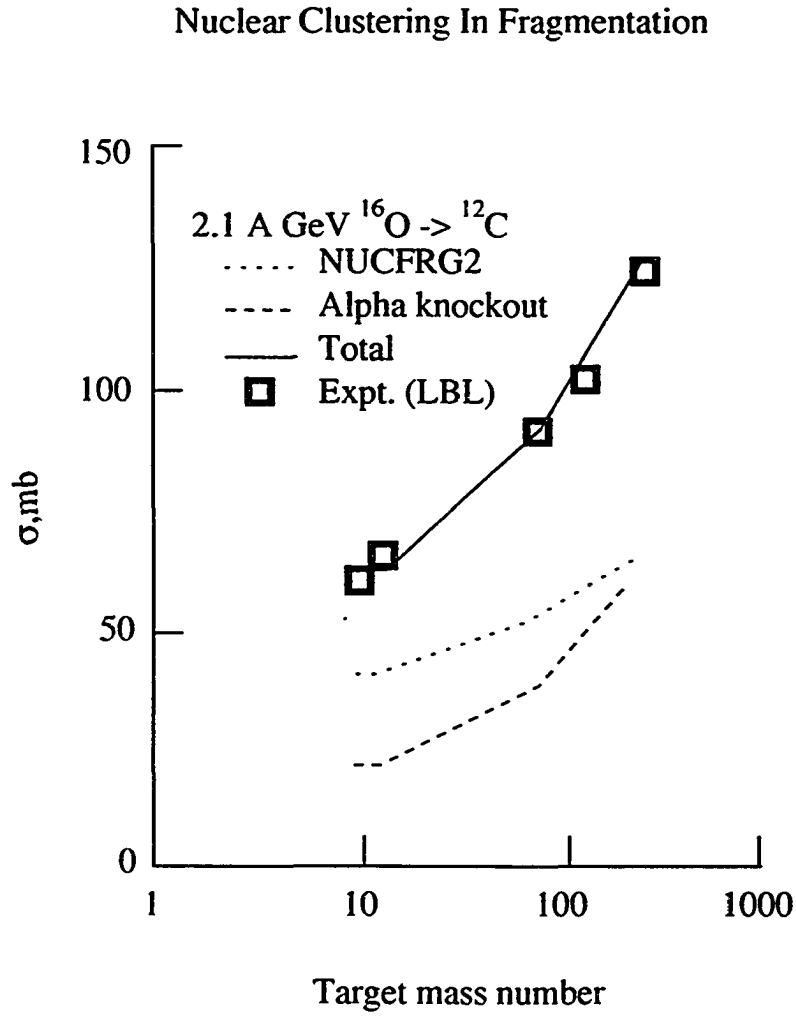

Figure 15. The clustering effects for an ^{16}O projectile at 2.1 A GeV bombarded on several targets is presented as a function of target mass number.

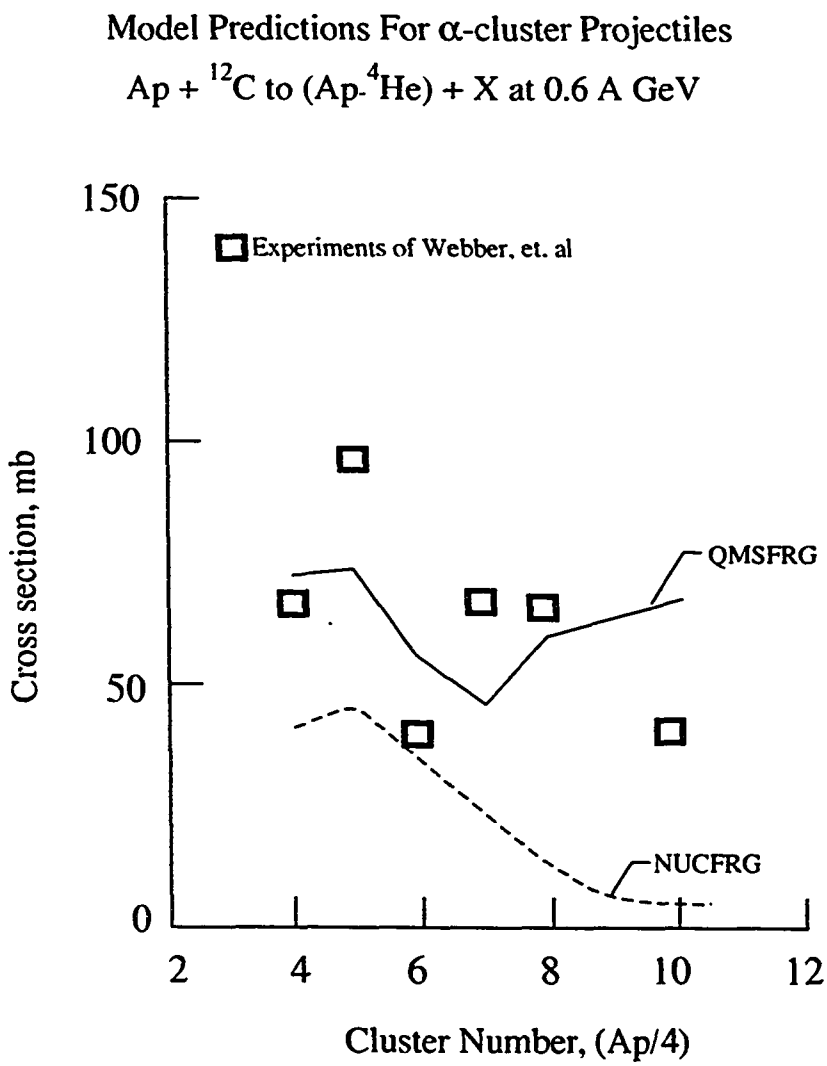

Figure 16. Model predictions for alpha-cluster projectiles with 600 A MeV beam energy on a ^{12}C target.

energy incident on a ^{12}C target. The dashed line shows the nucleon knockout cross section. The solid curve shows the total (nucleon + alpha) knockout cross section. The experimental data is taken from Webber et. al. [109]. The theoretical total knockout cross section is in good agreement with experiment. The sharp dip in the solid curve may be due to the uncertainty in the spectroscopic factors (Table 3). The unsystematic behavior suggests structure dependent effects and perhaps results from the fact that nuclei with large atomic masses consist of integral numbers of highly stable alpha particles.

Further development of the cluster model will be helpful in resolving discrepancies in these cross sections and we hope that such results will be available in the future. Most important in this respect is the strong energy dependence in the cluster knockout cross sections as seen in Figure 17. This Figure represents the alpha knockout cross section as a function of energy (for ^{16}O projectile on several targets). We observe from the figure that the knockout cross section increases with energy. We see that as the target mass number becomes large, the knockout cross section increases sharply. The systematic behavior indicates that cluster knockout is dominant in the nuclei with large mass numbers at higher energies (500 A MeV - 10 A GeV).

One expects a large alpha knockout cross section for 4n nuclei such as ^{20}Ne, ^{24}Mg, and ^{28}Si that are important contributors to GCR exposure. Also, knockout of other light clusters will be important in heavy-ion fragmentation for all nuclei that have large spectroscopic constants for clusters outside the

Table 3. Spectroscopic Factors

System	l=0		l=2		l=4	
	value	range	value	range	value	range
^{12}C - ^{8}Be	.558	.29 - .70	1.74	.29 - 1.7	.203	---
^{16}O - ^{12}C	.244	.23 - .98	1.26	.78 - 1.2	.205	---
^{20}Ne - ^{16}O	.202	.15 - 1.3	.18	---	.4	---
^{24}Mg - ^{20}Ne	.23	.23 - 1.0	.2	.2 - .9	.9	---
^{28}Si - ^{24}Mg	.24	.24 - 1.0	.4	.4 - 1.5	.17	---
^{40}Ca - ^{36}Ar	.5	.5 - 2.1	.18	.18 - 1.0	.33	---

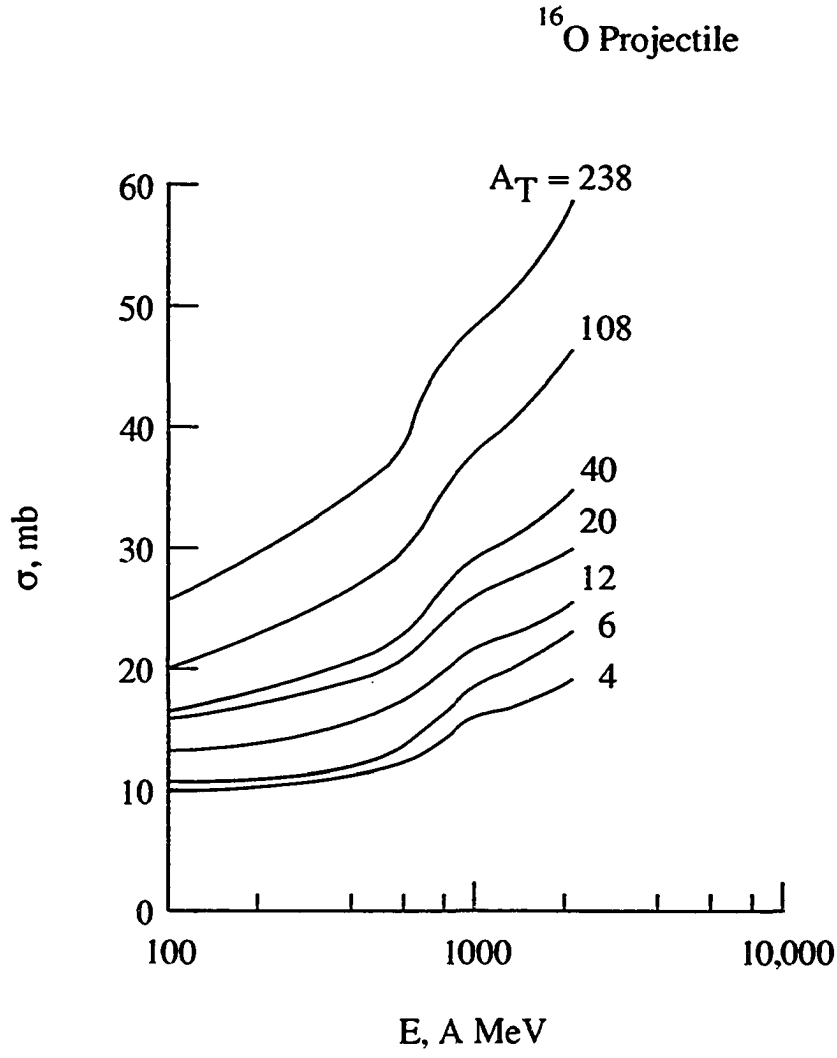

Figure 17. The energy dependence of the cluster knockout cross sections is presented as a function of energy for several targets.

closed sub shells in the ground state of the projectile or the target. There is a strong energy dependence associated with the nuclear form factors and the effects of pion production as clearly shown in the few hundred MeV to one GeV region in Figure 17. Fortunately the energy dependence is less severe for light targets and low projectile energy, which is helpful in developing medical therapy beams. Therefore, it is clear from the present study that a final database generator will require cluster models for light ions.

6.3 BRYNTRN Code and Mono-energetic Proton Beam

In Figure 18, we show the secondary charged particle spectra ϕ at several depths in an aluminum shield for a 200 MeV proton beam. The dashed line corresponds to the evaporation part of the spectrum. The inclusion of the knockout cross sections (solid line) is clearly seen to increase the flux ϕ. We see that for greater depths the secondaries produced from the targets fall off as the beam energy is degraded. In alpha and helion particle emission, we see a sharp drop in the flux at higher depths.

In Figure 19, we show the results of calculations of the absorbed dose as a function of depth in water shields for a 200 MeV proton beam. In Figure 19, we also show the contributions from the knockout cross sections. This Figure provides the break down of the contributions from the primary proton (dotted line), secondary proton (dash-dot line), and all the other secondaries (dashed line). The increase in the secondary contributions to the absorbed dose

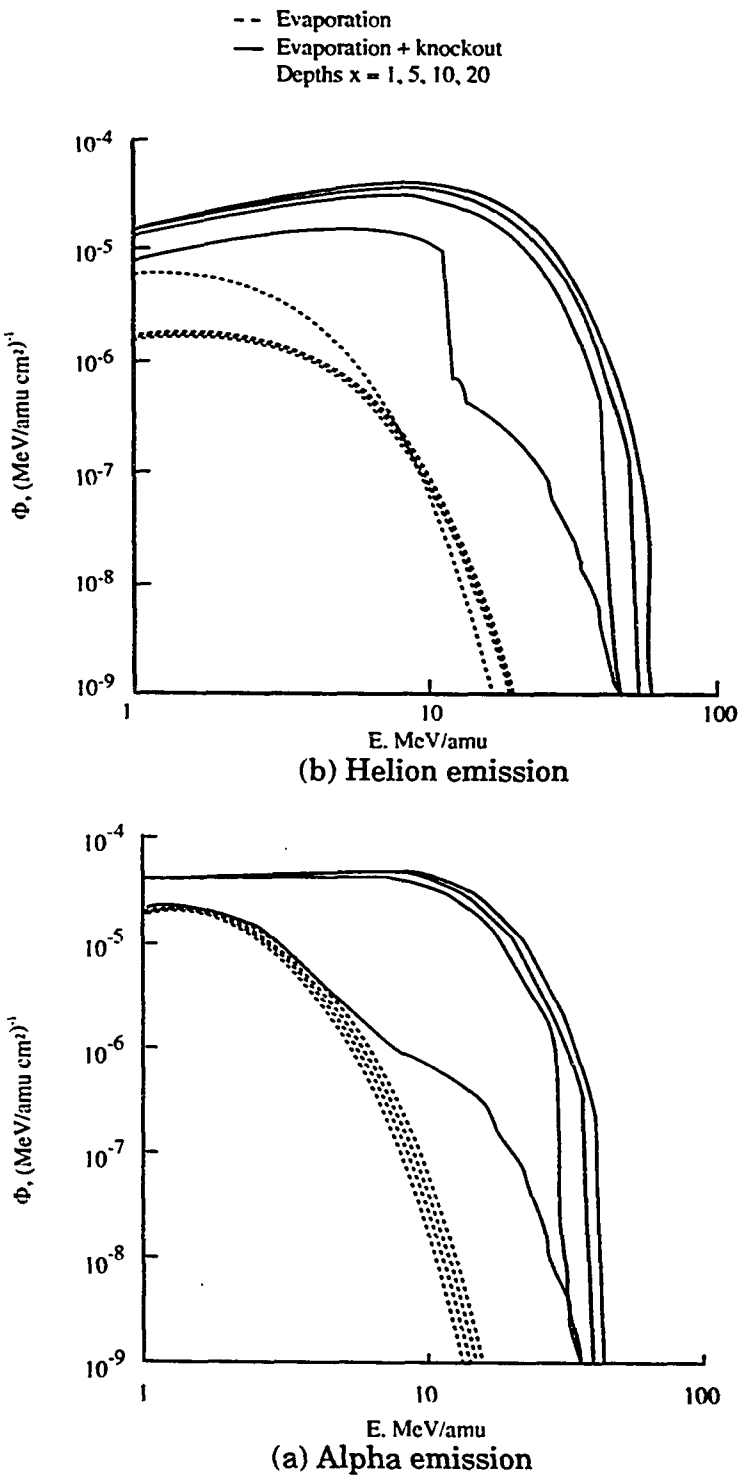

Figure 18. Theoretical light ion spectrum per primary proton in aluminum shields for a primary proton beam at 200 MeV/amu.

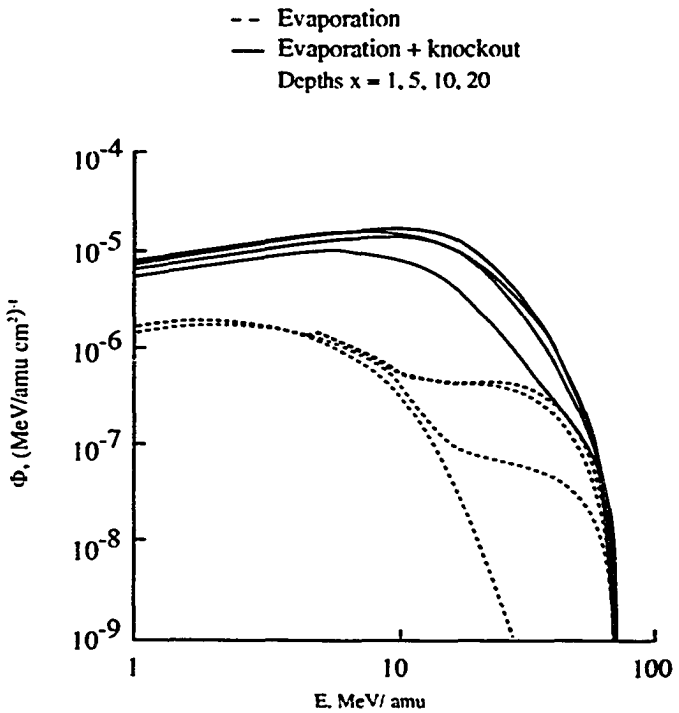

(d) Deuteron emission

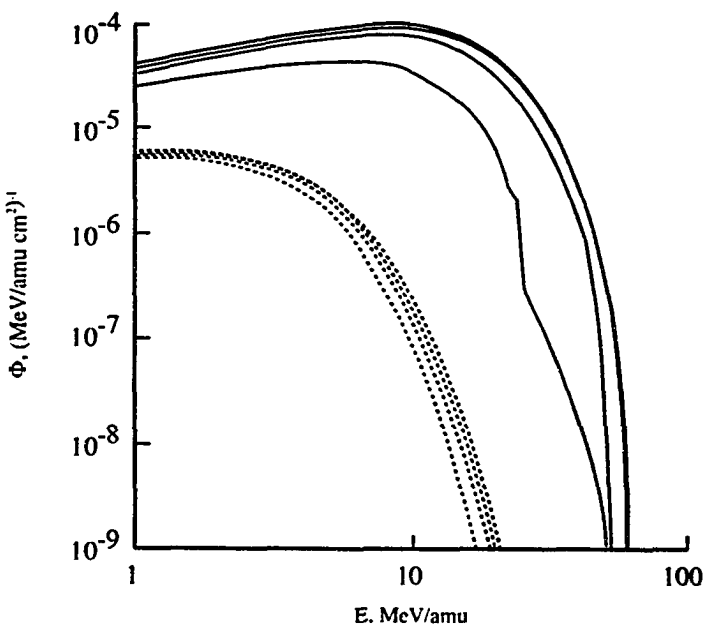

(c) Triton emission

Figure 18, continued

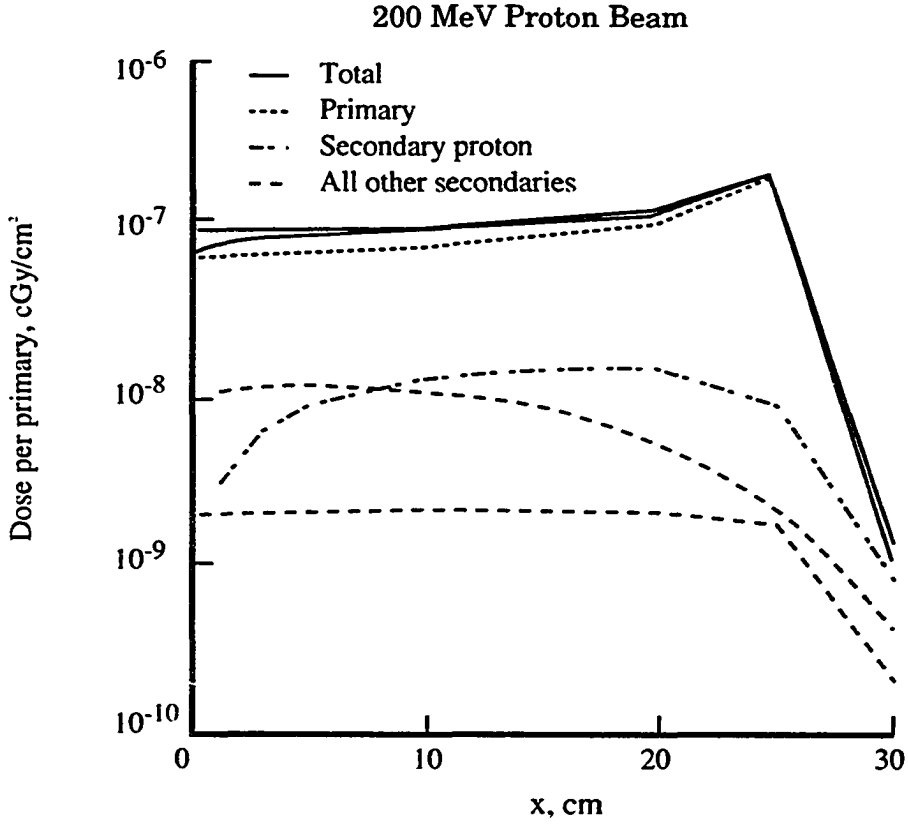

Figure 19. Depth-dose curves for a proton beam at 200 MeV in water.

is apparent when we include the knockout cross sections. We also observe an increase in the total (solid line) absorbed dose.

In Figure 20, we show the results of calculations of the dose equivalent as a function of depth in water shields for a 200 MeV proton beam. Features similar to the absorbed dose as discussed in the previous paragraph are observed.

6.4 Trapped Proton Energy Spectrum

The trapped protons surrounding the earth can be conveniently described as existing in two partially distinct regions. In each region, protons spiral around the geomagnetic field lines moving towards and away from the magnetic poles. In addition, the trapped protons drift westward. Since these trapped protons occupy a limited volume in space, they are important in low earth-orbiting missions. The most intense region is located between Africa and South America, where the spiraling protons dip closer than usual to the earth. Extensive information on the energy spectra of the trapped protons has been accumulated from orbiting spacecrafts over the past three decades. In this section, we describe the energy spectra for the trapped protons and compare them with the observations made by a solid-state charged particle telescope in the mid-deck of a Space Shuttle during the period of solar maximum. The telescope was flown in high altitude flights at 57^0 inclination. These observations show the presence of the secondary deuterons, tritons as well as

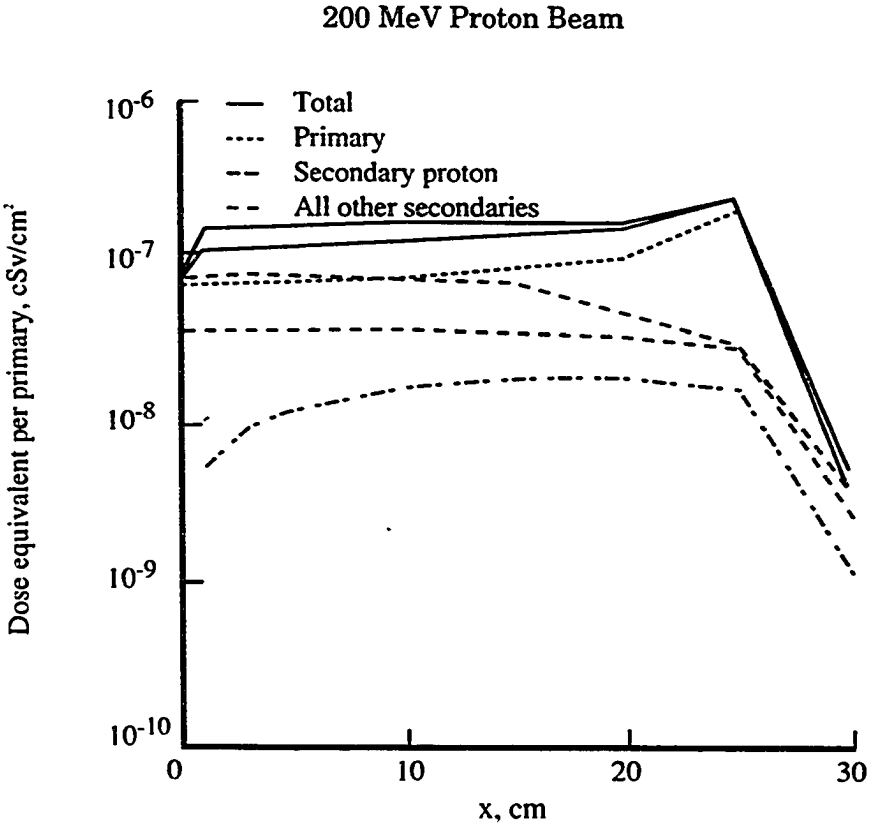

Figure 20. Dose equivalent curves for a proton beam at 200 MeV in water.

helions and alpha particles.

In Figure 21, we show the energy spectra of secondary (trapped) helion and alpha particles assuming that the angular distribution of the particles incident on the telescope is isotropic. The solid line corresponds to the helion and the dashed line corresponds to the alpha particles. The calculations are based on the BRYNTRN transport code. Figure 22 shows the energy spectra for the trapped deuteron and triton particles. A comparison of the results of calculations is made with the STS-48 observations [110]. Clearly, the model calculations and observations are in good agreement. A discrepancy can be seen for the low energy case. The discrepancy may be due to the fact that the angular distribution of these particles may not be isotropic at low energy. It is not quite clear at present how these effects can be separated. Care should be taken in including the contributions of these particles in model calculations.

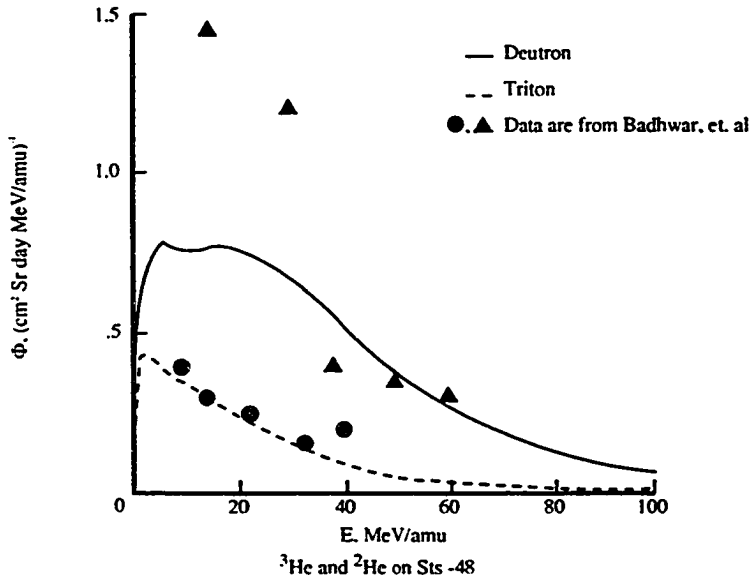

Figure 22. Comparision of secondary deutron and triton energy spectra using the BRYNTRN transport code.

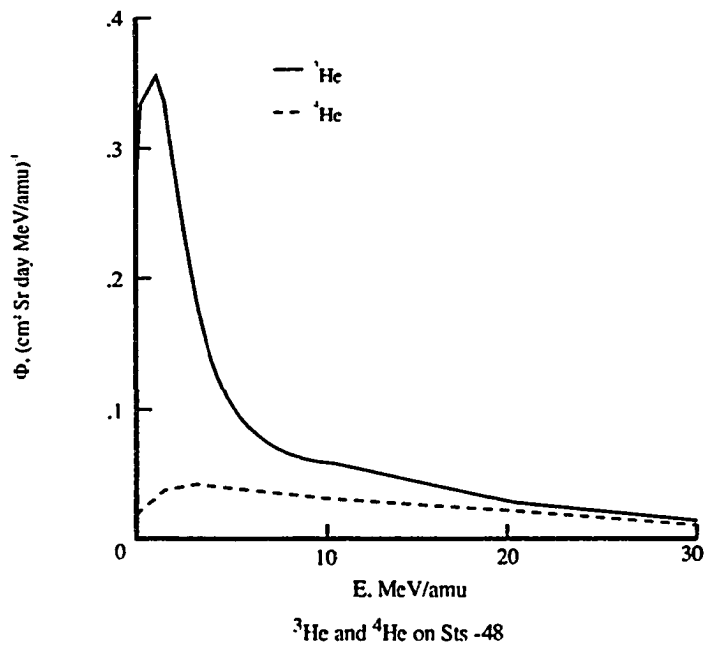

Figure 21. Comparision of secondary helion and alpha energy spectra using the BRYNTRN transport code.

Bibliography

1. J.W. Wilson, L.W. Townsend, W. Schimmerling, G.S. Khandelwal, F. Khan, J.E. Nealy, F.A. Cucinotta, L.C. Simonsen, J.L. Shinn, and J.W. Norbury, NASA RP 1257, 1991
2. F.A. Cucinotta, L. W. Townsend, J.W. Wilson, J.L. Shinn, G.D. Badhwar, and R.R. Dubey, Adv. in Space Res. **17**, 77, (1996).
3. D.L. Dye, and J.C. Noyes, J. Astronaut Sci., **7**, 64, (1960).
4. B. H. Bethe, American Inst. of Physics handbook, Edited by D.E. Gray, (McGraw-Hill Publication, 1963).
5. M.C. Walske, and H.A. Bethe, Phy. Rev. **83**, 457, (1951).
6. G.S. Khandelwal, Nucl. Phys. **A116**, 97, (1968).
7. G.S. Khandelwal, Phys. Rev. A **26**, 2983, (1982).
8. Y.J. Xu, G.S. Khandelwal, and J.W. Wilson, Phys. Rev. A **32**, 629, (1985).
9. S.L. Lamkin, Ph. D. Thesis, Old Dominion University, 1994.
10. R.R. Dubey, G.S. Khandelwal, and W.M. Pritchard, J. Phys. B **24**, 57, (1991).
11. S.Y. Chun, Ph. D. Thesis, Old dominion University, 1994.
12. G.S. Khandelwal, and E. Merzbacher, Phys. Rev. **144**, 349, (1966).
13. J.W. Wilson, L.W. Townsend, J.E. Nealy, S.Y. Chun, B.S. Hong, W.W. Buck, S.L. Lamkin, B.D. Ganapol, F. Khan, and F.A. Cucinotta, NASA TP-2887, 1989.

14. J.W. Wilson, and S. L. Lamkin, Nucl. Sci. & Eng. **57**, 292, (1975).

15. J.W. Wilson, L.W. Townsend, J.L. Shinn, F.A. Cucinotta, R.C. Costen, F.F. Badavi, and S.L. Lamkin, Adv. Space Red. **14**, 841, (1994).

16. F.A. Cucinotta, L.W. Townsend, and J.W. Wilson, NASA TP-3285, 1993.

17. F.A. Cucinotta, NASA TP-3354, 1993.

18. ICRP-60, Ann. of the ICRP **21**, (Pergamon Press, New York,1991).

19. J.W. Wilson, and L.W. Townsend, J. Phys. **59**, 1569, (1981).

20. L.W. Townsend, and J.W. Wilson, NASA RP-1134, 1985.

21. R.R. Dubey, G.S. Khandelwal, F.A. Cucinotta, and K.M. Maung, NASA TP 3498, 1995.

22. R.R. Dubey, G.S. Khandelwal, F.A. Cucinotta, and J.W. Wilson, J. of Phys. G (Submitted).

23. F.A. Cucinotta, K. Katz, J.W. Wilson, and R.R. Dubey, NASA TP-3497, 1995.

24. A. Picklesimer, and R.M. Thaler, Phys. Rev. C **23**, 42, 1981.

25. A. Picklesimer, P.C. Tandy, and R.M. Thaler, Phys. Rev. C **25**, 1215, (1982).

26. A. Picklesimer, P.C. Tandy, and R.M. Thaler, Phys. Rev. C **25**, 1233, (1982).

27. D.H. Wolf, M.V. Hynes, A. Picklesimer, P.C. Tandy, and R.M. Thaler, (AIP Conference Proceeding No. 97), edited by H.O. Meyer, 149, 1983.

28. C.R. Chinn, Ch. Elster, and R.M. Thaler, Phys. Rev. C **48**, 2956, (1993).

29. A.K. Kerman, H. McManus, and R.M. Thaler, Ann. of Phys. **8**, 551, (1959).

30. K.M. Watson, Phys. Rev. **89**, 575, (1953).

31. H.F. Arellano, F.A. Brieva, and W.G. Love, Phys. Rev. Lett. **63**, 605, (1989).

32. Ch. Elster, T. Cheon, E.F. Redish, and P.C. Tandy, Phys. Rev. C **41**, 814, (1994).

33. R. Crespo, R.C. Johnson, and J.A. Tostevin, Phys. Rev. C **41**, 2257, (1990).

34. H.F. Arellano, F.A. Brieva, and W.G. Love, Phys. Rev. C **41**, 2188, (1990).

35. J.W. Wilson, Ph.D. Diss., College of William and Mary, 1975.

36. J.W. Wilson, Phys. Lett. B **52**, 149, (1974).

37. C.J. Joachain, Quantum Collision Theory, (North-Holland Publication, 1987).

38. F.A. Cucinotta, Ph.D. Diss., Old Dominion Univ. 1988.

39. F.A. Cucinotta, G.S. Khandelwal, K.M. Maung, L.W., Townsend, and J.W. Wilson, NASA TP-2830, 1988.

40. F.A. Cucinotta, and R.R. Dubey, Phys. Rev. C **50**, 979, (1994).

41. R.J. Glauber, "Lecture in Theoretical Physics", edited by, W.E. Brittin, and L.G. Dunham (Interscience Publication, New York), **1**, 315, 1959.

42. M. Ostrofsky, G. Breit, and D. Johnson, Phys. Rev. **49**, 22, (1936).

43. H.A. Bethe, Phys. Rev. **57**, 1125, (1940).

44. S. Fernbach, R. Serber, and T. Taylor, Phys. Rev. **75**, 1352, (1949).

45. G.Z. Moliere, Z. Naturferch **2A**, 133, (1947).

46. R.J. Glauber, Phys. Rev. **91**, 459, (1953).

47. R.J. Glauber, Phys. Rev. **100**, 242, (1955).

48. D.T. Khoa, W. von Oertzen, and H.G. Bohlem, Phys. Rev. C **49**, 1652, (1994).

49. W.W. Buck, J.W. Norbury, L.W. Townsend, and J.W. Wilson, Phys. Rev. C **33**, 234, (1986).

50. G.R. Satchler, and W.G. Love, Phys. Rev. **55**, 183, (1979).

51. A.M. Kobos, B.A. Brown, P.E. Hodgson, G.R. Satchler, and A. Budzanowski, Nucl. Phys. **A384**, 65, (1982).

52. A.M. Kobos, B.A. Brown, R. Lindsay, and G.R. Satchler, Nucl. Phys. **A425**, 205, (1984).

53. R. Crespo, R.C. Johnson, and J.A. Tostevin, Phys. Rev. C **44**, 1735, (1991).

54. R. Crespo, R.C. Johnson, and J.A. Tostevin, Phys. Rev. C **46**, 279, (1992).

55. L. Ray, Phys. Rev. C **39**, 1170, (1989).

56. L. Ray, Phys. Rev. C **47**, 2236, (1993).

57. D.T. Khoa, and W. von Oertzen, Phys. Lett. B **304**, 8, (1993).

58. J.P. Jeukenne, A. Lejeune, and C. Mahaux, Phys. Rev. C **10**, 1391, (1974).

59. T. Cheon, and E.F. redish, Phys. Rev. C **39**, 331, (1989).

60. H. Feshbach, Ann. Phys. **5**, 357, (1958).

61. M.B. Johnson, and A. Picklesimer, Relativistic Dynamics and Quark Nuclear Physics, (Wiley Publication, 1986).

62. K.M. Maung, P.A. Deutchman, and W.D. Royalty, Canadian J. Phys. **67**, 95, (1989).

63. B. ter Haar, and R. Malfliet, Phys. Rev. C **36**, 1611, (1987).

64. A. Bohnet, N. Ohtsuka, J. Aichelin, R. Linden, and A. Faessler, Nucl. Phys. **A494**, 349, (1989).

65. J.R. Shepard, J.A. McNeil, and S.J. Wallace, Phys. Rev. Lett. **50**, 1443, (1983).

66. D.P. Murdock, and C.J. Horowitz, Phys. Rev. C **35**, 1442, (1987).

67. L. Ray, and G.W. Hoffmann, Phys. Rev. C **31**, 538, (1985).

68. K.M. Maung, and F. Gross, Phys. Rev. C **42**, 1681, (1990).

69. J. Janicke, J. Aichelin, N. Ohtsuka, R. Linden, and A. Faessler, Nucl. Phys. **A536**, 201, (1992).

70. G.Q. Li, and R. Machleidt, Phys. Rev. C **48**, 1702, (1993).

71. G.Q. Li, and R. Machleidt, Phys. Rev. C **49**, 566, (1994).

72. W.G. Love, and M.A. Franey, Phys. Rev. C **24**, 1073, (1981).

73. A. Picklesimer, and G.E. Walker, Phys. Rev. C **17**, 237, (1978).

74. J. of Comp. Phy. **3**, 332, (1968).

75. R. Serber, Phys. Rev. **72**, 1008, (1947).

76. J.D. Bowman, W.J. Swiatecki, and C.F. Tsang, Report LBL-2908, 1973.

77. J. Hufner, K. Schafer, and B. Schurmann, Phys. Rev. C **12**, 1888, (1973).

78. M. Blesznski, and C. Sanders, Nucl. Phys. **A326**, 525, (1979).

79. L.F. Oliveria, R. Donangelo, and J.O. Rasmussen, Phys. Rev. C **19**, 826, (1979).

80. J.J. Gaimard, and K.H. Schmidt, Nucl. Phys. **A531**, 709, (1991).

81. G. Faldt, and L. Gislen, Nucl. Phys., **A254**, 341, (1975).

82. N. Masuda, and F. Uchiyama, Phys. Rev. C **15**, 972, (1977).

83. T. Kodama, S.B. Duarte, K.C. Chang, and R. Nazareth, Phys. Rev. Lett. **49**, 536, (1982).

84. D.M. Brink, Proceeding of the International School of Physics " Enrico fermi," Course 36, (Academic Press, New York, 1966).

85. J. Zhank, and W.O.M. Rae, Nucl. Phys. **A564**, 252, (1993).

86. R.D. Viollier, and E. Turtschi, Ann. Phys. (N.Y.), **124**, 290, (1980).

87. F.A. Cucinotta, L.W. Townsend, J.W. Wilson, Phys. Rev. C **46**, 1451, (1992).

88. F.A. Cucinotta, and R.R. Dubey NASA Report TP-3353, 1993.

89. H.T. Coelho, Phys. Rev. C **7**, 2340, (1973).

90. W.F. Hornyak, Nuclear Structure, (Academic Press, New York, 1975).

91. J.V. Noble, Phys. Rev. C **1**, 1900, (1970).

92. H.P. Grotz, L. Lehmann, E. Rossle, M. Schmitt, and L. Schmitt, Nucl. Phys. **A490**, 667, (1988).

93. L. Shiver, and T. Kanai, NIRS-M-82.

94. S. Kox, A. Gamp, R. Cherkaoui, A. Cole, N. Longequeue, J. Menot, J.C. Perrin, and J.B. Viaano, Nucl Phys. **A420**, 162, (1984).

95. W. Bauhoff, Atomic Data and Nuclear Data Tables, **35**, 429, (1986).

96. A.M. Sourkes, A. Houdayer, and W.T.H. Van Oers, Phys. Rev. C **13**, 451, (1976).

97. F.A. Cucinotta, G.S. Khandelwal, L.W. Townsend, and J.W. Wilson, Phys. Rev. Lett. B **223**, 127, (1989).

98. F.A Cucinotta, L.W. Townsend, and J.W. Wilson, NASA TM-4314,1991.

99. A. Auce, R.F. Carlson, A.J. Cox, A. Ingemarsson, R. Johansson, P.U. Renberg, O. Sundberg, G. Tibell, and R. Zorro, Phys. Rev. C **50**, 871, (1994).

100. J. Engelage, et. al., Phys. Lett. B **173**, 34, (1986).

101. F. Ajzenberg-Selove, Nucl. Phys. **A506**, 1, (1990).

102. G.S. Blanpied, G.W. Hoffmann, M.L. Barlett, J.A. McGill, S.J. Greene, L. Ray, O.B. Van Dyck, J. Amann, and H.A. Thiessen, Phys. Rev. C **23**, 2599, (1981).

103. A. Chaumeaux, G. Bruge, T. Bauer, R. Bertini, A. Boudard, H. Catz, P. Couvert, H.H. Duhm, J.M. Fontaine, D. Garreta, J.C. Lugol, V. Layly, and R. Schaeffer, Nucl. Phys. **A267**, 413, (1976).

104. F.A. Cucinotta, G.S. Khandelwal, K.M. Maung, L.W. Townsend, and J.W. Wilson, NASA Report TP-2830, 1988.

105. F.A. Cucinotta, L.W. Townsend, and J.W. Wilson, J. Phys. G **18**, 889, (1992).

106. F.A. Cucinotta, Unpublished.

107. M.L. Webb, et. al., Phys. Rev. C **36**, 193, (1987).

108. D.L. Olson, B.L. Berman, D.E. Greiner, H.H. Heckman, P.J. Lindstrom, and H.J. Crawford, Phys., Rev. C **28**, 1602, (1983).

109. W.R. Webber, J.C. Kish, and D.A. Schrier, Phys. Rev. C **41**, 547, (1990).

110. G.D. Badhwar, J.U. Patel, A. Konradi, F.A. Cucinotta, and J.W. Kern, Adv. in Space Research, (in Press)

Rajendra R. Dubey

Rajendra R. Dubey, a native of India, was born on March 24, 1964 in a small town named Gorakhpur. He graduated from Marwari Vidyalya High School, Bombay, India in June, 1979. He entered Jaihind College, Bombay, India in 1979 and graduated from the University of Bombay, with a B. Sc. degree in August, 1984. He received his M. Sc. degree in August, 1986 from the University of Bombay.

After working as a lecturer at K.C. College, Bombay for a year, he joined Old Dominion University in Norfolk, Virginia in August, 1988. After arriving at ODU, Mr. Dubey sought the guidance of Dr. Govind S. Khandelwal, Department of Physics, Old Dominion University. His master of science degree at ODU was awarded in December, 1991. Since January, 1992, Mr. Dubey has pursued his Doctoral research in conjunction with the NASA Langley Research Center, under the supervision of Dr. Francis A. Cucinotta. His Research publications are in Atomic, Nuclear, and Radiation Physics. Mr. Dubey has worked on several heavy-ion nuclear physics projects requiring high level modeling and simulation on several computational systems. His work has been documented in over fifteen national and international publications and conference presentations.

In 1984, Mr. Dubey was the recipient of the best student award at Jaihind College, Bombay. He has served on several technical review committees for NASA Langley Research Center publications. He is a member of the American Physical Society, Virginia Academy of Science, and Sigma Pi Sigma (an honorary physics society).

Mr. Dubey was married to his wife Sudha in June 1981. His daughter Pryanka was born in December 1984 and his son Prasant was born in September 1988.

PUBLICATIONS

National and International Journals

1. R.R. Dubey, G.S. Khandelwal, F.A. Cucinotta, and J.W. Wilson: Microscopic Optical Model Calculations of Heavy Ion Absorption Cross Sections: *J. Phys. G,* (Submitted).

2. F.A. Cucinotta, L.W. Townsend, J.W. Wilson, J.L. Shinn, G.D. Badhwar, and R.R. Dubey: Light Ion Components of the Galactic Cosmic Rays: Nuclear Interactions and Transport Theory, *Adv. Space Res.* **17,** 77, 1995.

3. F.A. Cucinotta, K. Katz, J.W. Wilson, and R.R. Dubey: Heavy Ion Track-Structure Calculations for Radial Dose in Arbitrary Materials: NASA TP-3497, February 1995.

4. R.R. Dubey, G.S. Khandelwal, F.A. Cucinotta, and K.M. Moung: Comparison of Exact Solution to Eikonal Approximation for the Elastic Heavy Ion Scattering: NASA TP-3498 February 1995.

5. F.A. Cucinotta, and R.R. Dubey: Alpha-Cluster Description of Excitation Energies in $^{12}C(^{12}C, 3\alpha)X$ at 2.1 A GeV: *Phys. Rev. C* **50,** August 1994.

6. F.A. Cucinotta, L.W. Townsend, and R.R. Dubey: Energy-Loss Cross Section for Inclusive Nuclear Collisions: NASA TP 4522, November 1993.

7. F.A. Cucinotta, and R.R. Dubey: Final State interactions and Inclusive Nuclear Collisions: NASA TP 3353, August 1993.

8. R.R. Dubey, G.S. Khandelwal, and W.M. Pritchard: Asymptotic Expansion of hydrogenic Radial Dipole Integral: *J. Phys. B* **24,** 1991, pp. 57-63.

Conference Presentations

1. F.A. Cucinotta, J.W. Wilson, K.M. Maung, T. Christian, R.K. Tripathi, and R.R. Dubey: Nuclear Interactions Models in the Development of Cross Section Libraries for Cosmic Ray Studies: Paper submitted for the 1996 Radiation Protection and Shielding Division Topical Meeting, Falmouth, MA, April 1996.

2. R.R. Dubey, G.S. Khandelwal, F.A. Cucinotta, and J.W. Wilson: α-Clustering Effects in the Fragmentation of Heavy Ions: Paper to be presented at the APS division of nuclear physics fall meeting, October, 1995.

3. R.R. Dubey, G.S. Khandelwal, F.A. Cucinotta, and J.W. Wilson: α-Production Cross Section in Heavy-Ion Fragmentation Under Abrasion-Ablation Models: Paper presented at the joint meeting of CAP (Canada) and SMF (Mexico), June 1995.

4. R.R. Dubey, G.S. Khandelwal, F.A. Cucinotta, and L.W. Townsend: Model for the Multiple Knockouts During Quasi-Elastic Charge Exchange Reactions: Paper presented at the APS General Meeting, Crystal City, Virginia, April 1994.

5. R.R. Dubey, G.S. Khandelwal, F.A. Cucinotta, L.W. Townsend, and K.M. Moung: Nucleus-Nucleus Scattering Using First Order Optical Potential: Paper presented at the Annual Meeting of the APS Division of Nuclear Physics, Asilomar, California, October 1993.

6. R.R. Dubey, G.S. Khandelwal, F.A. Cucinotta, and L.W. Townsend: Final State Interaction Effects on the Quasi-Elastic Peak for Proton-Nucleus Scattering: Paper presented at the 70th Annual Conference of Virginia Academy of Science, Richmond, Virginia, May 1992.

7. F.A. Cucinotta, S.M. Beck, L.W. Townsend, J.W. Wilson, R.K. Tripathi, and R.R. Dubey: Final State Interaction Effects on the Quasi-Elastic Peak for Proton-Nucleus Scattering: Paper presented at the APS General Meeting, Washington, D.C., April 1992.

8. R.R. Dubey, G.S. Khandelwal, F.A. Cucinotta, and L.W. Townsend: Parameterization of Off-Shell α-α Transition Amplitude: Paper presented at the 69th Annual Conference of Virginia Academy of Science, Blacksburg, Virginia, May 1991.

Coauthor on Old Dominion University/NASA Progress Reports

1. A Study of Physical Process for Space Radiation Protection, Tech. Rep., NASA, PTR-90-1, 1990.

2. A Study of Physical Process for Space Radiation Protection, Tech. Rep., NASA, PTR-90-5, 1990.

3. A Study of Physical Process for Space Radiation Protection, Tech. Rep., NASA, PTR-91-1, 1991.

4. A Study of Physical Process for Space Radiation Protection, Tech. Rep., NASA, PTR-91-2, 1991.

5. A Study of Physical Process for Space Radiation Protection, Tech. Rep., NASA, PTR-92-2, 1992.

6. A Study of Physical Process for Space Radiation Protection, Tech. Rep., NASA, PTR-92-5, 1992.

7. A Study of Physical Process for Space Radiation Protection, Tech. Rep., NASA, PTR-93-2, 1993.

8. A Study of Physical Process for Space Radiation Protection, Tech. Rep., NASA, PTR-93-5, 1993.